Louisiana State University
LSU Scholarly Repository

LSU Master's Theses | Graduate School

July 2021

Evaluation of Cell Concentration and Viability By Impedance Spectroscopy On Microfluidic Devices

Jason Eades
Louisiana State University and Agricultural and Mechanical College

Follow this and additional works at: https://repository.lsu.edu/gradschool_theses

 Part of the Biological Engineering Commons

Recommended Citation

Eades, Jason, "Evaluation of Cell Concentration and Viability By Impedance Spectroscopy On Microfluidic Devices" (2021). *LSU Master's Theses*. 5421.
https://repository.lsu.edu/gradschool_theses/5421

This Thesis is brought to you for free and open access by the Graduate School at LSU Scholarly Repository. It has been accepted for inclusion in LSU Master's Theses by an authorized graduate school editor of LSU Scholarly Repository. For more information, please contact gradetd@lsu.edu.

EVALUATION OF CELL CONCENTRATION AND VIABILITY BY IMPEDANCE SPECTROSCOPY ON MICROFLUIDIC DEVICES

A Thesis

Submitted to the Graduate Faculty of the
Louisiana State University and
Agricultural and Mechanical College
in partial fulfillment of the
requirements for the degree of
Master of Science

in

The Department of Biological and Agricultural Engineering

by
Jason Clark Eades
B.S., Louisiana State University, 2016
August 2021

Acknowledgments

First and foremost, I would like to thank my advisor, Dr. W. Todd Monroe, for his unwavering support. As a dedicated educator, Dr. Monroe clearly considers the professional and personal development of his students to be of utmost importance, and I consider myself fortunate to have been an observer and a direct recipient of that commitment.

I also want to express my gratitude to the other members of my thesis committee, Dr. Terrence Tiersch and Dr. Jin-Woo Choi. After years of working with them, I have learned countless lessons, both technical and personal, that I expect will serve me for the rest of my career. Their efforts to create effective and enjoyable collaborative relationships provide wonderful examples which I aspire to follow.

I must also thank the large number of people with whom I have had the fortune of working including Dr. Yue Liu, Dr. Hamed Shamkhalichenar, Dr. Jorge Belgodere, Nick Lombardo, Nik Zuchowicz, Jonathan Thomas, Val Browning, Jack North, Clint Graham, Mustafa Alam, Nate Semmes, and Julie Armand. I value deeply the camaraderie that has existed in this group.

I would like to thank my family for their support. I am grateful to my parents who have taught me to embrace and enjoy challenges and value the hard work and determination required to overcome them. There is no question that I would not have been able to navigate this experience without your examples and encouragement.

Finally, I want to thank Kelly for her love and encouragement. Her exceptional support has been and continues to be invaluable to me.

I acknowledge support from the National Institutes of Health, Office of Research Infrastructure Programs (R24-OD010441), with additional support provided by the National Institute of Food and Agriculture, United States Department of Agriculture (Hatch project NC1194), and the LSU-ACRES (Audubon Center for Research of Endangered Species) Collaborative Program.

Preface

This document describes two distinct platforms that implement electrochemical impedance spectroscopy (EIS) within microfluidic devices for rapid, label-free cell analysis. Each study provides proof-of-concept evaluations of these devices for cell counting and viability analysis applications to mitigate some of the challenges associated with conventional methods. Chapter one includes background information on each version of EIS selected and motivations for the studies conducted. Chapter two describes the design and fabrication of a modular, reusable microfluidic device. Additionally, the methodology for and results from the application of this platform for the measurement of zebrafish sperm cell concentrations are presented. Chapter three describes a microfluidic impedance flow cytometer created by a computer-aided manufacturing method for parallel electrode geometry fabrication. This device was used for single-cell viability testing of Jurkat cells on a continuous flow basis. Cell detection events and discrimination of intact and disrupted cells on the basis of their membrane properties was performed using a custom Matlab script. Major contributions to this project were made by Dr. Julianne Audiffred and Micah Fincher including device design and fabrication, maintenance of cell lines, and raw signal collection, that are shown in Dr. Audiffred's dissertation "Quantitative Macro- and Microscale Methods for Characterizing Cell Viability" (Louisiana State University, 2009). My contribution to this project, as detailed in Chapter 3, was to perform a more thorough COMSOL simulation of parallel versus coplanar electrode geometry performance in impedance cytometry applications, and to create a signal processing algorithm to re-analyze the raw experimental data to improve upon the work pursuant to viability status discrimination. As such, this work will be the basis of a co-authored manuscript

that has been significantly re-written to include comparisons with microfluidic impedance cytometry devices that have published more recently. Chapter four includes a summary of conclusions from these efforts and a discussion of proposed future directions.

Table of Contents

List of Tables

List of Figures

Chapter 1. Background and Significance

1.1. Need for a Sperm Cell Counting Platform

The determination of sperm cell concentration is an integral factor in many agricultural, research, clinical, and repository applications. Implementation of reliable and robust methods for cell counting is imperative for these operations. For example, sperm counts are a critical component in the diagnosis and prognosis of fertility, according to World Health Organization (WHO) guidelines (Research 1992). Traditionally, this has been performed by optical means whereby cells are counted by manual observation with a microscope. However, manual counting is generally tedious, time consuming, and prone to erroneous results (Auger 2000). Automated cell counting platforms capable of accurate concentration measurements of a number of cell types are commercially available. However, their cost and incompatibility with cell types such as sperm limit their use. A recent review found significant differences in the correlations among various counting methods of sperm cells (Kumar, Reddy, and Krishna n.d.). Thus, sperm cell counting remains a challenge.

Zebrafish (*danio rerio*) have been used increasingly in research settings as a model organism for embryology and genetics studies, with more than 30,000 distinct genetic lines created to date. Effective maintenance and distribution of the gametes of these lines is necessary for implementation and protection of these research resources (Jing et al. 2009). Cell concentration has been shown to be a fundamental consideration required for effective implementation of various methods of preservation, fertilization, and distribution of sperm cell lines from aquatic species. However, users often neglect to perform cell

concentration measurements or adjust concentration to establish values which significantly affects the efficacy of cell-preservation efforts (Dong, Huang, and Tiersch 2007). Moreover, manual optical observation continues to be a predominant method for counting this cell type. Potentially lacking in accuracy and repeatability, this approach acts as a barrier to standardization of techniques for handling and use of zebrafish sperm cells.

1.2. Electrochemical Impedance Spectroscopy (EIS)

Leveraging the electrochemical properties of biological cells for analysis is an inherently rapid and automatable approach compared to many other methods. In general, electrochemical analyses involve the study of the nature and extent of changes in chemical properties that result from the application of a direct or alternating electrical current to the system being studied. Among the variations of this class of analysis methods, electrochemical impedance spectroscopy (EIS) has become widely used for evaluating biological samples owing to advantages including high sensitivity and low limits of detection. The basic mechanism of EIS involves application of an AC voltage and the measurement of the subsequent transfer function of the current response in the frequency domain (Lasia 2014). This response is typically measured as electrical impedance, a complex number with the form:

$$Z = R + jX \tag{1.1}$$

where R = resistance, X = reactance, and j = an imaginary number. Instruments that interrogate systems and collect impedance measurements typically do so in terms of changes in the amplitude of the applied current, denoted as impedance magnitude, and a shift in the phase of the applied signal. These components can be related to the real and

imaginary properties of impedance by:

$$|Z| = \sqrt{R^2 + X^2} \tag{1.2}$$

$$\theta = tan^{-1}(\frac{X}{R}) \tag{1.3}$$

where $|Z|$ = impedance magnitude and θ = phase. Using a knowledge of the dimensions of the system under study and the frequency of the applied AC, these values can be converted into and expressed in terms of constituent and related properties such as resistivity, capacitance, and permittivity.

1.2.1. Base Elements of EIS

While impedance spectroscopy is a powerful technique for the analysis of biological cell samples, a number of important design considerations must be made to achieve sufficient device accuracy and sensitivity. Impedance spectroscopy tools generally consist of several basic elements (each of which comprise a number of variations). Typically, EIS is applied to biological samples of cells in liquid electrolyte solutions. A set of electrodes is arranged adjacent to the sample, and voltage is applied via an excitation electrode by a signal generation instrument. The change in the applied signal is carried to a signal analysis apparatus (sometimes coupled with the generator) by a sensing electrode.

1.2.2. Electrode Geometry and Material

Traditionally, a three-electrode system has been used for impedance spectroscopy where the third electrode, a reference electrode, measures and contributes to the subtraction of the impedance signal corresponding to the cell-free electrolyte solution (Brosel-Oliu et al. 2019). Early versions of dielectric spectroscopy tools for analysis of liquid samples implemented coaxial probes (Raicu 1995) or parallel plate capacitors

(Hollingsworth and Saville 2003). These methods provided for simple data analysis due to their defined dimensions (Liu, Qiang, and Du 2021). Additionally, the large surface areas offered by these geometries provide high measurement sensitivity. However, despite these advantages, large-scale geometries suffer from an important drawback relevant to the analysis of biological samples. Because of their large surface areas, macro-scale electrode geometries do not offer high signal-to-noise ratios. As a result, contributions by small biological cells and relevant physical phenomena can be neglected (Varshney and Y. Li 2009). Instead, electrodes with dimensions at the micro-meter scale have improved abilities to resolve small changes in impedance signals. Specifically, interdigitated electrode arrays (IDEAs), arrays of symmetrical coplanar geometries wherein "fingers" alternate from excitation and sensing electrode sources as shown in Figure 1.1, are often utilized (Varshney and Y. Li 2009).

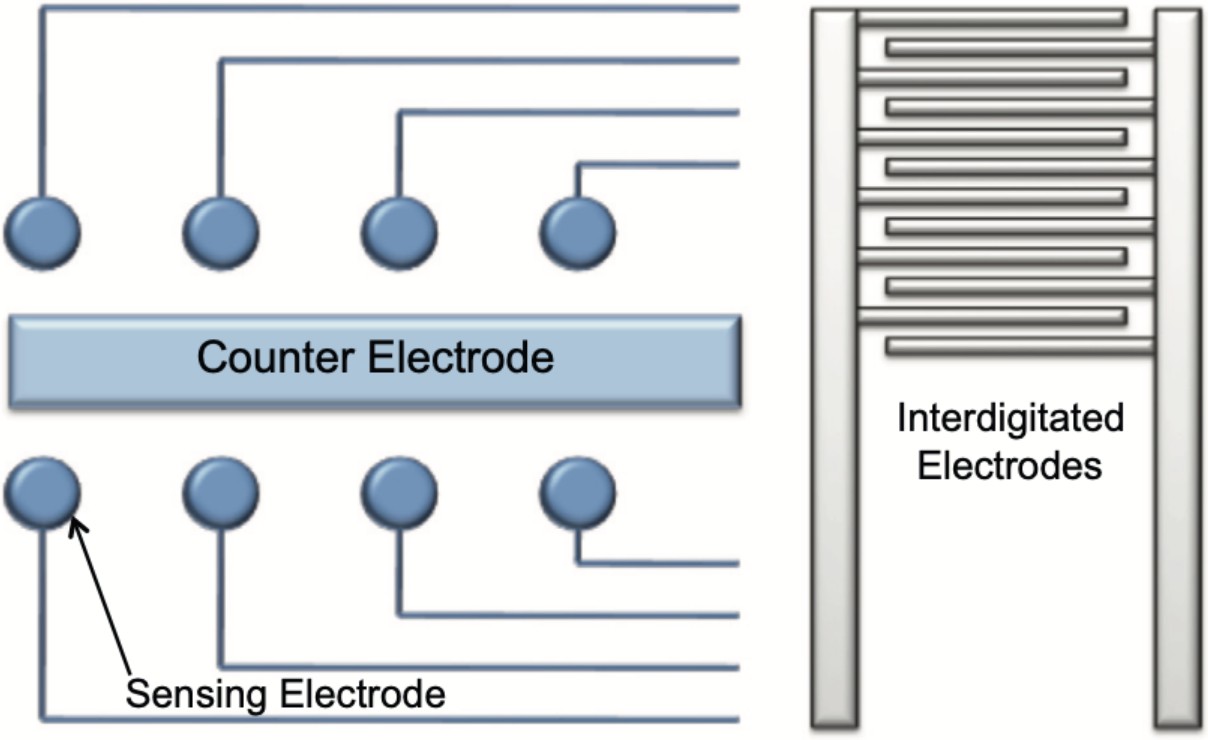

Figure 1.1. Illustration of an interdigitated electrode array (Source: Heileman, Daoud, and Tabrizian 2013.)

These designs balance the advantages of an overall large surface area and the high signal-to-noise ratio of microscale features. The performances of simple two-rail, coplanar interdigitated, and rectangular parallel plate electrode geometries were compared for cancer cell analysis (Demircan Yalçın et al. 2019). The parallel plate configuration demonstrated the greatest sensitivity to changes in the cell sample while the coplanar interdigitated array significantly outperformed the simple two-rail geometry. However, because parallel electrode geometries require complex fabrication methods, IDEAs are often favored.

While alternative materials are being developed and studied for specific applications of impedance spectroscopy (Cesewski and Johnson 2020), metals such as gold and platinum are used most often because their high conductivities allow for

sensitive measurements of more resistive solutions. Additionally, fabrication methods for generation of thin-film microelectrode geometries, such as by vapor deposition (Hierlemann et al. 2003) or screen printing (Taleat, Khoshroo, and Mazloum-Ardakani 2014) are well-established.

1.2.3. Electrode Modifications

Electrical impedance spectroscopy can generally be divided into two categories of physical orientation of cell samples: analysis of cells in suspension, and analysis of cells adhered onto a substrate. Most commonly, EIS devices implement immobilization layers on electrode surfaces consisting of nonspecific binding sites or specific conjugate molecules corresponding to cells or molecules of interest. Importantly, this technique restricts cells to regions near the electrode surface, increasing the probability of interaction with the applied electric field. However, these functional elements are often difficult to regenerate rendering them appropriate for single-use, and they can be cost prohibitive for users seeking multi-use solutions (Cesewski and Johnson 2020). Conversely, interrogation of suspended cells can be performed without the need to prepare or regenerate any labels or binding sites. Designing testing platforms without additional elements decreases cost and complexity while maintaining the potential for device reusability.

Electrodes can also be modified by the addition of a passivation layer. These consist of micron-height (or smaller) layers of resistive materials deposited onto electrode surfaces. Advantages of this approach include protection of vulnerable thin-film electrode materials from degradation by physical contact and fouling. These layers can also allow users to reduce the impacts of the interaction of the electrode material with electrolyte

solutions providing for easier analysis on the basis of their capacitive properties (Tsouti et al. 2011). However, despite these advantages, the use of passivation layers has been shown to inhibit achievable device sensitivity (Narayanan et al. 2010) thereby making the approach less feasible for some biologically relevant applications. Additionally, analyses conducted using passivated electrodes are often limited to capacitive measurements and therefore may not be suitable for applications requiring observation of resistive properties (Couniot et al. 2015).

1.2.4. Buffer Properties

Impedance spectroscopy has also been shown to be sensitive to the properties of the cell buffers. Detection of water-polluting bacteria was attempted in both high-conductivity and low-conductivity liquids. Although samples with cells could not be distinguished in the high-conductivity solution, cell concentration could be measured in a low-conductivity liquid. This could hinder cell detection by multiple mechanisms. First, if cells must be analyzed on the basis of conductivity, use of a conductive buffer may limit measurement sensitivity enough that properties cannot be discriminated from the background solution. Conversely, if cells are expected to be analyzed on the basis of their resistance in a conductive solution, a portion of the applied electric field is likely to bypass cells by taking the path of least electrical resistance. Similarly, solutions with high resistivities may also limit sensitivity as the applied electric field may be dampened or absorbed by the buffer. As a result, an appropriate balance must be tuned between the properties of the target cell and its liquid media to achieve sensitive cell analysis.

1.2.5. Integration of Microfluidic Technology

Microfluidic, or lab-on-a-chip, technology has revolutionized *in vitro* cell analysis efforts in recent years. Microfluidic chips require microliter sample volumes and offer greater standardization than larger-scale techniques (Petchakup, K. Li, and Hou 2017). Additionally, because these devices can be fabricated at dimensional scales similar to the sizes of cells, improved sensitivity of EIS tools can be achieved by restricting cells to the physical region immediately adjacent to the electrodes without the use of binding elements. As a result, in recent years, a new field of study, micro-electrochemical impedance spectroscopy (μEIS), has emerged in which microfluidic devices are developed for the application of impedance spectroscopy.

1.3. Data Collection and Processing

While a number of variations of impedance spectroscopy have been demonstrated, this technique generally involves measurement of the current response resulting from the application of a voltage over a range of frequencies, termed a frequency sweep. Data collected by this method can be presented in various ways. Bode plots are among the most commonly used methods for visualizing this type of data because they show the components of measured impedance values, whether magnitude and phase or resistance and reactance, in the frequency domain (Randviir and Banks 2013). Importantly, these plots can be used to evaluate potential frequency-dependent physical phenomena that may be occurring within a given system.

1.3.1. Data Validation

However, this characteristic of impedance spectroscopy offers advantages over other electrical analysis methods (e.g., voltammetry, conductometry, etc.) in that multiple properties and processes can be measured simultaneously. Impedance spectroscopy data in the frequency domain must meet certain criteria - stability, linearity, and causality - to be considered valid (Barsoukov and J. R. Macdonald 2005). The Kramers-Kronig relations are a set of mathematical expressions based on the rule of causality inherent to the real and imaginary components of complex functions. These relations can be used to predict the imaginary components of electrical impedance in electrochemical systems from measured real component values and vice versa. By comparing predicted and measured values of each component, users can test the stability and the linearity of an electrochemical system by these relations (Daniels and Pourmand 2007,Schönleber, Klotz, and Ivers-Tiffée 2014).

1.3.2. Frequency Dependence of Electrochemical Systems

Although different electrochemical systems exhibit differences in measured impedance spectra, a number of important principles are conserved that can be used to acquire understanding of liquid sample characteristics (Barsoukov and J. R. Macdonald 2005). Dielectric electrochemical systems can typically be analyzed on the basis of dispersion events observed over sweeps of applied AC frequencies. These dielectric dispersion, or relaxation, events result from the reordering of polarizable molecules in the liquid due to changes in the applied electric field. These events can be used to identify distinct frequency ranges in which applied electric fields interact with specific

portions of the sample. Aqueous solutions generally display a characteristic relaxation event at low frequencies. The presence of other molecules in solution can also create additional dispersions at other frequencies based on their unique polarization properties. Importantly, biological cells create these events (Figure 1.2) at frequencies and to extents dependent on their biophysical properties (Schwan 1957).

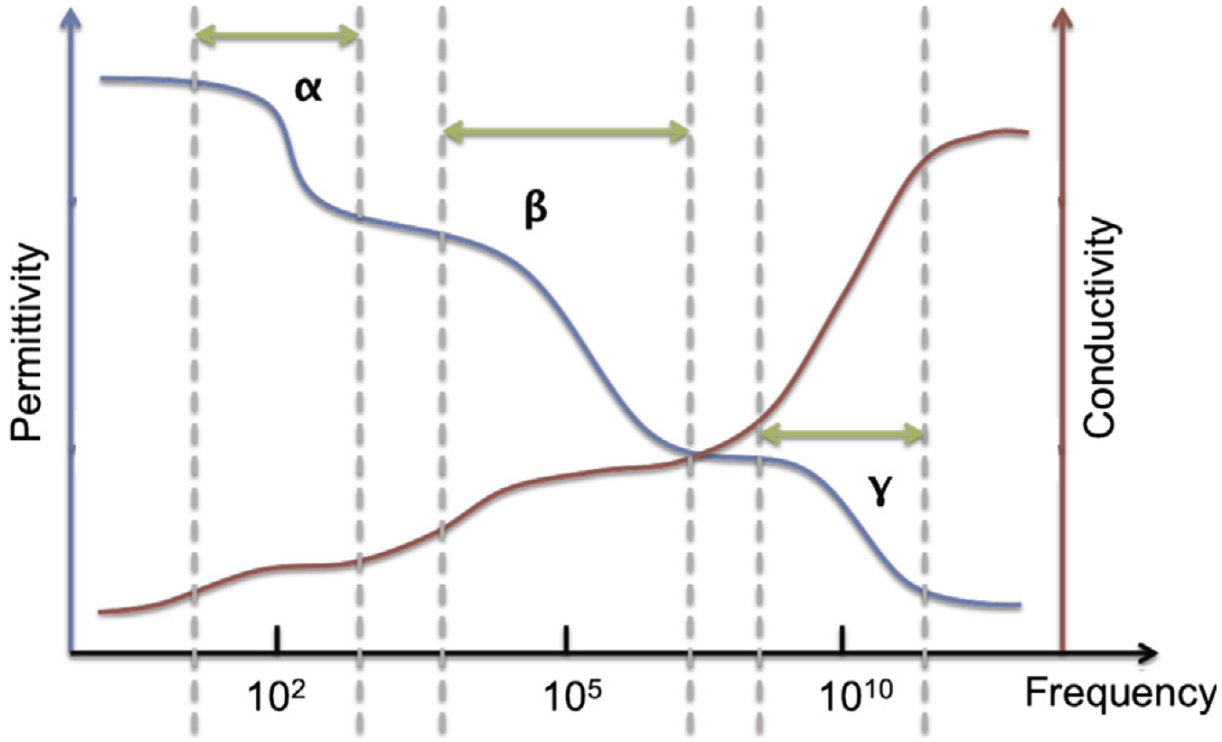

Figure 1.2. A typical profile of permittivity and conductivity of biological cells and tissues over applied AC frequencies (Source: Heileman, Daoud, and Tabrizian 2013)

Cell samples typically show a characteristic low-frequency α-dispersion below which applied electric fields often induce polarization of ions around external interfaces generating double layers near the excitation electrode surface. This first relaxation event results from the movement of ions and the dissolution of the electrical double layer, and measured resistances in this range of frequencies sometimes reflect these

movements (Lei 2014). As frequency increases above the first relaxation event, the double layer dissipates, and impedance signals often become dominated by the overall solution impedance properties. The second relaxation event, termed β-dispersion, results from the polarization of ions around the membranes of cells. Impedance measurements collected above this frequency typically reflect the resistive and capacitive properties of these charged interfaces. These phenomena, along with a basic understanding of the physical elements in analyzed samples, provide a framework for the interpretation of impedance spectra and correlation to important biophysical properties.

1.4. Microfluidic Impedance Cytometry

In recent years, a variation of the micro-electrochemical impedance spectroscopy technique has been implemented for the analysis of cellular properties. Motivated by the need to identify heterogeneities in cell properties within the bulk sample measurement methods, this tool combines the advantages of microfluidic technologies with impedance spectroscopy. First demonstrated by Gawad et al. in 2001 (S. Gawad, Schild, and Ph. Renaud 2001), this technique incorporates excitation and sensing electrodes immediately adjacent to or near a liquid solution containing cells (Figure 1.3).

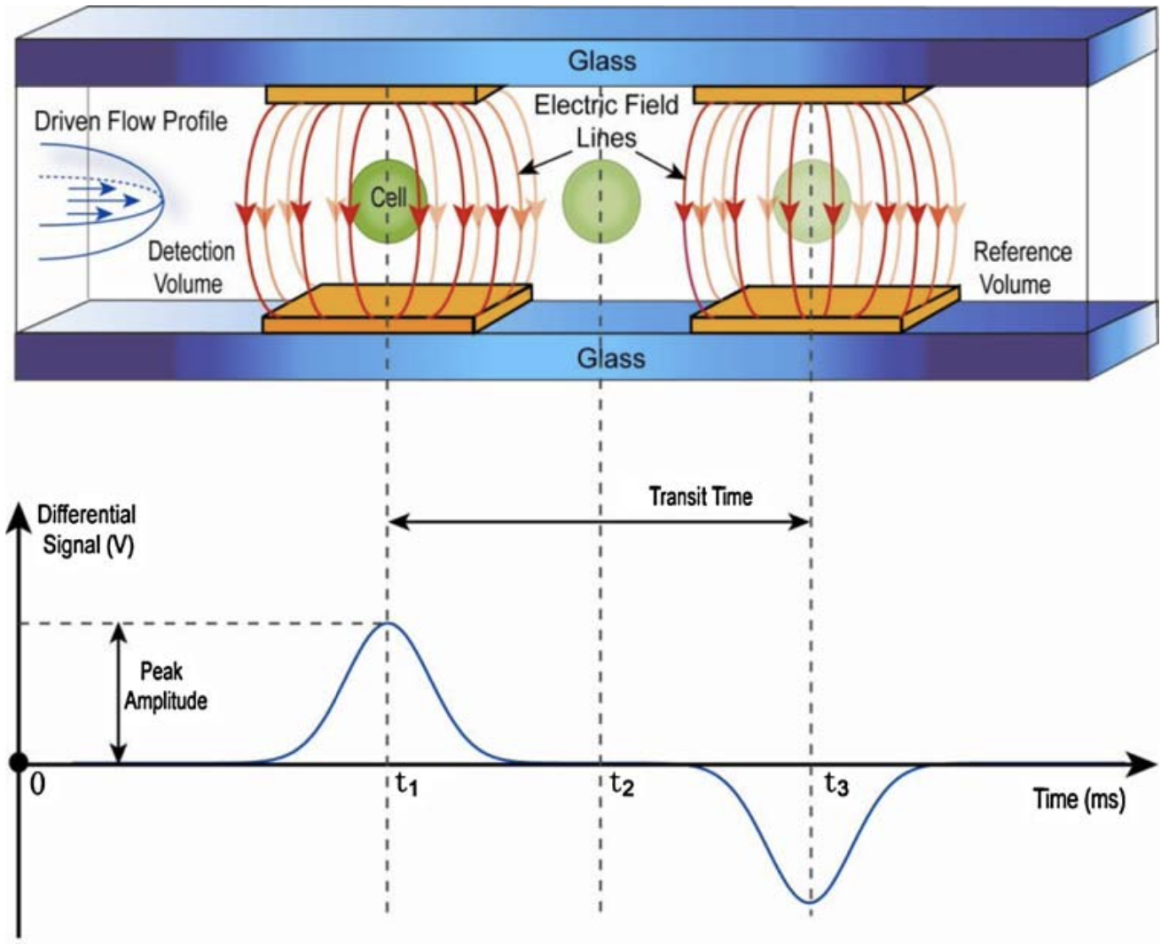

Figure 1.3. Elements of the basic structure and mechanism of microfluidic impedance cytometry including a microchannel, two electrode pairs, and the form of a typical impedance signature acquired by this technique (Sun et al. 2009).

An AC voltage is applied across the electrodes continuously at a single frequency (or pair of frequencies). The differential measurement of the impedance change as cells pass through the interrogation region (corresponding to the induced electric field) is collected. This frequency-dependent response of cell samples can then be correlated to important biophysical properties using similar considerations to those used for basic EIS.

1.5. Significance

The devices and methods described herein provide means for biological analyses on the basis of the direct relationship between cell biophysical characteristics and their electrochemical properties. First, a modular, reusable microfluidic device with an integrated interdigitated electrode array and a custom electrode connector unit is described. This device allows for the repeated use of microfluidic and microelectrode components. Additionally, the modular nature of this device provides an opportunity for integration of supplementary microfluidic control or cell analysis elements.

The determination of zebrafish sperm concentration is demonstrated with the device in low-conductivity media. Second, a microfluidic impedance cytometer with parallel vertical sidewall electrodes is used for single-cell discrimination of Jurkat cell viability status. A custom signal processing algorithm was developed to extract cell detection events from noisy baseline data using a correlation to the mathematical function that time series data is expected to fit according to the simulated electric field created by the device electrode design. Overall, each of these electrical analysis tools integrates microfluidic technologies to address challenges associated with conventional analysis tools by providing rapid, easy-to-use platforms for cell counting and viability analysis.

Chapter 2. Quantification of Zebrafish Sperm Cell Concentration by Impedance Spectroscopy on a Modular, Reusable Microfluidic Device

2.1. Abstract

Zebrafish (*danio rerio*) are an important model organism used for a wide variety of applications. Sperm cell concentration measurement and adjustment have been established as vital, but often neglected, steps for effective implementation of reproductive procedures and cryopreservation. To address the lack of standardization associated with conventional methods for cell counting, alternative options are being explored. In this study, electrochemical impedance spectroscopy (EIS) was applied on a modular microfluidic assembly with a reusable microelectrode connector unit for zebrafish sperm cell measurements. Cell detection was shown to be achievable in an isosmotic low-conductivity sucrose solution but less sensitive in typical Hanks' balanced salt solution used with these cells. Various concentrations of cells from 1E5 to 1E7 cells per mL in the sucrose solution were discriminated at a sensitivity of 9.7E-7 ± 4.5E-12 mS (cells per mL)$^{-1}$ based on a linear relationship between sample conductance and cell concentration. To evaluate a possible basis for conductive measurement of cell concentration, cells were maintained temporarily in the sucrose solution and removed, and the conditioned sucrose media was tested. The conductivities of this conditioned media correlated linearly with the cell concentrations at a sensitivity of 16.6E-7 ± 20.0E-12 mS (cells per mL)$^{-1}$. This suggested that zebrafish sperm cells change the properties of the media by increasing conductivity. Evaluation of cell samples by microscopy showed that cell membrane disruption occurred over time, likely causing intracellular ions to be released into the

sucrose solution and thus affecting its conductivity. Further evaluation is warranted to confirm the cause of and identify the time-dependence of the cell-lysis events. The use of a low-conductivity, buffered, and isosmotic solution should be further explored for impedance spectroscopy of intact zebrafish sperm cells.

2.2. Introduction

Zebrafish (*danio rerio*) have been established as an important model organism for developmental, genetic, and medical research (Westerfield 2000) due to a number of factors including similarities with human genomic structures and tractability and the optical clarity of their embryos and larvae (Lieschke and Currie 2007). To best protect and share thousands of developed zebrafish lines, proper handling of gametes is necessary (Lawrence 2007). Sperm concentration has been established as an important consideration for effective implementation of multiple processes (Jing et al. 2009); however, cell concentration is often not controlled for implementation of cryopreservation which often leads to inconsistent results and waste (Dong, Huang, and Tiersch 2007).

The traditional method for sperm sample concentration is manual counting by observation of cells by microscopy (Brito et al. 2016). In the case of zebrafish sperm which are smaller than blood cells for which hemocytometers are designed, the sample is constrained to a short focal plane on specialized platforms like the Makler® counting chamber and cells are counted on an individual basis (Torres et al. 2017). However, this method is laborious and time-consuming and canv produce errors in cell counts. Alternatively, automatic cell counting methods including flow cytometry (Yang, Daly, and Tiersch 2016) and microspectrophotometry (Tan, Yang, and Tiersch 2010) have been

demonstrated for zebrafish sperm cells. However, while these methods are well-established, each has challenges or limitations associated with its use. Generally, these methods detect cells at a low throughput, require complex and expensive equipment or software, and can involve binding with a labeling molecule that perturbs cells (Rollo et al. 2017). As a result, zebrafish repositories and laboratories that use sperm seek inexpensive, easy-to-use alternatives for standardized cell counting (Yang, Daly, and Tiersch 2016).

Electrochemical impedance spectroscopy (EIS) has been demonstrated to be an effective tool for the analysis of biological samples for a number of applications including cell detection and measurement of cell concentrations (Cheng et al. 2007, Jönsson et al. 2006, Kadan-Jamal et al. 2020). Variations of EIS devices exist, and key design features have been shown to affect performance, sensitivity, and accuracy, and usability. For instance, the majority of device designs include functional elements on electrode surfaces for cell or molecule recognition and immobilization. However, while this technique has advantages of specificity and positioning of analytes immediately adjacent to electrodes, electrodes containing adherent layers cannot easily be regenerated for reuse, thereby increasing their cost and complexity. Conversely, impedance spectroscopy of cells in liquid suspensions obviates the need for preparation and regeneration of recognition elements. As a result, there is opportunity for developing reusable EIS platforms, thereby reducing their cost. However, despite this potential, design features and operating conditions of devices that measure suspended cells must be optimized to achieve sufficient sensitivity for most applications.

The materials and design of the electrodes used to apply and sense electrical signals have been shown to influence sensitivity and signal-to-noise ratio in these systems

(Demircan Yalçın et al. 2019). Electrode designs integrated with microfluidic devices can be fabricated at macro- or micro-scales and are often implemented in parallel or coplanar orientations. Coplanar thin-film interdigitated electrode arrays (IDEAs) are often an effective design, combining the sensitivity of large electrode surface areas with high signal-to-noise ratio associated with designs on the scale of the cells being analyzed. Additionally, fabrication of this electrode geometry and its integration on microfluidic chips is easier to achieve than many other designs. However, one important drawback of this configuration results from the non-uniform electric field induced. That is, the shape of the electric field created between coplanar excitation and sensing electrodes varies with increasing distance from the electrode plane. As a result, variations in the vertical position of cells being analyzed can have an effect on the impedance observed (Daguerre et al. 2020).

The electrical properties of the cell buffer have been utilized with EIS tools to detect the presence of cells. For example, (Houssin et al. 2010) impedance spectra of samples of *C. parvum* oocysts in high-conductivity and low-conductivity solutions were compared, and cell detection was more reliable in the low conductivity buffer. During manipulation prior to evaluation of motility, zebrafish sperm cells are typically maintained in 300 mOsm/kg Hanks' balanced salt solution (HBSS), a high conductivity media, but have also shown viability in lower conductivity media such as sucrose solutions (Jing et al. 2009, Wilson-Leedy, Kanuga, and Ingermann 2009).

Lab-on-a-chip, or microfluidic, devices provide alternative solutions to challenges faced in larger-scale laboratory techniques, offering advantages such as low sample consumption, improved standardization, and greater sensitivity. As a result, integration

of electrical impedance spectroscopy on microfluidic devices (μEIS) provides a platform for the combination of the advantages of each technology. However, standard methods for the fabrication of microfluidic devices can prevent easy use and reuse, as most require the irreversible bonding of material layers to generate regions for fluid confinement. As a result, alternative methods for fabrication of modular, reversibly sealed microfluidic platforms should be considered to allow for repeated disassembly, cleaning, and reassembly. Modular device designs have been developed using a variety of methods (Anwar, T. Han, and Kim 2011, Temiz et al. 2015).

Mechanical clamping for chip assembly has been demonstrated whereby the application of pressure to elastic polydimethylsiloxane (PDMS) layers in contact with a rigid substrate provided a sufficient sealing force (Skafte-Pedersen et al. 2013, Dekker et al. 2018). Importantly, use of magnets for the application of a compressive force provided a method for easy device assembly (Rasponi et al. 2011). Traditionally, connection of thin-film microelectrodes to signal generation and analysis instrumentation is made by application of a permanent conductive adhesive. However, this approach is not amenable to repeated assembly and disassembly. As a result, in addition to the implementation of a modular fluidic assembly, a reversible mechanism for microelectrode connection should be considered.

In recent years, three-dimensional (3D) printing has gained popularity as a low-cost fabrication method for microfluidic device components (N. P. Macdonald et al. 2017, Gale et al. 2018, Waheed et al. 2016) as the increasing availability of low-cost printers continues to open access to new user groups. Microfabrication research groups are embracing consumer-grade printers to create channel features less than 50 μm in scale and chip build

times on the order of minutes (reviewed by Nielsen et al. 2020). Particularly attractive are the masked LCD stereolithography (MSLA) resin printers that with single-voxel resolution of 35 × 35 × 10 µm and costs of approximately 200 USD, make rapid prototyping of microfluidic chips possible (Zuchowicz et al).

In addition to the physical elements used for design and operation of a µEIS device, careful consideration must be given to the method for processing data and drawing conclusions relevant to the system under study. Due to the frequency-dependence of electrochemical systems including biological samples, impedance spectroscopy can reveal insights into biophysical properties and molecular phenomena. However, extraction of these characteristics from spectral data is challenging. To aid these efforts, data are often analyzed by fitting to analytical models such as equivalent circuit models (Barsoukov and J. R. Macdonald 2005). In some cases, these models have been applied such that the system is treated as a black box with no physical relevance, receiving criticism (Lasia 2014). As a result, an evaluation of the physical elements of a given system and consideration of common frequency-specific characteristics should be made.

For systems containing bare conductive metal electrodes (e.g., without any functional element or passivation layer) in an electrolyte solution at the micron scale, there are key characteristics of impedance spectra that are often observed in distinct frequency ranges (Lei 2014). At low frequencies (up to low kHz), the induced electric field causes ions in the electrolyte solution to polarize near the excitation electrode surface forming a capacitive double layer. In this range of frequencies, impedance spectra are typically dominated by the capacitance of that double layer and a resistance resulting from the movement of ions. At intermediate frequencies (kHz to low MHz), the ions that

formed the capacitive double layer disperse and the inherent resistance of the solution dominates. For samples containing biological cells, this solution resistance may contain contributions from cell membranes (typically resistive) and the electrical properties of the solution itself. Finally, at frequencies above 1 MHz, ion polarization results from the capacitive properties of the bulk solution. These frequency ranges can be discerned from one another by the observation of dielectric relaxation events in which rearrangement of ions within the solution cause changes in impedance values.

Sensitive cell detection and concentration measurement has been demonstrated using a unique application of impedance spectroscopy whereby conductivity changes in cell solutions resulting from ions released from lysed cells are measured. While yet to be documented for sperm cells, this approach has been demonstrated for cell detection and concentration measurements for various cell types including blood mononuclear cells (Cheng et al. 2007), synthetic liposomes (Damhorst et al. 2013), HIV cells (Demircan Yalçın et al. 2019), and parasitic bacteria (Houssin et al. 2010). Concentration measurement of lysed cells by impedance spectroscopy eliminates the need for maintenance and monitoring of cell viability over time. As a result, analysis of less stable cell types can be performed at any time.

The goal of this study was to develop a modular, low-cost, easy-to-use microfluidic platform for quantification of zebrafish sperm cell concentration by electrical impedance spectroscopy. Design features and tools implemented for device fabrication and data analysis were selected on the basis of providing accessible solutions to previously demonstrated barriers for concentration measurement. Specific objectives were to: 1) evaluate effects of cell vertical position on impedance signals using finite element

analysis; 2) design, implement, and evaluate a low-cost, modular microfluidic assembly unit for electrical analysis of cell suspensions; 3) design and integrate an easy-to-use instrumentation-to-electrode connector into the assembly unit; 4) measure the impedance spectra of known concentrations of zebrafish sperm cells in high-conductivity and low-conductivity solutions; and 5) demonstrate potential for concentration measurement on fixed frequency basis and generate a calibration curve at an appropriate frequency. A 3D-printed reversible assembly unit with magnetic clamping was used to identify a linear correlation between solution conductance and cell concentration resulting from the release of intracellular ions resulting from membrane lysis.

2.3. Materials and Methods

2.3.1. Microelectrodes

A custom interdigitated microelectrode array (IDEA) was designed using AutoCAD (Version Q.46.M.184, AutoDesk Inc., California) to produce a 6 mm x 11 mm rectangular array. The electrode fingers were designed on the basis that, to maximize the signal-to-noise ratio associated with any signal changes caused by cellular properties or phenomena at the cellular scale, the electrode dimensions should be as close to the size of the cells as possible. Because the head of zebrafish sperm cells (which is expected to contribute most prominently to impedance signals) is approximately 2 µm in diameter (Hagedorn et al. 2009), design features as close to this dimension as possible were targeted. Specifically, due to limitations in standard fabrication methods, the electrode fingers were designed to be 10 µm in width and spacing. The IDEA slides were fabricated by and purchased from the Guangdong Provincial Key Laboratory of Sensor Technology

and Biomedical Instrument (Sun Yat-Sen University, Guangzhou, China). The slides contained a 100-nm layer of gold on a 30-nm adhesive layer of titanium on approximately 0.25 mm thick quartz glass (Figure 2.1).

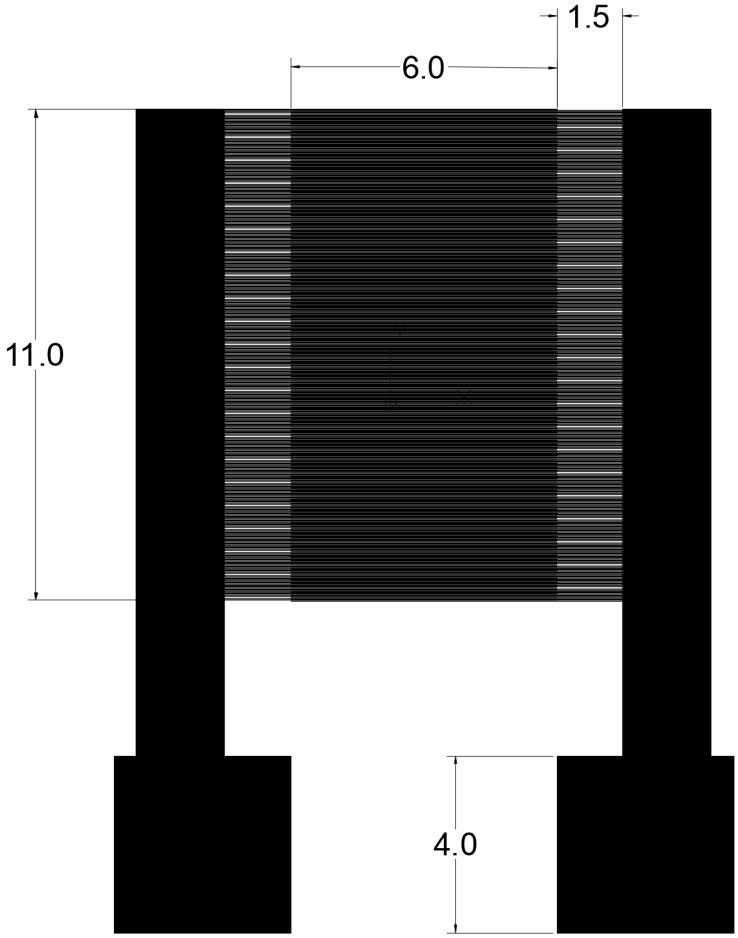

Figure 2.1. Design of the interdigitated electrode array used in this study. All dimensions are in mm. The electrode fingers were 10 µm wide with 10 µm gaps.

2.3.2. Finite element analysis

Finite element analysis was performed using the AC/DC module of Comsol (v5.3, COMSOL Inc., Stockholm, Sweden). Three-dimensional geometries consisting of a 90 µm x 90 µm chamber with a height of 50 µm were created. The chamber included two pairs of 10 µm-wide excitation and sensing electrodes with 10 µm spacing to replicate a small

region of the IDEAs used in this study. Two 2 µm-diameter spheres were created and placed at midlines between electrode pairs to simulate the presence of zebrafish sperm cell heads in the device interrogation region. A parametric sweep was conducted to vary the vertical position of the cells (concurrently) within the microfluidic chamber.

The solution was assigned a conductivity of 0.016 mS/cm and a relative permittivity of 134 to match the values collected for the sucrose formulation used in this study with cells at a concentration of 1E-5 cells/mL. The cell was approximated as an insulator with a conductivity of 1E-12 mS/cm and a relative permittivity of 6 to approximate the cell membrane. A 250-mV voltage was applied at a frequency of 10 kHz to each of the excitation electrodes, and the resulting system impedance was measured using the COMSOL ec.Z11 term.

2.3.3. Microfluidic Chamber

A microfluidic chamber was designed to position cells in the vicinity of the microelectrodes. This dimensions of the chamber were set such that samples would completely cover the interrogation region of the electrode array (where electrode fingers from opposite sources overlap) (Figure 2.1). The chamber was formed using a PDMS gasket. A 10:1 mixture of Sylgard 184 polydimethylsiloxane (PDMS, DOW Corning, Inc.) elastomer:curing agent was hand-mixed for 10 min. A 76 mm x 127 mm x 3 mm polymethylmethacrylate (PMMA) slide was placed on a spin coater chuck (WS-650-23B, Laurell Technologies, North Wales, PA). Approximately 3 mL of the PDMS mixture was poured on the poly(methyl methacrylate) (PMMA) slide, and the slide was spun at 500 rpm and 300 rpm/s for 10 s then at 2570 rpm and 300 rpm/s for 5 min to create a 10-µm

layer. The PDMS (on PMMA) was degassed at 600 mmHg vacuum and cured for 1.5 hr at 75^oC in an oven. A 8 mm x 13 mm rectangle was cut into the PDMS using a single pass cut with a 50-W CO_2 laser engraver (FLUX Beambox Pro, FLUX, Inc., Nangang Dist., Taipei), set to 25% current, 25% power, 100% speed. The PDMS inside of the rectangle was gently rubbed away to create an open chamber. For simple chamber loading, one 1.5 mm-diameter hole was engraved through the PMMA using eight passes of the laser engraver at 100% current, power, and speed.

The thickness of the PDMS, which governs the height of the microfluidic chamber, was evaluated using optical profilometry. The PDMS and exposed PMMA region were sputter-coated with platinum (Pt) for 8 min (K550X, Emitech Inc., Fall River, MA). The slide was profiled using an optical profiler (Wyko Hi Res, Bruker Nano, Inc., Tuscon, AZ) using a step size of 50 µm. The resultant altitude profiles were processed using MountainsMap (v8, Digital Surf, Besançon, France). The differential parameters tool was used to calculate the height between the PDMS layer and PMMA substrate. A total of 13 replicates were fabricated and evaluated by this method.

2.3.4. Modular Assembly

A housing unit was designed to generate a modular assembly integrating a microelectrode slide and microfluidic chamber layer capable of easy reassembly. The housing was drawn in Fusion 360 (Version 2.0.10148, AutoDesk Inc., California) as separate top and bottom pieces each with inset regions of dimensions corresponding to the PMMA slide and microelectrode slide. Empty rectangular regions were designed in each piece to allow for microscopic observation of the sample. Four square open regions were

also removed near the corners of each piece for magnets. Another set of rectangular open regions were added to the design to accommodate connection of the electrical analysis instrumentation to the microelectrode pads.

The housing unit design was fabricated using MSLA 3D-printing (Anycubic Photon S, Anycubic, Shenzhen, China) with black AnyCubic UV resin (AnyCubic, Shenzhen, China) followed by post-processing sonication in isopropol alcohol for 30 min. The housing unit applied a clamping force to the assembly sufficient to seal injected liquid into the microfluidic chamber using 1/4-in. rare earth magnets (Magcraft Advanced Materials, Vienna, VA) placed in the smaller open squares on the periphery. The thickness of the PDMS gasket chamber under compression in the housing unit was evaluated using the same optical profilometry method (and same number of replicates) described in the previous section.

A 3D rendering of the modular assembly (Figure 2.2) was created in Blender (Version 2.93, Blender Foundation).

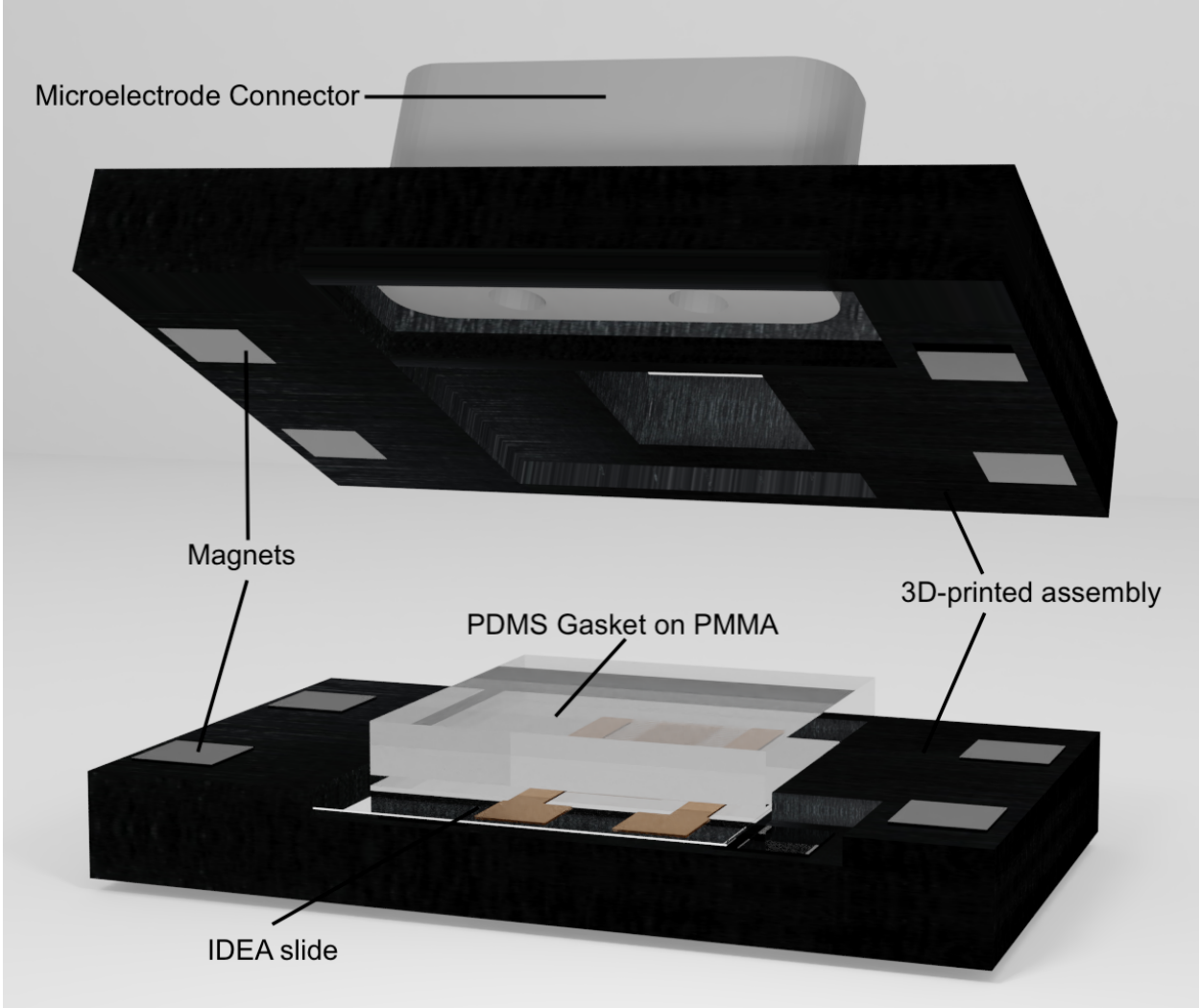

Figure 2.2. A three-dimensional rendering of the modular assembly including IDEA, microfluidic chamber (clear), and clamping magnets.

2.3.5. Microelectrode Connector

A reusable microelectrode connector unit was designed and fabricated to allow for reuse of IDEA slides. This unit consisted of two beryllium copper rolling spring-loaded (pogo) pin connectors (Mill-Max Mfg. Corp., Oyster Bay, NY) set into a standard 5-pin JST connector (Digi-Key Electronics, Thief River Falls, MN). A 5-pin connector was used to align the pin connects with the square pads on the microelectrode slides. A 3D-printed housing was fabricated to hold the JST connector and pins using the same printer and

resin described above. Open regions were included in the regions flanking the JST connector for the inclusion of magnets. Solid core wires were soldered onto the static ends of the pin connectors for connection to signal generation and analysis instrumentation.

For application of the connector to the microelectrode slide, magnets with polarity opposite to and spacing matching those in the connector unit were placed in the open region of the bottom piece of the modular assembly under and adjacent to the region occupied by the microelectrode pads. As a result, when the connector unit was brought in close contact with the pads, the magnets pulled the connector unit to the electrode slide creating strong contact. The rolling pogo pins allowed sufficient force to be applied for good electrical contact without scratching the gold on the electrode pad surfaces. Additionally, the dimensions of the open region of the 3D-printed modular assembly through which the microelectrode connector unit was applied restricted the degree of lateral translation, rotation, and tilting that could occur.

2.3.6. Cell Collection and Preparation

Practices for the use of animals in this study were reviewed and approved by the Louisiana State University Agricultural Center Institutional Animal Care and Use Committee. Zebrafish culture and sperm collection were performed as described previously (Beckham 2018). Zebrafish were obtained from the Zebrafish International Resource Center (Zebrafish International Resource Center, OR). Fish were maintained at target values of 28.5^{o}C, pH 8.5, and a 12-hr light:dark photoperiod. Additionally, water chemistry was monitored weekly; ammonia, nitrite, and nitrate levels were maintained below 1.0 mg/L, 0.8 mg/L, and 15 mg/L, respectively. Fish were fed a dry food mix (as

prescribed by ZIRC) every morning and Artemia (Brine Shrimp Direct, Ogden, Utah) every afternoon. To collect sperm cells, zebrafish were anesthetized using 0.01% MS-222 (tricaine methanesulfonate, Western Chemical, Inc. Ferndale, WA), placed ventral side up on a sponge, and collected by pipet Cells were diluted with HBSS at 297 mOsm/kg. Collected cells were counted on a Makler® chamber under phase-contrast microscopy. Various concentrations were prepared by serial dilution of collected samples.

Samples were centrifuged at 4^oC at 1000 rpm for 10 min. The supernatant was removed, and cells were resuspended in the appropriate buffer for each study including 297 mOsm HBSS/kg H_2O, 305 mM sucrose (305 mOsm sucrose/kg H_2O), and a 300 mOsm/kg H_2O Tris-HCl-buffered 305 mOsm/kg sucrose solution. These isosmotic solutions were used to prevent cells from becoming motile, as zebrafish sperm cells will activate when subjected to reduced osmolarity. Prior to testing, cells suspended in sucrose were observed by brightfield microscopy to ensure that they were not motile. To observe a range of concentrations relevant to cryopreservation processes commonly applied to zebrafish sperm, a range from approximately 1E5 to 1E8 cells/mL was tested. Additional experiments were performed to evaluate the potential for ion release into the sucrose media, where cells were maintained (following centrifugation and resuspension) for 20 min. The samples were centrifuged, and the supernatant solution was removed and tested by impedance spectroscopy. All samples were allowed to reach room temperature before testing. Buffer pH values were measured using a YSI Ecosense pH100a pH meter (YSI Incorporated, Yellow Springs, OH). Brightfield and phase-contrast microscopy was performed using a Nikon Ti-E microscope (Nikon Corporation, Tokyo, Japan). Using a

pipette, 20 µL of sample was deposited for each impedance measurement collected in the study.

2.3.7. Impedance Measurements

All samples were loaded into the microfluidic chamber using a standard mechanical micropipette (Gilson PIPETMAN L P20L, 2-20 µL, Gilson, Inc., Middleton, WI, USA). Impedance measurements were collected using an LCR Meter (E4980A, Agilent Technologies, Santa Clar, CA) at an applied voltage of 250 mV from 20 Hz to 2 MHz. The LCR meter was connected to a custom printed circuit board (PCB) that combined the high voltage and current and low voltage and current cables to create a two-probe measurement system. Male ends of breadboard jumper cables (Qwiic Cable, SparkFun Electronics, Niwot, CO) were soldered to the PCB while the female ends were used to connect to the wires on the custom microelectrode connector unit. The LCR Meter was controlled, and measured response signals were collected, using a custom Matlab script. A total of 3-5 replicates were collected for each measurement.

2.3.8. Data Analysis

Impedance data were validated using scripts implementing a previously reported (Murbach et al. 2020) Python-based impedance analysis package. The stability and linearity of all collected data were validated using a linear Kramers-Kronig test (Schönleber, Klotz, and Ivers-Tiffée 2014). Complete impedance spectra were displayed in the form of Bode plots to visualize the frequency-dependence of the system.

2.4. Results and Discussion

2.4.1. Effect of vertical positioning of cells on impedance

The effect of the height of the chamber (and location of the cells within the chamber) on impedance measurements was evaluated using finite element analysis simulations (Figure 2.3).

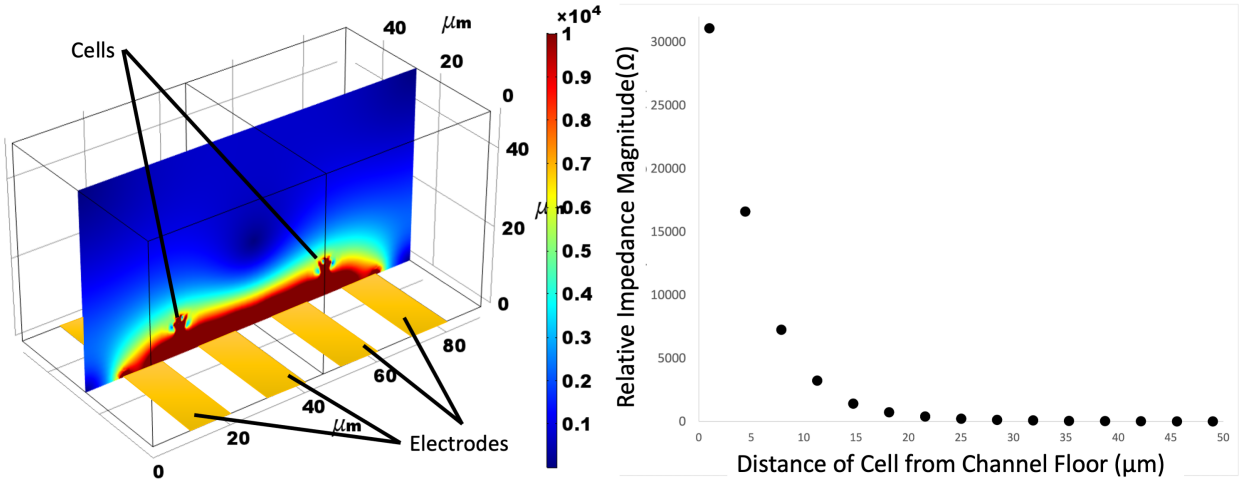

Figure 2.3. Finite element analysis of electric field strength throughout the height of a 50-μm-tall chamber (left) and theoretical relative impedance magnitude resulting from two cells at various distances from planar electrodes.

These results highlighted the importance of positioning cells near the interrogation electrodes in coplanar geometries. As the vertical position of the cell increased, the relative impedance magnitude measured by the electrodes decreased. With the electrode geometry used in this study and the conductivity of isosmotic sucrose with cells present, impedance measurements corresponding to cell heights (of the cell center) above some height may not be able to be distinguished from the impedance of the solution.

2.4.2. Microfluidic Chamber

The shallow microfluidic chamber was designed to minimize the variation in impedance measurements that can result from the electric field nonuniformity induced by coplanar electrode geometries. Optical profilometry was performed on the spun and laser-engraved PDMS on PMMA to evaluate the consistency of the PDMS gasket formation. Line scans were taken from various locations on the surface profile map across the laser-engraved chamber. To determine the actual height of the chamber during sample analysis, the procedure was performed on the PDMS/PMMA in the 3D-printed assembly. To compare the effects of the clamping force on the PDMS gasket chamber, the heights of PDMS gaskets in and out of the clamping setup were collected (Figure 2.4).

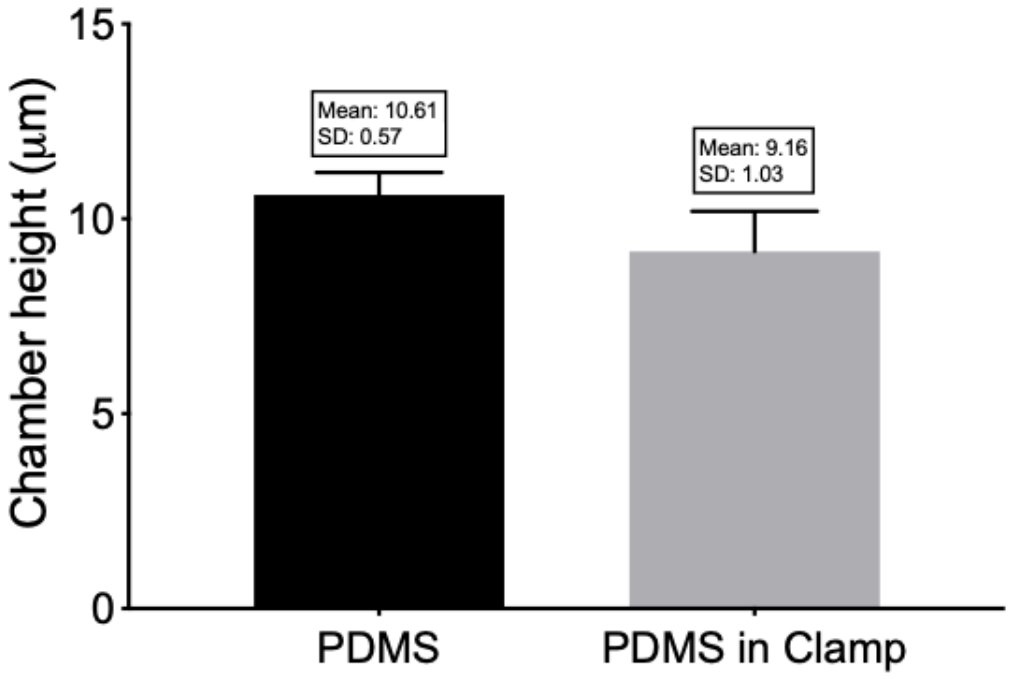

Figure 2.4. Heights of 13 replicates of PDMS gaskets outside (left) and inside (right) of the clamping assembly.

A student's t test was performed to determine whether the modular assembly compressed the PDMS. No statistical difference was found between the data corresponding to the PDMS gasket inside and outside of the assembly unit. As a result, while the compressive forces helped maintain a sufficient seal to keep fluid in the chamber, the PDMS gasket height was not significantly affected by the magnetic clamping force of the assembly.

2.4.3. Comparison of Zebrafish Sperm Cell Suspension Impedance Values in High- and Low- Conductivity Buffers

Prior to attempting to measure zebrafish sperm cell concentration, the efficacy of detecting cells in high-conductivity (HBSS) and low-conductivity (sucrose) solutions, was compared. In this case, cell samples near the minimum concentration of the target detectable range (i.e. approximately 1e5 cells/mL) were suspended in each of the buffers and tested (Figure 2.5).

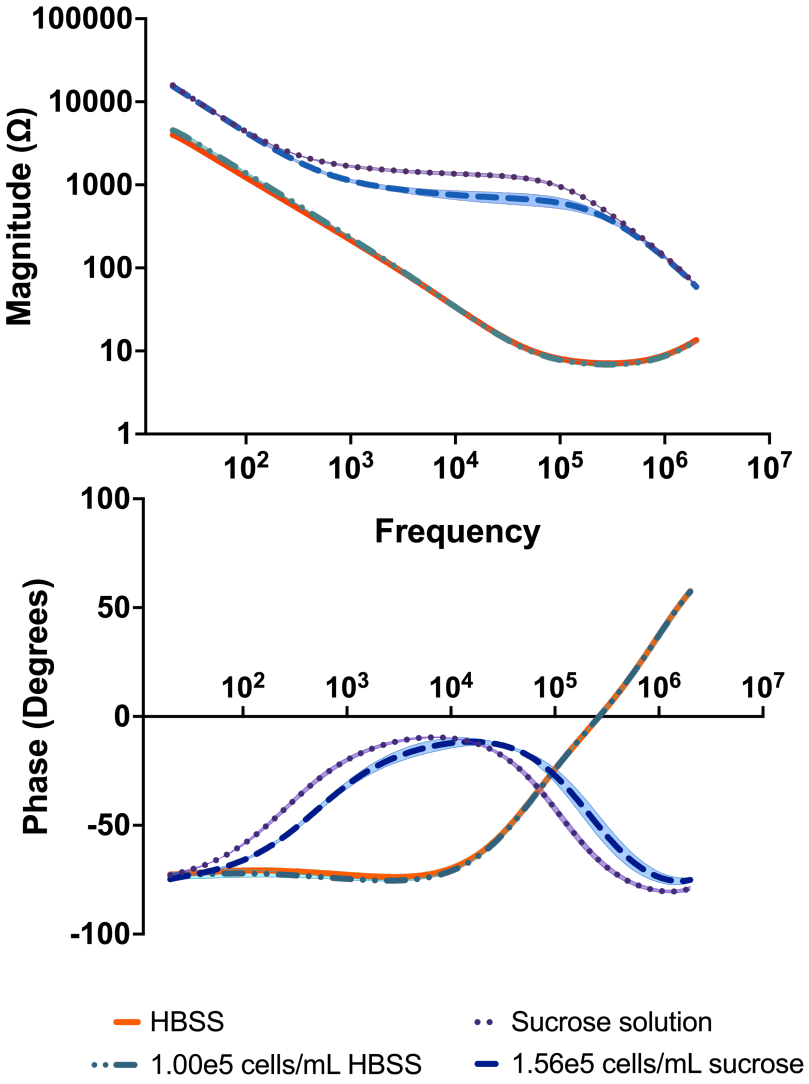

Figure 2.5. Bode plots (magnitude and phase) corresponding to zebrafish sperm cells in high-conductivity 297 mOsm/kg HBSS and low-conductivity (300 mM sucrose) isosmotic media. Shaded bands denote standard deviations of data (some error values are small enough that bands are not visible relative to line thicknesses).

As expected, due to the higher ion concentration and thus higher conductivity, samples containing HBSS had significantly lower impedance magnitudes than those in sucrose. This shows that there is little to no discernible difference in the impedance of samples containing different cell concentrations in HBSS, whereas samples containing different concentrations of cells suspended in sucrose created impedance spectra that

could be discriminated. Additionally, this highlights characteristics of impedance spectra of conductive solutions. The transition of the phase values from negative to positive at high frequencies can be attributed to inductive effects likely resulting from artifacts like wire inductance. The dielectric relaxation events (shown as sharp changes in impedance values) corresponding to the conductive samples appear to occur at significantly higher frequencies than those of the low-conductivity samples. In fact, as the leveling of the magnitude data only seems to occur when the inductive region is reached, no relaxation event appeared in the data corresponding to HBSS (and cells in HBSS) in the frequencies observed.

2.4.4. Zebrafish Sperm Cell Concentration Measurements

Upon suspension of cells in sucrose, samples were observed by brightfield microscopy to confirm the presence of intact, nonmotile sperm cells. To evaluate the efficacy of the approach presented in this study for zebrafish sperm cell concentration measurement, frequency sweeps of cells suspended in sucrose at various known concentrations were performed (Figure 2.6).

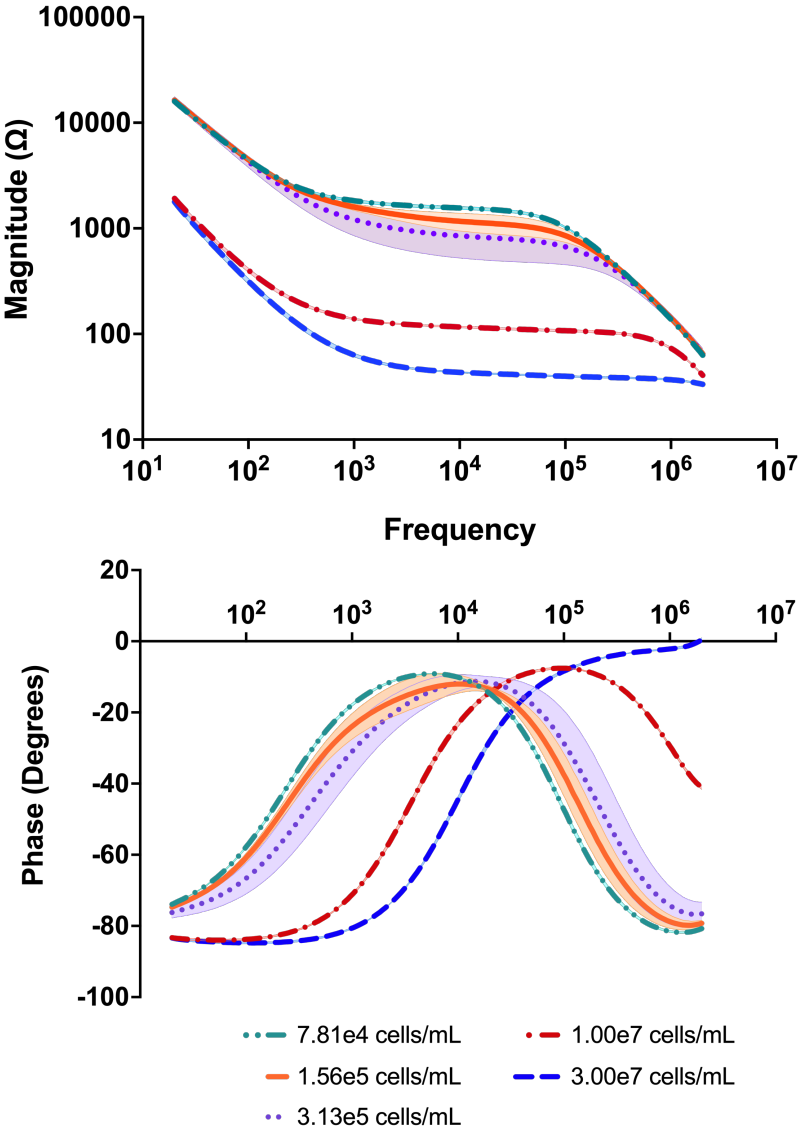

Figure 2.6. Bode plots (magnitude and phase) corresponding to various concentrations of zebrafish sperm cells in isosmotic sucrose solution.

The magnitude Bode plot shows that samples containing different concentrations of cells have impedance signals at different magnitude values that were inversely proportional to cell concentration. The most prominent differences in these magnitude values appeared in the frequency range between 1-100 kHz. The phase data showed that samples containing different cell concentrations underwent dielectric relaxation events

at different frequencies while the amplitude of the phase shifts did not appear different. The concurrence of these phenomena suggested that the most likely basis for effective concentration discrimination is differences in the resistances or conductances of the solutions. That is, increases in cell concentration appeared to correspond to an increase in sample conductance as the impedance magnitude and frequency of relaxation events were proportional and inversely proportional to cell concentration, respectively.

To establish a correlative relationship between cell concentration and measured impedance values, the solution conductance was calculated for each sample as the inverse of the overall system resistance at the frequency at which the minimum phase shifts (phase values near zero) occurred in data corresponding to each cell concentration. These points corresponded to the frequency region wherein little to no capacitance was detected, and measured impedance values were dominated by system resistance. Furthermore, because these events occurred in an intermediate frequency range (between 1 kHz and 1 MHz), measured resistance values could be expected to correlate to the solution conductance (as the inverse of measured resistances). However, because the near-zero phase region corresponding to a cell concentration of 1.00e8 cells/mL likely occurred at a frequency greater than the measurement interrogation frequency limit of 2 MHz, the concentrations used in the generation of the predictive relationship between sample conductance and cell concentration were limited to 3.00e7 cells/mL. Conductance terms as a function of cell concentration were evaluated and fit with a linear regression (with 95% confidence intervals) (Figure 2.7).

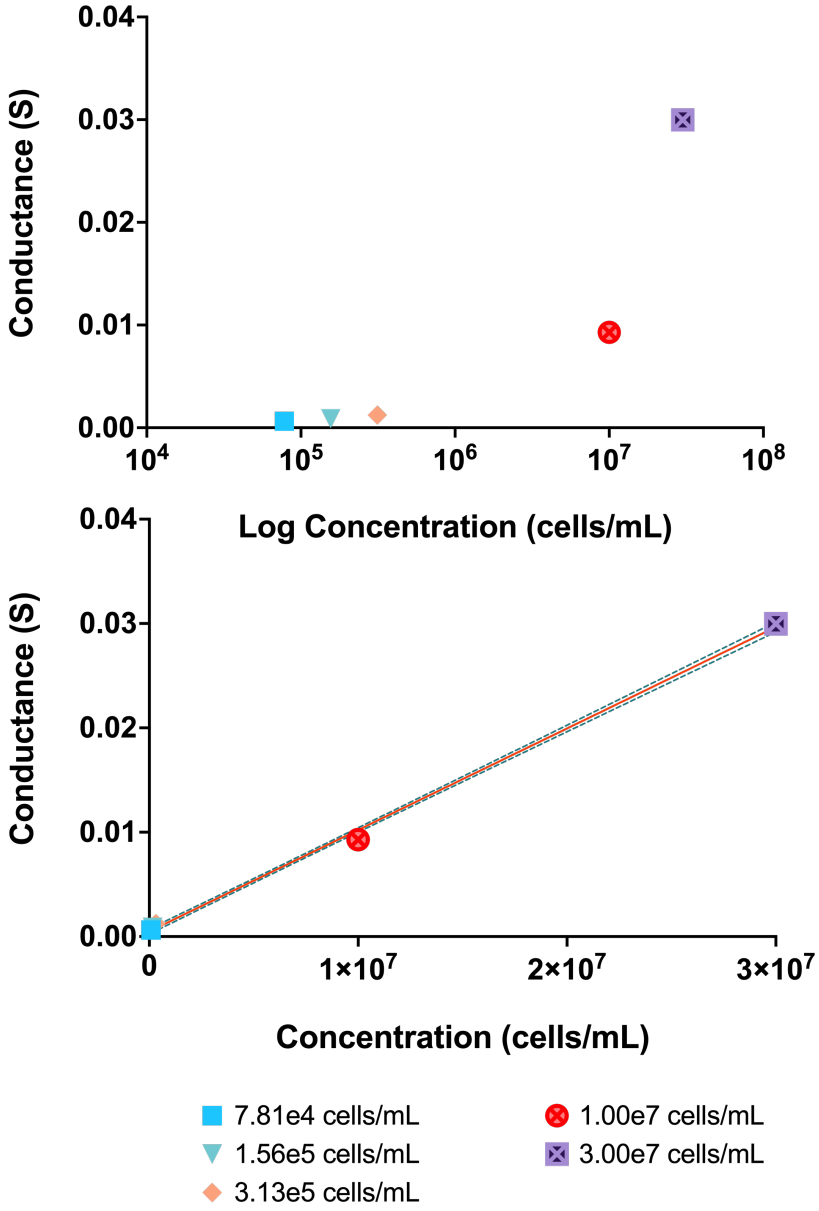

Figure 2.7. Sample conductance vs. log-scaled concentration (top) and linear-scaled concentration (bottom) from samples containing cells in 300 mM sucrose. In the plot on the bottom, a regression line with 95% confidence intervals is shown.

The resulting line of best fit had an R^2 value of 0.998 ± 5.37e-4. The slope of this line approximated the sensitivity of concentration measurements by this method as

9.73E-7 ± 4.51E-12 mS (cells per mL)$^{-1}$. This suggested a highly linear trend between sample conductance and cell concentration in the concentration range tested.

2.4.5. Evaluating the Basis of Concentration Discrimination

The relationship shown in Figure 2.6 suggested a prospective basis for use of the platform developed in this study as a concentration measurement tool. The proportionality between solution conductance and cell concentration in the intermediate frequency range was contrary to the trend that would be predicted by consideration of the high resistivity of cell membranes, which are often measured at those frequencies. However, in the event that cells released some of their ion content, whether by diffusion due to the existing ion concentration gradients or by disruption of cell membranes, the conductivity of the non-ionic sucrose solution would be expected to increase.

To explore whether ion release contributed as a basis by which cell concentration could be discriminated, samples containing various concentrations of cells were suspended in sucrose for 20 min centrifuged, and the supernatant was removed. The supernatant solutions were tested in the device (Figure 2.8).

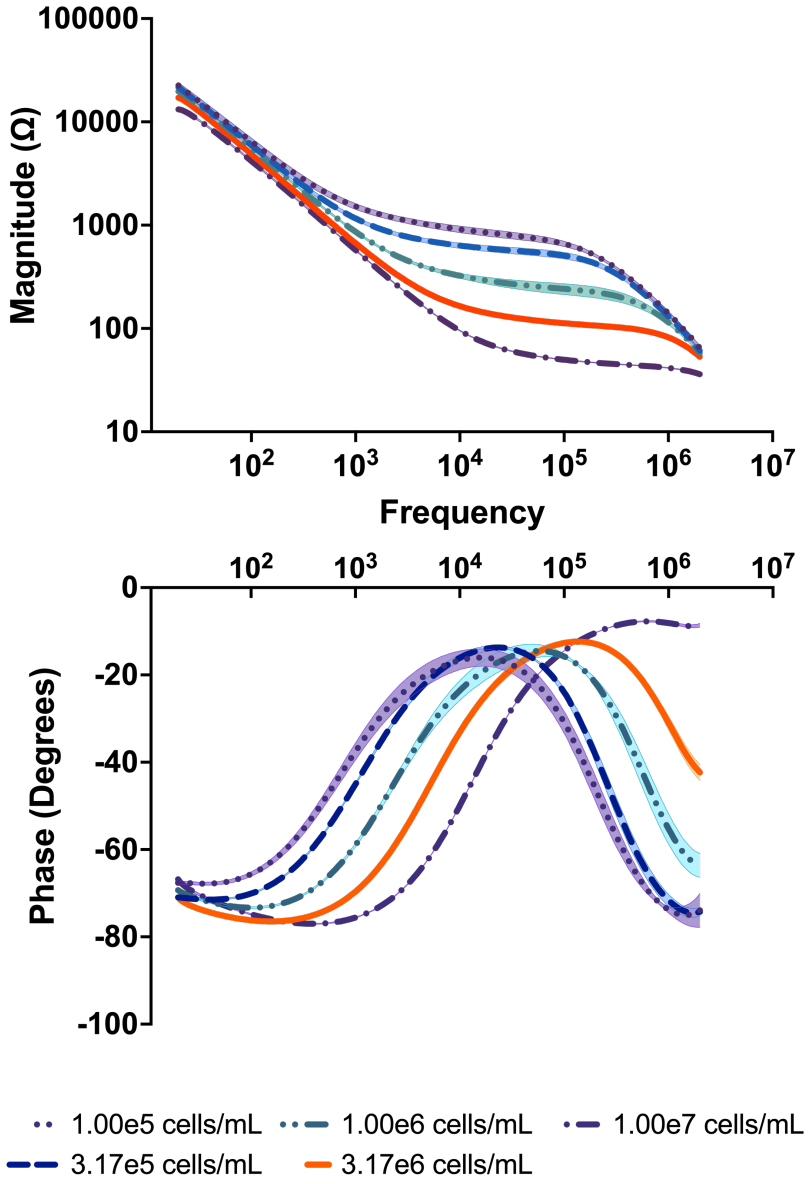

Figure 2.8. Bode plots (magnitude and phase) corresponding to conditioned sucrose media solutions conditioned by various cell concentrations.

These data followed a similar trend (Figure 2.9) to that observed in samples containing cells, which suggests that solution conductivities were modified by exposure to cells in a manner that is proportional to cell concentration.

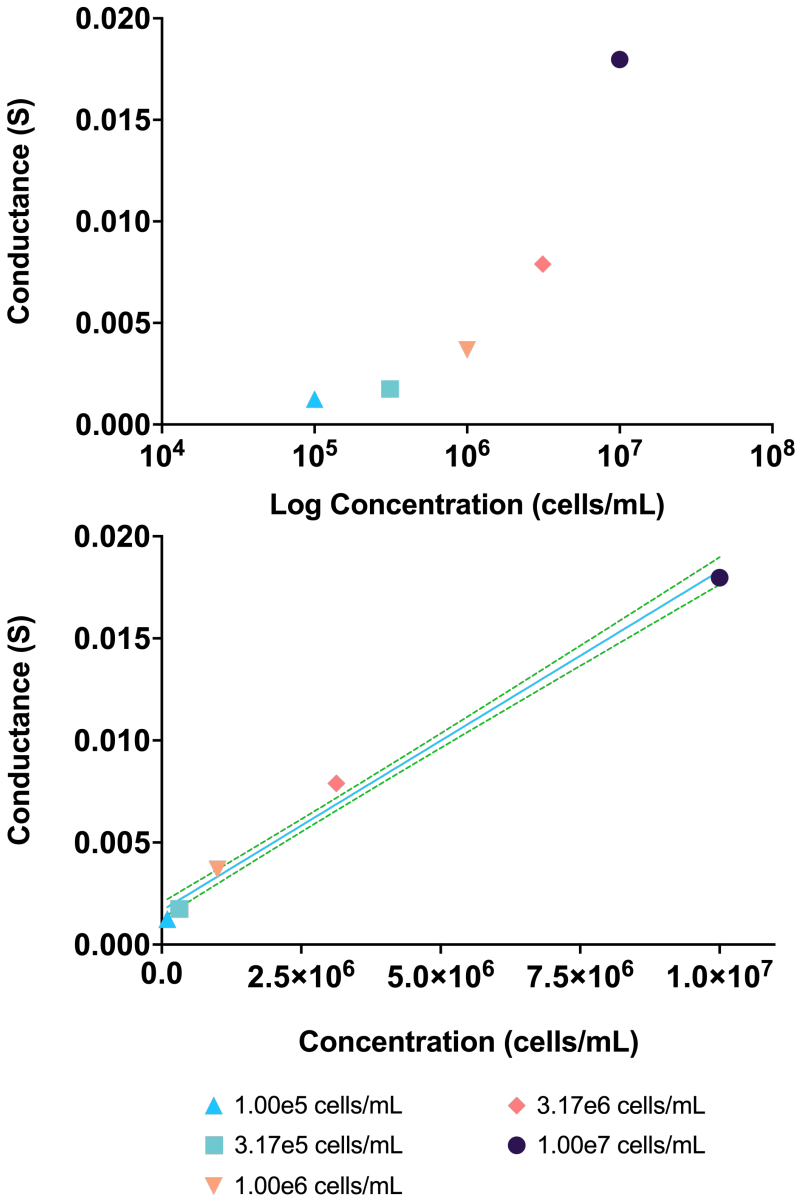

Figure 2.9. Sample conductance vs. log concentration (top) and concentration (bottom) corresponding to conditioned sucrose media after cells at various concentrations were removed. A regression line with 95% confidence intervals is shown.

The resulting line of best fit shows a comparable linearity to the relationship found for measurements conducted with cells present in solution with an R^2 value of 0.990 ± 6.61e-4. The sensitivity of this approach, as determined by the slope of the line of best fit, was found to be 16.64E-7 ± 19.97E-12 mS (cells per mL)$^{-1}$.

The lines of best fit from data collected with and without cells were compared (Figure 2.10).

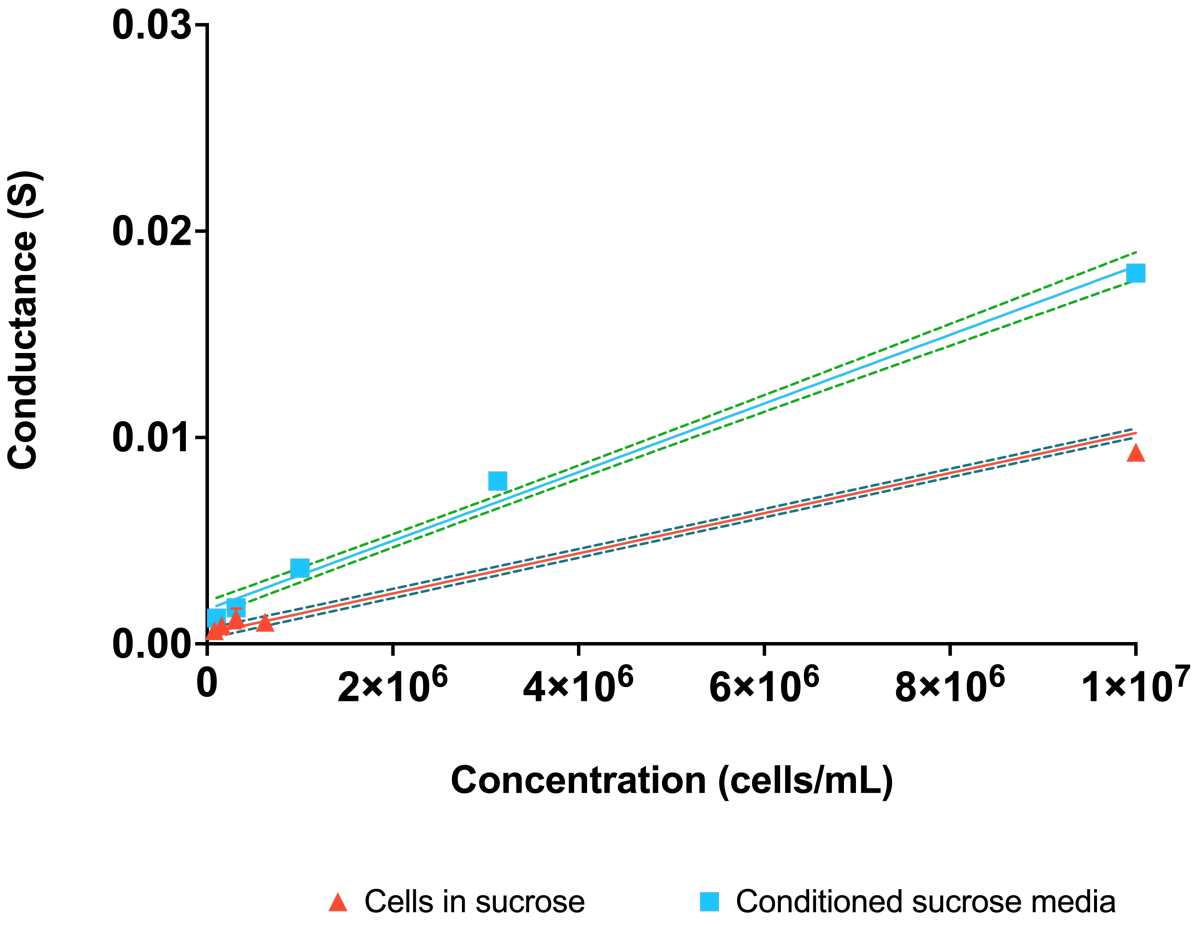

Figure 2.10. Comparison of sample conductance vs. concentration corresponding to samples consisting of cells in sucrose and conditioned sucrose media.

As illustrated above, each dataset showed linearity of conductance vs. concentration; however, the quality of the fit of the data from cells in sucrose was greater than that measured for conditioned sucrose media samples. Conversely, the higher slope of the line corresponding to the conditioned media samples suggested a greater sensitivity of measurements conducted under those conditions. Similarly, the conditioned media demonstrated a larger overall conductance than the samples containing cells. This

suggested that, in the intermediate frequency range, cells and debris may act as resistive elements to the applied electric field, dampening the increase in buffer conductivity, as reported by Cheng et al. Cheng et al. 2007 with T lymphocyte cells.

Comparison of the correlations between conductance and cell concentration of the cells in sucrose and the conditioned sucrose media (Table 2.1) demonstrated a stronger linear relationship than that found between absorbance and cell concentration during microspectrophotometry (Tan, Yang, and Tiersch 2010).

Table 2.1. Comparison of impedance data from cells in sucrose and conditioned sucrose media.

	Spectrophotometry	**EIS of Cells in Sucrose**	**EIS of Conditioned Sucrose Media**
Goodness-of-fit (R^2)	0.918	0.998	0.990
Sensitivity	2.5E-9 $(cells/mL)^{-1}$	9.7E-7 mS $(cells/mL)^{-1}$	16.6E-7 mS $(cells/mL)^{-1}$

To evaluate the stability of the sperm cells in the sucrose solution, time-series measurements were performed whereby fixed-frequency impedance data was collected for samples containing 1E5 and 1E7 cells/mL at the frequencies at which impedance phase was at its minimum. These measurements revealed that impedance values reached a steady state at approximately 12 minutes. Additionally, cells were observed by phase-contrast microscopy immediately and 20 minutes after suspension in the sucrose solution (Figure 2.11).

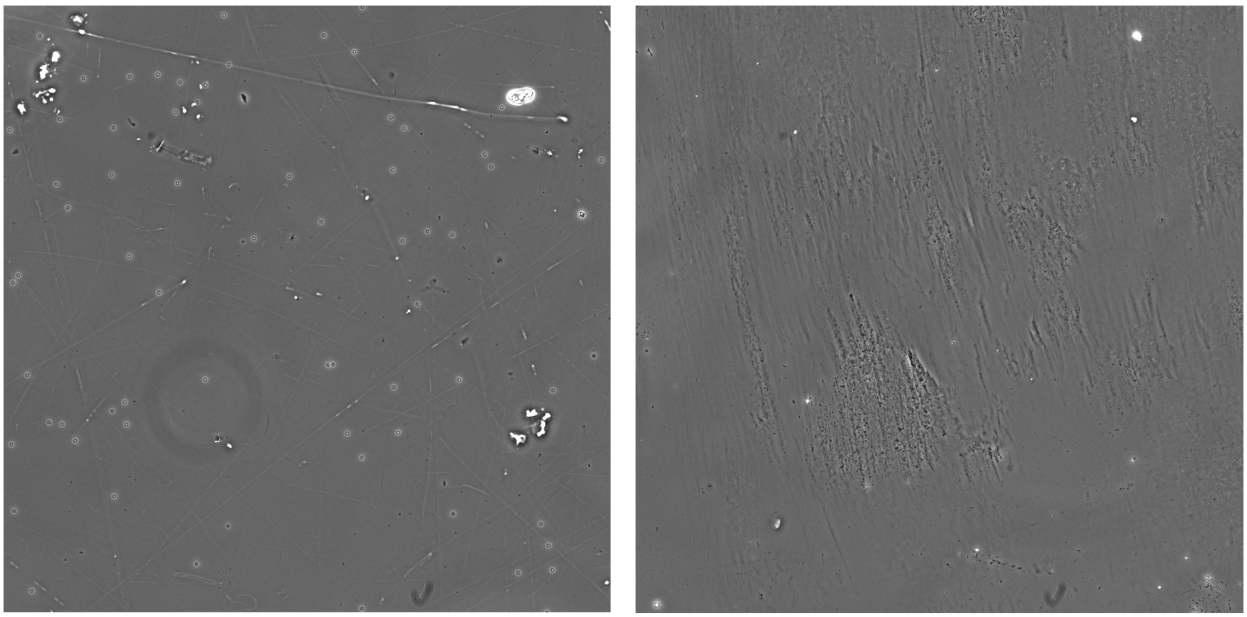

Figure 2.11. Phase-contrast microscopy images of sucrose solution shown immediately (left) and 20 minutes after (right) suspension of cells.

The number of intact cells that could be observed significantly decreased after the cells remained in the sucrose solution thereby indicating cell membrane disruption. This supported the conclusion that cell lysis occurred in the sucrose solution, increasing its conductivity.

To explore the cause of cell lysis in the non-buffered sucrose solution, the pH of the solution was measured and found to be approximately 5.6, consistent with values expected for deionized water in which carbon dioxide absorption has led to carbonic acid formation. Tris-HCl buffer (pH 9.5) was added to the acidic aqueous sucrose solution to create a Tris-sucrose buffered solution (TSBS) with a pH of 7.1. Cells were resuspended in this buffered solution for two hours and observed by phase-contrast microscopy (Figure 2.12).

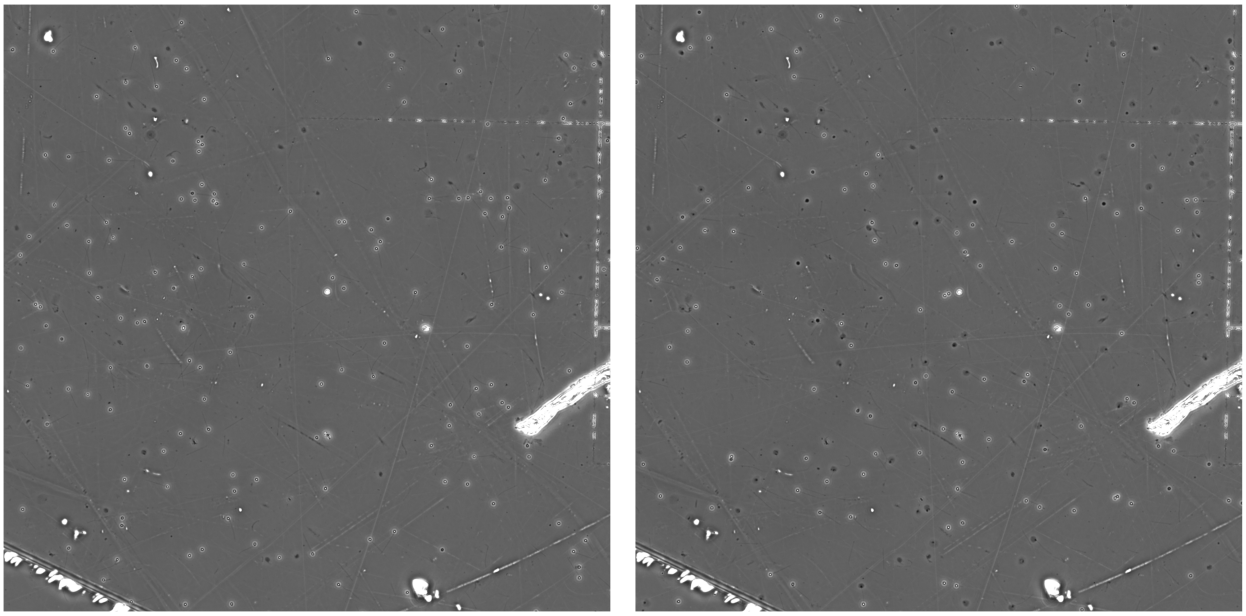

Figure 2.12. Phase-contrast microscopy images of Tris-HCl-buffered sucrose solution shown immediately (left) and 2 hours after (right) suspension of cells.

Cells appeared to be intact, suggesting that the TSBS solution would be more compatible with whole cell impedance measurements. Frequency sweep impedance spectroscopy data were collected for samples containing cells at concentrations between 1E5 and 1E7 cells/mL in TSBS (Figure 2.13).

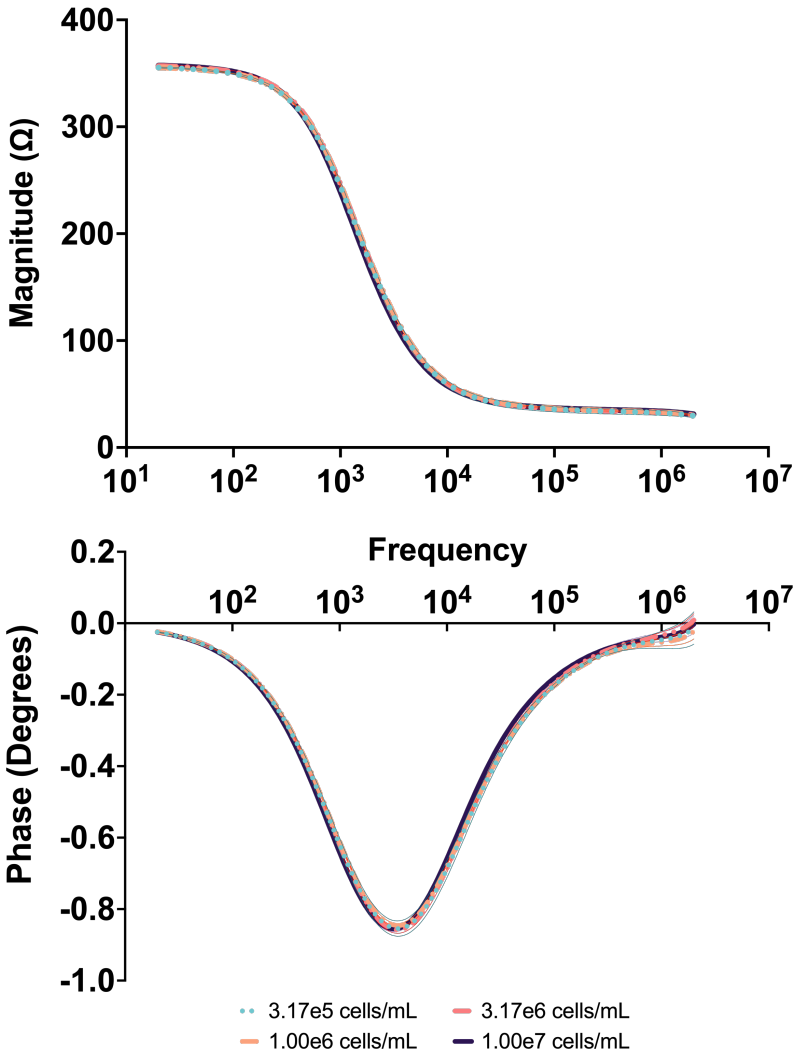

Figure 2.13. Bode plots (magnitude and phase) corresponding to cells in Tris-HCl-buffered sucrose solution.

No difference between the impedance signals corresponding to samples containing different concentrations of cells could be resolved up to 2 MHz. A single dielectric relaxation event could be observed at approximately 1 kHz. For Bode plots of this form, the solution resistance can typically be estimated as the maximum-frequency resistance value in the plateau that forms after the relaxation event. However, in this case, there was no significant difference between the measured resistance values for samples containing

different concentrations of cells. Typically, impedance measurements from electrolyte solutions containing biological cells reveal information about the cell membranes at frequencies above the second dielectric relaxation event. While frequencies greater than 2 MHz were not possible with the instrumentation used in these studies, further studies are warranted to interrogate intact cells in the buffered sucrose solution at higher frequencies to elucidate whether the contributions of the membranes of the cells in the solution can be detected and correlated to cell concentration.

2.5. Conclusions

Because the conventional methods for zebrafish sperm cell concentration measurement are labor-intensive and time-consuming, an easy and rapid tool is needed to support research and germplasm repository efforts. The incorporation of electrochemical impedance spectroscopy modalities on microfluidic chips provides an opportunity to overcome some of the challenges associated with conventional cell counting methods. The goal of this study was to develop a modular, reusable µEIS device whereby zebrafish sperm cell concentration could be measured at levels relevant to reproductive biology practices. A custom 3D-printed modular assembly unit with a pogo pin-enabled reversible connector was developed and utilized for impedance spectroscopy measurements of cell suspensions.

Cell detection was compared in an isosmotic (approximately 300 mOsm/kg) high-conductivity buffer (HBSS) and a low-conductivity solution (sucrose). Signals corresponding to samples containing cells in sucrose were able to be discriminated from the background media while signals from cells in HBSS could not be discriminated.

Various concentrations of cells in sucrose were assessed and a quantitative relationship between sample conductance and cell concentration was identified. To explore the basis for the observed trend of increasing sample conductance with increasing cell concentration, impedance spectra were collected corresponding to sucrose samples in which cells were stored (for 20 min) and removed. The relationship between sample conductance and the concentration of the conditioned sucrose media was found to have a larger measurement sensitivity and a larger overall conductance. This suggests that the cells modified the media likely by some conductive species, such as ion release by diffusion, while cells and debris acted as resistive elements in the intermediate frequency range, reducing the impact of the increase in conductivity. Because the cell-containing samples demonstrated a significantly greater goodness-of-fit by linear regression, there existed a trade-off in the selection of the most appropriate method for cell concentration measurement based on sensitivity or accuracy. Analyzing supernatant samples, wherein cells were held in sucrose solution and removed, may provide a greater sensitivity to differences in concentration, but interrogation of samples containing cells may provide greater measurement accuracy. The choice between these methods could depend on the application and the requirements for subsequent sample analysis, such as motility evaluation or cryopreservation.

To evaluate the mechanism by which cells conditioned the sucrose solution, cells were stored in isosmotic sucrose and observed by microscopy. Likely affected by the low pH of the aqueous sucrose solution, few intact cells were found while a significant amount of debris appeared to be present. This suggests that the increase in sucrose solution conductivity is a result of the release of intracellular ions while cells and cell debris provide some resistance at intermediate frequencies.

Cells were stored in the aqueous sucrose solution and observed by phase-contrast microscopy. After 20 minutes, very few cells could be observed, indicating the cell membranes have been disrupted. Additionally, time-series impedance measurements indicated that cells suspended in the acidic sucrose solution reached a steady state after 12 minutes. These observations suggest that cell lysis, and therefore the cause of sucrose media conditioning, is caused by the low pH of the non-buffered sucrose solution. Cells were also suspended in a Tris-HCl-buffered sucrose solution and observed by microscopy. In this case, after two hours, a large number of cells appeared to remain intact. However, impedance spectroscopy measurements of samples consisting of various concentrations of cells in the buffered solution did not show adequate sensitivity for reliable cell detection or concentration discrimination. This evidence supports the superior sensitivity of cell detection and concentration measurement of zebrafish sperm cells as observed by cell-lysate impedance spectroscopy measurements as observed in other cell types (Cheng et al. 2007). Selection of a suitable low-conductivity, buffered, isosmotic solution for impedance spectroscopy of zebrafish sperm cells is worthy of future exploration, as is additional studies on intact cells in the buffered sucrose solution at frequencies above 2 MHz to elucidate whether contributions of cell membranes to impedance measurements can be detected and correlated to cell concentration.

Chapter 3. A Simple Microfluidic Impedance Cytometer and Detection Algorithm for Cell Viability Analysis

3.1. Abstract

Microfluidic impedance cytometry has been demonstrated as an effective platform for single cell analysis, taking advantage of microfabricated features and dielectric cell sensing methods. In this study, we present a simple microfluidic device to improve sensitivity, accuracy, and throughput of single suspension cell viability analysis using vertical sidewall electrodes fabricated by a widely accessible negative manufacturing method. A microchannel milled through a 75 µm platinum wire created a pair of parallel vertical sidewall platinum electrodes. Jurkat cells were interrogated in a custom low-conductivity buffer (1.2 ± 0.04 mS/cm) to reduce current leakage and increase device sensitivity. Confirmed by live/dead staining and electron microscopy, a single optimum excitation frequency of 2 MHz was identified at which live and dead cells were discriminated based on the disruption in the cell membrane associated with cell death. At this frequency, live cells were found to exhibit changes in impedance phase with no appreciable change in magnitude, while dead cells displayed the opposite behavior. Correlated with video microscopy, a computational algorithm was created that is able to identify cell detection events and discriminate between live and dead cells by application of a mathematical correlation method.

3.2. Introduction

Elucidation of the heterogeneities inherent to all populations of biological cells has a significant impact on researchers' and clinicians' abilities to understand the mechanisms of and develop effective treatments for important diseases (Buettner et al. 2015, Suresh

2007). As a result, considerable effort has been directed to the development of tools capable of measuring cells' biophysical properties on a single cell basis at sufficient throughputs to gather population- level data. Traditional methods for single-cell property measurement analyze one cell or a small population of cells in batch conditions and are therefore unsuitable for this purpose (Heath, Ribas, and Mischel 2016). Flow cytometry offers a more rapid, high-throughput method for single-cell analysis, but conventional flow technologies, such as fluorescence-activated cell sorting (FACS), require extensive sample processing for conjugation of fluorescent labels with cells of interest prior to cytometric detection. Such label-dependent strategies are necessarily labor-intensive and invasive to cells and can render samples unsuitable for many subsequent uses (Seidl, Knuechel, and Kunz-Schughart 1999). Additionally, while optical flow cytometry techniques have been proven effective in probing biochemical properties, conventional methods are not well suited to analysis of cells' biophysical properties. Alternatively, analysis of cells on the basis of their dielectric properties is an inherently rapid, non-invasive, and label-free approach and provides the opportunity for direct correlation of measurements to relevant biophysical properties for electrical phenotyping. The advent of microfluidic technology has provided a means to overcome many of the challenges associated with single cell analysis by reducing the cost and complexity of integrated tools while increasing sensitivity and throughput (Murphy et al. 2018). In 2001, Gawad et al. (S. Gawad, Schild, and Ph. Renaud 2001) demonstrated a microfabricated impedance flow cytometer, which combined the advantages of microfluidic technology with the basic functionality of standard electrical analysis methods for continuous flow-through single-cell dielectric property measurements. The mechanism employed by this device fundamentally involved

passing cells through a microchannel flanked by a pair of electrodes, applying a voltage potential between the electrodes, and measuring the differential current change caused by the impedance of the cell and suspending buffer. By combining an understanding of the frequency dependence of the current response induced by biological cells with simplified electrical models of a cell, impedance measurements can be correlated to important biophysical characteristics including size and shape of the cell, properties of its membrane, conditions of intracellular structures, etc. However, while many efforts have necessarily been directed to the advancement of novel device designs and informational multiparametric (multifrequency) analysis, costs of many tools required for fabrication and operation of these devices may be prohibitive to some users. As a result, in addition to the development of greater analysis capabilities, implementation of widely accessible fabrication and measurement tools should be considered.

In any case, accurate and sensitive application of this technique relies on optimization of key features of the device design and operating conditions. There are two standard electrode configurations commonly utilized on microchips for impedance analysis of single cells: coplanar and top/bottom parallel geometries. Coplanar electrode geometries, in which electrodes are arranged on the same physical plane, are often used due to the relative simplicity of their fabrication. However, the electric field generated by these geometries is highly nonuniform, which leads to a significant positional dependence of measured impedance values on the height of the cell in the channel that cannot be easily resolved to generate accurate measurements. As a result, various methods have been devoted to the mitigation of this positional dependence including use of flow focusing techniques (Bernabini, Holmes, and Morgan 2011, Mernier, Duqi, and Philippe Renaud

2012, Tang et al. 2017), novel electrode configurations (Mernier, Duqi, and Philippe Renaud 2012, Solsona et al. 2019, Spencer and Morgan 2020, Wang, Sobahi, and A. Han 2017), and advanced signal processing methods (Caselli, De Ninno, et al. 2018). The reader is directed to the recent review of methods used to account for or reduce positional dependence by Daguerre et al. (Daguerre et al. 2020) However, in many cases, these methods require complex fluid manipulation strategies, result in reduced sensitivity, and/or perform measurements using more than two electrodes, which increases the risk of coincidence events in which impedance measurements are distorted by the presence of multiple cells within the detection region. Conversely, in parallel electrode geometries, the generated electric field is much more uniform, and the dependence of measurements on cell position is significantly reduced throughout most of the detection region. However, despite the advantages of electric field homogeneity offered by parallel electrodes, coplanar geometries are often favored as standard methods for fabrication of devices with top/bottom parallel electrode geometries in a microfluidic chip are complex (Cheung, Shady Gawad, and Philippe Renaud 2005) and require advanced alignment capabilities. Alternatively, vertical parallel sidewall electrode geometries have been shown to generate vertically homogeneous electric fields thereby mitigating the sensitivity of impedance measurements to cell height (Rollo et al. 2017). To date, the inclusion of vertical electrodes has not been widely adopted in the field of microfluidic impedance cytometry. However, advances in subtractive manufacturing techniques provide new opportunites for rapid, low-cost fabrication of microscale features with geometries that have otherwise been difficult to access. Properties of the cell-carrying buffer can also be optimized to maximize the contribution of cells to measured impedance values and thereby

maximize device sensitivity. Typically, 1x phosphate-buffered saline (PBS) is used as the cell-containing buffer for biologically relevant analytes; however, while this solution does effectively maintain physiologic osmolality and pH (thereby not affecting cell viability), its relatively high electrical conductivity can lead to a significant portion of the applied electric field bypassing cells. Constriction channels (Chen et al. 2011) and constraining sheath flows (Bernabini, Holmes, and Morgan 2011) have been implemented in attempts to mitigate this current leakage and increase sensitivity. However, these techniques risk channel clogging and require additional instrumentation for flow control, respectively. Use of reduced conductivity buffers consisting of diluted PBS (Clausen et al. 2018) and of a PBS-sucrose mixture (Ostermann et al. 2020) have been demonstrated previously for impedance flow cytometry.

The difficulty of achieving sufficient sensitivity of impedance flow cytometry is also reflected in the extensive efforts undertaken, as reviewed recently by Honrado et al. (Honrado et al. 2021), to effectively process impedance signatures and accurately identify cell detection events. These events can be isolated from raw signals amidst noise and baseline drift by correlation to a mathematical function that corresponds to the expected profile, which is dictated by device design parameters including electrode width and spacing, microchannel dimensions, buffer properties, interrogation frequency, and cell biophysical properties and location (Caselli, De Ninno, et al. 2018, De Ninno, Errico, et al. 2017, Sun et al. 2009). As a result, analytical or numerical analysis tools should be applied to identify the expected impedance profile for a given device design and to evaluate the effects of positional dependence on that profile (Daguerre et al. 2020). Microfluidic impedance cytometry has gained significant interest as a cell viability

detection tool that can be integrated directly with various other biological analysis tools (Luongo et al. 2013, Xu et al. 2016). The application of microfluidic impedance cytometry for viability analysis of T lymphocyte cells specifically has been tested previously by others (Palego et al. 2013, Schade-Kampmann et al. 2008), but each of these devices required the use of constriction channels or ancillary particle focusing or trapping tools that reduced their throughput and/or added complexity to their operation. Recently, De Ninno et al. (De Ninno, Reale, et al. 2020) showed the discrimination of live, necrotic, and apoptotic lymphoma cells interrogated at multiple frequencies in a continuous flow-through cytometer with coplanar electrodes.

Similarly, advancements in electrical measurement instrumentation has significantly reduced obstructions to use of electrical interrogation techniques. This study seeks to build upon the aforementioned works to develop a microfluidic impedance cytometer capable of Jurkat cell viability discrimination that is optimized for sensitivity and simplicity with the use of widely accessible fabrication techniques and operational instrumentation. The specific objectives of this study were to: 1) design and evaluate a microfluidic impedance cytometer with parallel vertical sidewall electrodes; 2) fabricate the device using a widely accessible manufacturing technique; 3) maximize device simplicity by demonstrating a microfluidic chip that does not require use of constriction channels, particle focusing, or other convoluting or limiting features; 4) optimize device configuration and operation conditions for sensitive viability testing by use of a custom cell buffer and optimum excitation frequency selection; 5) demonstrate reliable discrimination of live and dead cell status with high sensitivity using a custom signal

processing algorithm; and 6) compare optical imaging of cells to qualitatively validate theoretical basis of dielectric live/dead discrimination.

3.3. Materials and Methods

3.3.1. Simulations of Electrode Geometries

Computational simulations of parallel and coplanar electrode geometries were generated in the AC/DC module in COMSOL Multiphysics (COMSOL Inc., Stockholm, Sweden) by adapting the approach described by Cottet et al. (Cottet et al. 2019). This method involves the approximation of a single cell as an 11 µm diameter spherical region of the microchannel with electrical properties differing from those of the fluid in the channel and corresponding to estimated values expected to be exhibited by the cell of interest. Electrode geometry parameters were kept consistent for congruency. For both configurations, the electrode diameters and spacing were 76 µm and 50 µm, respectively. The microchannel height and width were 80 µm and 50 µm, respectively. Synthetic impedance signals consisting of 50 data points longitudinally at 20 discrete distances relative to the electrodes were taken for each geometry.

3.3.2. Microfluidic Chip Design and Fabrication of Polymer-Based Device

A microfluidic device comprised of a single microchannel in a poly(methyl methacrylate), PMMA, chip with a pair of vertical platinum (Pt) side-wall electrodes (Fig. 3.1a) was fabricated using methods adapted from Adams et al. (Adams et al. 2008). The microfabrication procedure involved micromilling (KERN MMP 522, KERN Micro- and Feinwerktechnik GmbH and Co.KG; Germany) holes in a 3.2 mm thick PMMA substrate (GoodFellow Corp). Pt wires (76 µm, Sigma Aldrich) were threaded into the

holes in the PMMA and hot-embossed at 160 oC for 4 minutes to embed the wire into the polymer. A single 50 um-wide microchannel was then milled through the PMMA and wire, orthogonally to the wire orientation, to create access for fluid samples to be passed directly between the two cut edges of the wire that comprise sidewall electrodes (Fig. 3.1c). PMMA was selected as the substrate due to its good machinability and ability to form structures, its minimal nonspecific binding of cells to the material surface, and its clear optical properties for visualizing cells in the microchannel detection region (for correlation to electrical signatures) (Adams et al. 2008).

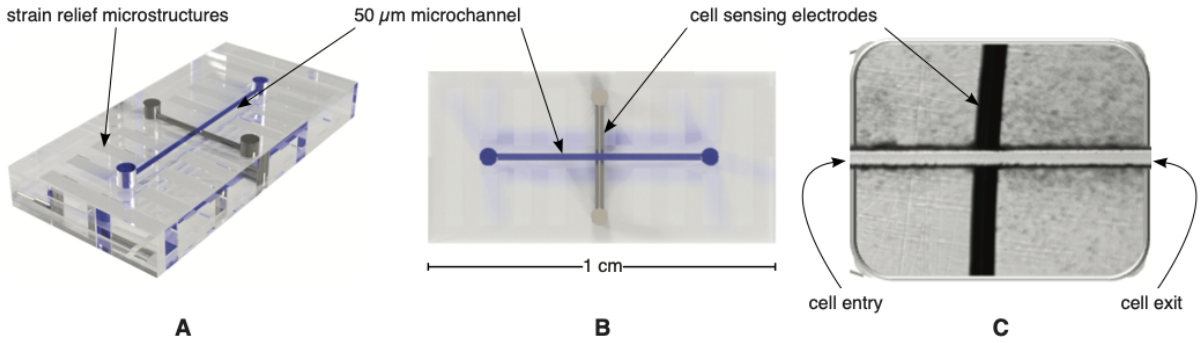

Figure 3.1. (A) Schematic of the cell viability PMMA chip, (B) simplified design of the single channel layout, and (C) integrated cell sensing electrodes consisting of cylindrical Pt electrodes 76 µm in diameter with a 50 µm spacing between the pair of electrodes.

3.3.3. Cell Culture and Buffer

As a model for human T-lymphocyte cells, Jurkat cells (E6.1, ATCC) were used in this study, maintained in 25 cm^2 flasks with 5 mL of classical RPMI-1640 culture media supplemented with 10% fetal bovine serum (FBS) and incubated at 37^{o}C in a humidified atmosphere containing 5% CO2. For the dead experimental control, Jurkat cells were incubated in a 12-well plate with 4 mM hydrogen peroxide in RPMI for 18 hr prior to analysis. Impedance experiments were carried out in a custom low-conductivity buffer

at physiological pH and approximately 300 mOsm unless otherwise stated. Air, dI water, TrisGly+Sucrose+BSA (Tris, Glycine, sucrose, and 1% BSA), and PBS were characterized by pH, osmolarity, and conductivity at room temperature prior to testing in the device. Cell buffer conductivity was measured at room temperature using an Omega #VDH-7X conductivity meter (Omega, Stamford, CT), and osmolality was measured using a Wescor #5520 osmometer (Wescor Inc., Logan, UT). Electrical impedance magnitude and phase data of these media were collected by list sweep measurements which were performed over the frequency range of 20 kHz to 2 MHz using the impedance analyzer described below.

3.3.4. Impedance Data Collection and Processing

NE-500 syringe pumps (New Era Pump Systems, Inc; Wantagh, NY) were controlled to provide pressure-driven flow in the microdevice. The syringe pump was programmed to generate a flow rate of 1 uL/hr, and the cell concentration was adjusted to approximately 1x105 cells mL-1 to obtain an optimum rate of cells passing between the excitation and sensing electrodes to be compatible with video microscopy. Electrical signals from the microdevice were acquired using an Agilent E4980A Precision LCR Meter (Agilent Technologies, Irvine, CA) at an operating voltage of 1 V and over a frequency range of 20 kHz to 2 MHz. The impedance analyzer was self-calibrated using short- and open- calibrations before samples were analyzed. For control sample impedance measurements, the measurement time was set to short scans taken at 1.0, 1.5, and 2.0 MHz. Impedance data acquisition was performed using a National Instruments VI with custom programming (National Instruments, Austin, TX). The impedance data were further processed by correlation to the appropriate mathematical function using a custom

digital signal processing algorithm developed in Matlab (The MathWorks, Inc., Natick, MA).

3.3.5. Video Microscopy

Brightfield and fluorescence video microscopy were used to visually confirm cell presence and viability during detection events in comparison to cell impedance detection events. Live and dead cell viability control treatments were conducted wherein Calcein AM was used as a fluorescent viability indicator. In the microdevice, fluorescent video microscopy stream acquisition was acquired at 3 frames per second (fps) to capture Calcein fluorescence with an exposure time of 250 ms. Images were captured with an inverted Eclipse TS100 Nikon fluorescence microscope using 10× and 20× objective lenses and a CoolSnapFX camera (Photometrics, Tucson, AZ). Time-lapse images were acquired to determine cell velocimetry (ranging from 25-75 um/sec). Image processing was performed on a Windows computer using MetaVue software (Universal Imaging Corporation, West Chester, PA).

3.4. Results and Discussion

3.4.1. Simulations of Vertical and Coplanar Electrode Geometries

A device employing a single pair of electrodes was used to minimize the complexity of fabrication, operation, and signal processing. This configuration also offers greater sensitivity implementing more than two electrodes as the volume of the induced electric field, and thus the interrogation region, is minimized thereby maximizing the volume fraction occupied by cells. Additionally, the minimization of the volume of the

interrogation region reduces the probability of a coincidence event in which multiple cells were interrogated simultaneously.

Finite element analysis has been proven to be a useful tool for the study of various electrode configurations and microfluidic geometries for impedance cytometry. A COMSOL model of the device reported herein including an 11 µm diameter spherical region with appropriate dielectric properties representing a Jurkat cell was generated to evaluate the efficacy of the Gaussian function for application of the correlation method. A second model with similar dimensions, yet coplanar electrode orientation, was evaluated to compare the vertical positional dependence between the two approaches. Figure 3.2 shows distributions of the electric field strengths and relative impedance signals resulting from translation of an insulating sphere through each of these geometries at varying heights (where cell heights and Z values refer to the vertical distance between the center of the cell) from the channel floor.

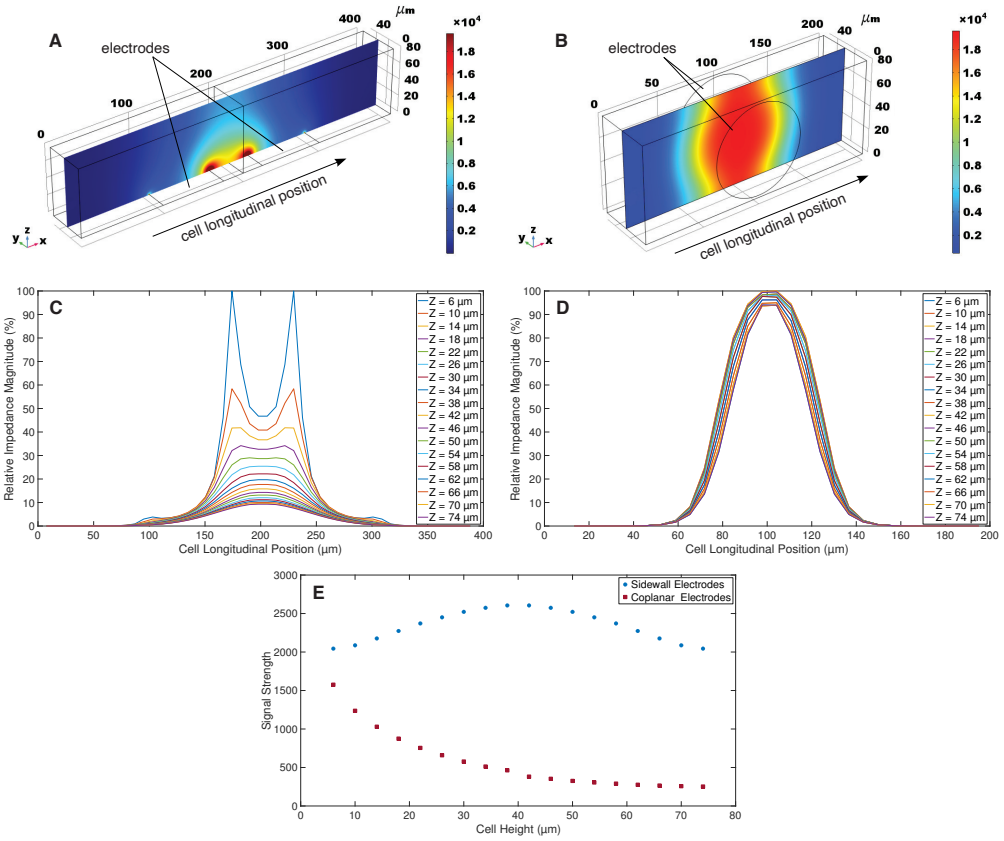

Figure 3.2. (A) Map of electric field strength through the microchannel centerline created by coplanar electrode geometry, (B) map of electric field strength through the microchannel centerline created by parallel electrode geometry, (C) relative impedance magnitude variation (%) of insulating sphere passing between coplanar electrodes, (D) relative impedance magnitude variation (%) of insulating sphere passing between parallel electrodes, and (E) areas under the curves corresponding to each impedance magnitude profile from both electrode geometries. Each plot line corresponds to a pathway through the channel at the longitudinal centerline at various heights ranging from the top to the bottom of the microchannel. Cell heights and Z values refer to positions of the center of the insulating sphere.

In microfluidic impedance cytometers utilizing coplanar electrodes, the nonuniformity of the electric field can create significant current leakage and reduced sensitivity. Conversely, as illustrated by the electric field maps (Fig. 3.2a,b), the strength of the electric field from the parallel sidewall electrodes is maintained through the height of the channel. This phenomenon, which is also reflected by the larger relative

amplitudes of the weakest impedance signal created by a cell passing between the sidewall electrodes compared to the weakest signal created by the coplanar electrodes (Fig. 3.2c,d), demonstrates the improved sensitivity achieved by the vertical parallel configuration.

To compare the vertical positional dependences of impedance signals generated by the two electrode configurations independent of any curve fitting, the strengths of the impedance magnitude signals were measured in terms of the area under the curves (similarly to the root mean square analyses commonly performed on power spectral density data). For congruency, these area values (Fig. 3.2e) were calculated based on the relative impedance magnitude variations and normalized cell longitudinal positions. The difference in these areas between the strongest and weakest signals from each of the parallel and coplanar electrode configurations were 21.5% and 83.7%, respectively. This demonstrates that the uniformity in the electric field created by the sidewall electrode geometry leads to more reliable and accurate measurement capability. Additionally, the inconsistency in the shape of the impedance profiles that occur at different heights in the channel between coplanar electrodes are not suitable for signal processing methods that rely on the correlation method; as a result, processing signals obtained by devices using this configuration can be a significant obstacle.

The quality of the fit of the expected impedance signals at various heights to a Gaussian function was also evaluated using goodness of fit (R2) values. For the electrode and microchannel geometry used in this study, the R2 values for pure magnitude profiles was 0.993 ± 0.004. This suggests that the single pulse Gaussian profile is an appropriate template function for extraction of cell detection events from raw impedance signals. As a result, this function was used for the signal processing algorithms employed in this study.

To evaluate the effect of noise on the quality of the fit, artificial noise was added to the impedance profiles using a periodic function and random number generator in Matlab at an amplitude that corresponded to the noise observed from the measurement system used in this study (raw data shown below in Fig. 3.3). The resulting average goodness of fit value with the added noise was 0.821 ± 0.094.

3.4.2. Cell Buffer

Important parameters of the cell media such as osmolarity, pH, and conductivity must be optimized to maintain eukaryotic cell viability and compatibility with the impedance measurement system. Optimal cell buffer properties include physiological osmolarity (300 mOsm for cell water balance) and physiological pH (7.4). To maximize device sensitivity, it is advantageous to choose a buffer that maximizes the interactions of cells with the electrical energy applied via electrodes. That is, the media should not be so conductive that the energy preferentially bypasses the cells. Often supplemented with sucrose (8.5% w/v) and dextrose (0.3% w/v), phosphate-buffered saline (PBS) is commonly used as the base for the suspending cell media (Cheng et al. 2007; Cheung, Shady Gawad, and Philippe Renaud 2005). To optimize the conditions described above, a custom 25 mM Tris, 192 mM Glycine, 83 mM Sucrose, and 1% BSA low-conductivity cell buffer was developed. As shown in Table 1, the characteristic complex impedances of various cell buffers in the microchip device were evaluated to determine the optimum conditions for maintaining and measuring cell viability.

Table 3.1. Optimization of cell buffers for cell viability maintenance (low conductivity, physiological pH, and osmolality) and compatibility with impedance detection.

Cell Buffer Solution	**Conductivity**	**Osmolality**	**pH**
	mS/cm	**mM/kg**	
di Water	0.002 ± 0.04	0	6.4
25mM Tris, 192mM Glycine	0.35 ± 0.04	180	8.3
25mM Tris, 192mM Glycine+83mM Sucrose+1% BSA	1.2 ± 0.04	292	7.6
0.1x PBS	1.2 ± 0.04	56	7.4
1x PBS	9.3 ± 0.04	300	74

3.4.3. Identification of Optimum Frequency

In a previous report of a flow-through application of microfluidic impedance measurement of T lymphocyte cell viability, cells were interrogated at 0.5 and 10 MHz. While multifrequency analyses using low and high frequencies simultaneously can uncover useful information about more subtle cellular properties, multiple sensing electrodes are generally required, as well as more expensive instrumentation than utilized here. One goal of this study was to identify a single frequency at which the impedance signatures of live and dead cells could be easily detected and discriminated on a continuous basis. Impedance measurements for live and dead cell control samples at several frequencies were collected independently and analyzed. Frequencies at the lower end of the intermediate frequency range (described above) up to the highest achievable frequency by the Agilent LCR Meter (2 MHz) were chosen in an attempt to capture both the resistive and

capacitive behaviors of interrogated cells. Impedance magnitude and phase signals were collected for live and dead cell control samples at frequencies of 1.0, 1.5, and 2.0 MHz as shown in Fig. 3.3.

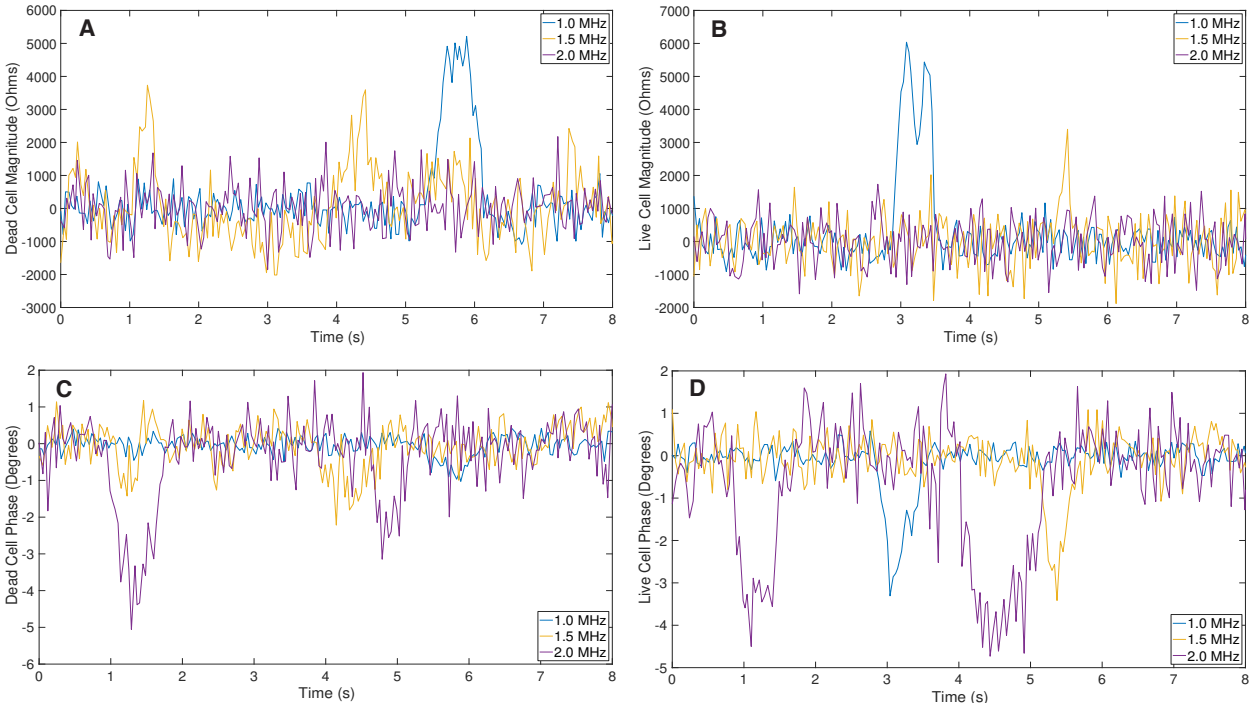

Figure 3.3. Relative changes in impedance magnitude of dead (A) and live (B) cells at 1, 1.5 and 2 MHz interrogation frequencies. Relative impedance phase changes of dead (C) and live (D) cells.

As illustrated above, raw output signals often have baseline drift and high levels of noise that can make extracting useful information challenging. As a result, although the data samples shown above were chosen on the basis of their clarity for illustration, quantitative and reliable identification of cell detection events is often difficult to achieve reliably. A few methods have been demonsrated previously for digital impedance signal processing including Savitzky-Golay smoothing (Evander et al. 2013) and the correlation method (Caselli and Bisegna 2016). Savitzky-Golay smoothing, a widely used alternative to moving average filtering for noise reduction in some fields (e.g., analytical chemistry),

applies a low pass polynomial filter by mathematical convolution and is dependent on an input order and frame length of the applied filter.

When compared with video microscopy, live single-cell events were observed to correlate with a measured change in the impedance phase signal, while dead single cell events displayed a change in the impedance magnitude at all frequencies tested. Importantly, at 2 MHz, live and dead cells displayed those expected dielectric responses without displaying the converse behaviors. That is, at this frequency, interrogation of live single cells created changes in the measured impedance phase without any appreciable change in magnitude while dead cells induced impedance magnitude changes without any significant phase change. Compared to previously reported devices for viability testing of T lymphocyte cells, the selection and application of an electric field at an optimum frequency allows for interrogation of cells at a single frequency thereby removing the need for more complex equipment capable of multifrequency analyses.

In low MHz ranges, alternating currents can induce polarization of membrane ions in live cells leading to membrane capacitance, which is proportional to the amplitude of changes in impedance phase. Because the membrane is disrupted upon cell death, the ion polarization events that lead to capacitance do not occur. Instead, the electric current interacts only with resistive elements of the cell. As a result, combining consideration of the effects of the frequency of the applied electric current on the nature of its interaction with the cell being analyzed and the effects of cell death on cell biophysical characteristics leads to the conclusion that live and dead cells of the same type can exhibit entirely different impedimetric behaviors at a single frequency. Therefore, at an optimum frequency (in this case, 2 MHz), live cells can be discriminated simply by observing

relative changes in the impedance phase with no change in magnitude, while dead cells show relative changes in impedance magnitude with no change in phase.

3.4.4. Live and Dead Control Sample Interrogation at 2 MHz

Once the frequency appropriate for cell status discrimination was determined, live and dead cell control samples were tested at an excitation frequency of 2 MHz, and observations were validated by comparison to fluorescence microscopy. Figure 3.4 shows the processed, detrended data corresponding to raw data shown in Fig. 3.3 plotted against the complete output of the signal detection algorithm.

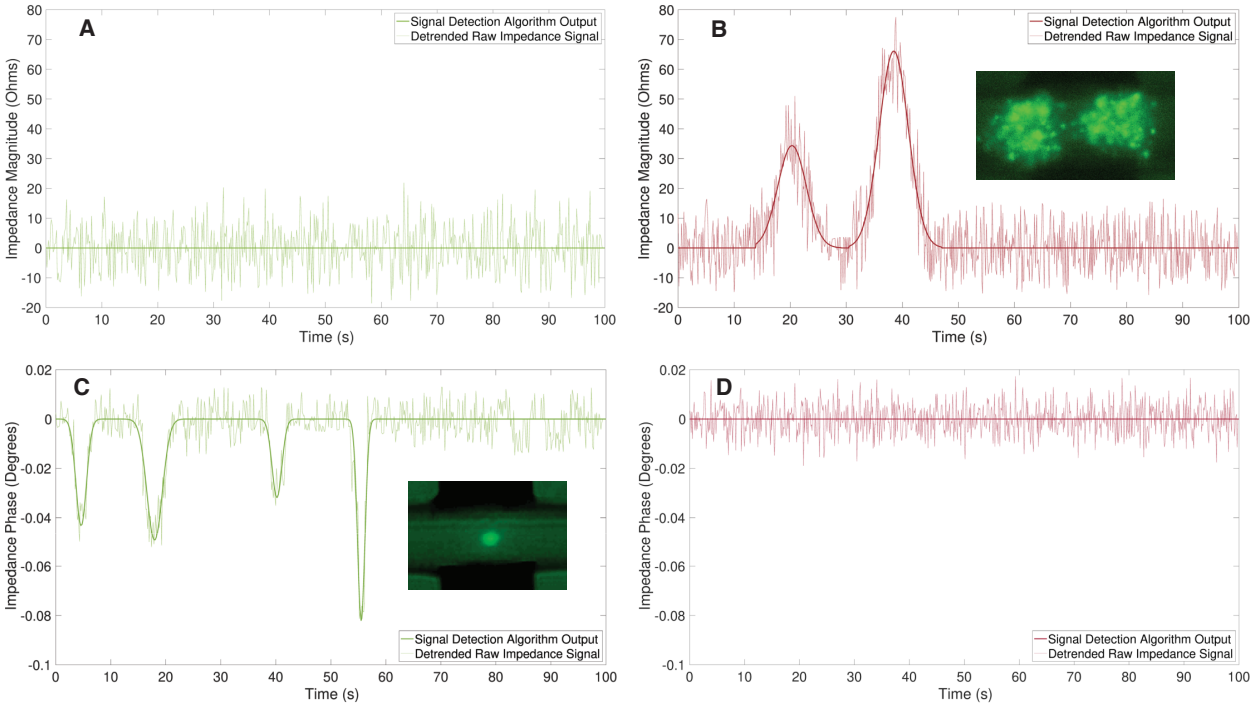

Figure 3.4. Signal detection algorithm output plotted against detrended noisy impedance output profiles corresponding to A) impedance magnitude of live cells, B) impedance magnitude of dead cells, C) impedance phase of live cells, and D) impedance phase of dead cells.

At 2 MHz, live and dead cells can easily be discriminated by identifying cell detection events in impedance magnitude and phase profiles. Live cells clearly display

impedance phase changes with no discernable impedance magnitude change whereas dead cells display impedance magnitude changes with no evident changes in impedance phase. Additionally, the signal detection algorithm is able to effectively process raw data to eliminate baseline drift and identify cell detection events without reducing the amplitude of signal peaks despite significant noise. Based on the combination of the hardware microfluidic chip geometry utilized, an estimated maximum throughput for detection of Jurkat cell viability is 1800 cells per minute. To illustrate the limitations of commonly used smoothing techniques, the results of moving average and Savitzky-Golay processing methods were applied to characteristic signals collected during this study. Moving average filters were applied with window sizes of 5 and 50 to explore the effects of small and large window sizes, respectively, while three combinations of orders and frame lengths for Savitzky-Golay filtering were applied to illustrate their effects. As shown in Fig. 3.5, moving average filters that incorporate too few data point do not adequately smooth noisy data. Conversely, as the window size is increased, the amplitudes of signal peaks are dampened. This leads to reduced sensitivity and an increased chance of missed cell detection events.

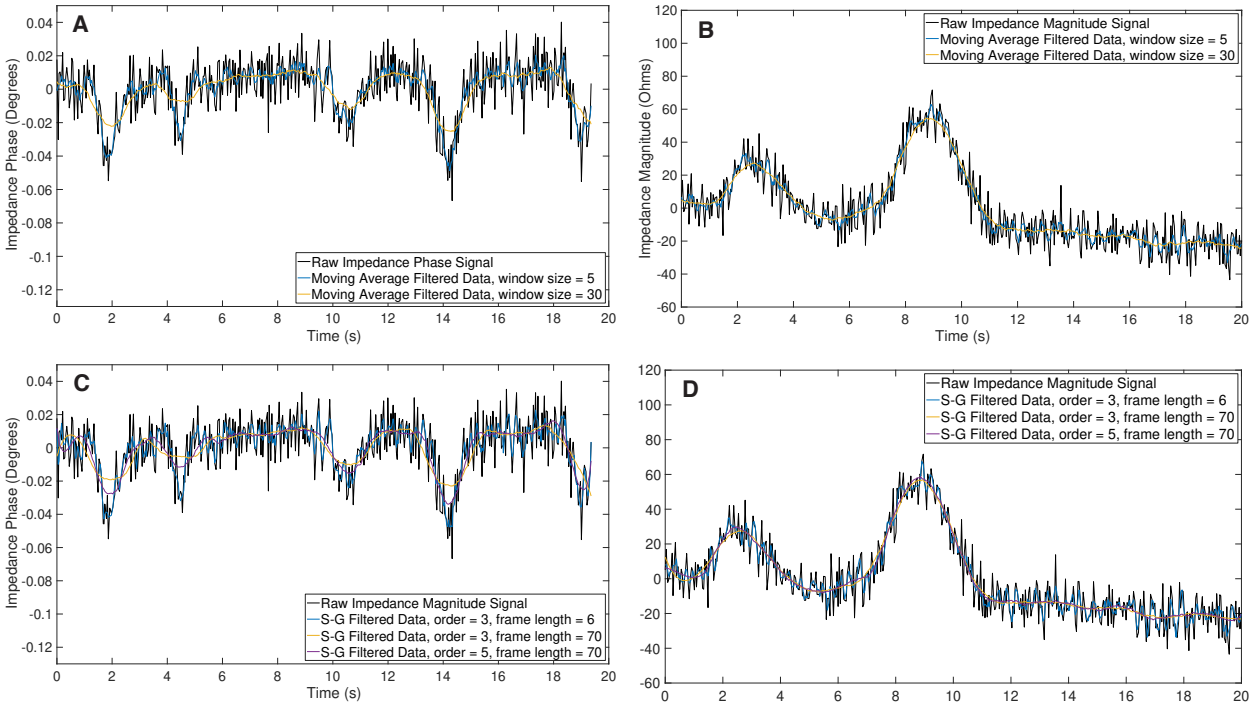

Figure 3.5. Relative changes in (A) impedance magnitude of dead cells including raw and moving average-filtered data, (B) impedance phase of live cells including raw and moving average-filtered data.

In Savitzky-Golay smoothing, there exists a similar compromise between noise reduction and preservation of peak amplitudes. Higher order filters do tend to maintain peak values but at the expense of noise reduction. Longer, lower-order filters, conversely, tend to more effectively reduce signal noise but dampen peak amplitude values. Identification of optimum order and frame length settings for noise reduction and peak preservation can be difficult or, in some cases, unachievable (Sun et al. 2009). Discrimination of cell viability states using the approach presented in this study can be more clearly demonstrated by plotting impedance magnitude and phase values (for live and dead cells) against one another using a scatter plot. To accomplish this, the signal processing algorithm was amended to record the peak magnitude of every positive signal detection event from collections of live and dead cells. That is, the algorithm identified

the signal peak corresponding to the impedance component that displays adequately Gaussian behavior, relative to the prescribed threshold for detection, and records the amplitude and index of that peak. If the converse impedance component does not display adequately Gaussian behavior as expected, that signal is averaged over a window of data points one-tenth of the data segment in length. Figure 3.6 shows the measured impedance magnitude and phase outputs resulting from signal processing plotted against one another.

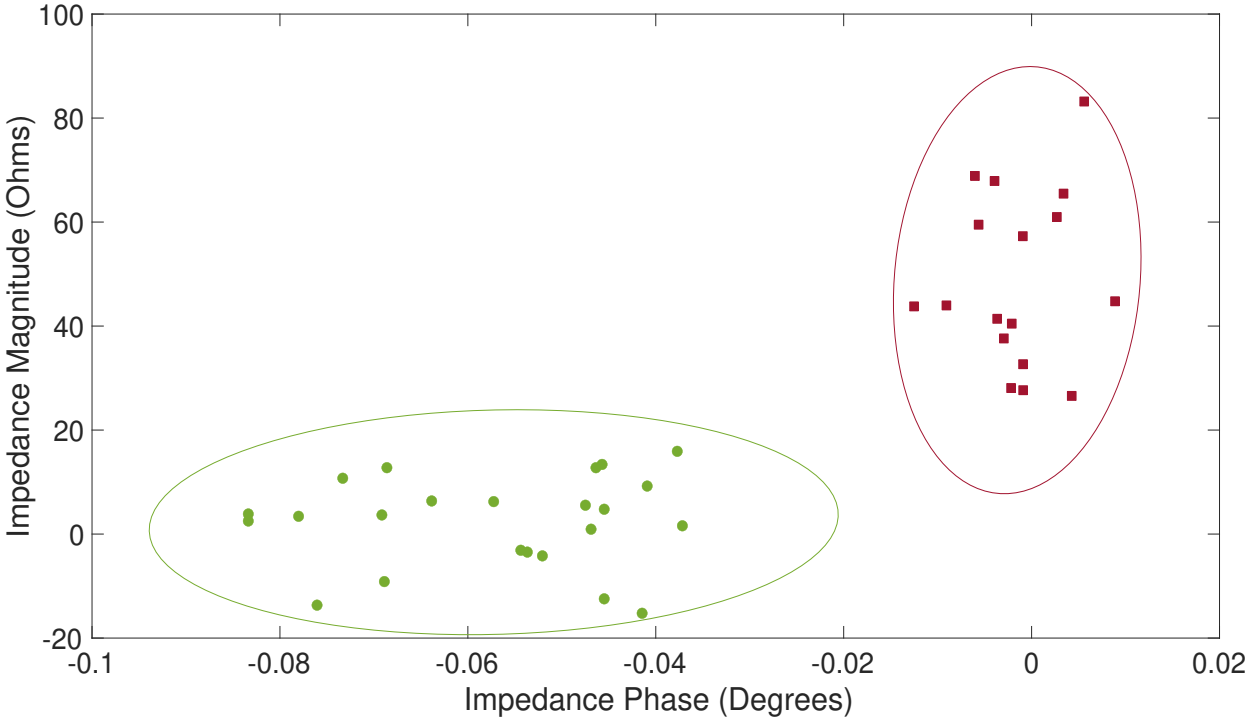

Figure 3.6. Representative 2D plot of change in magnitude versus phase, illustrating that live and dead cells can be discriminated using the designed microchip device with impedance measurements at 2 MHz.

This plot also contained 95% confidence ellipses for the sampled data collected from live and dead cell samples. Calculated in Matlab, the widths and angles of the major and minor axes of the ellipses were determined by the maximum and minimum eigenvalues of the covariance matrices of phase and magnitude values. As shown above, Jurkat cell

viability can be determined for at least 95% of interrogated cells using this device and signal detection algorithm.

3.5. Conclusions

This paper presents a microfluidic impedance cytometer optimized for sensitive, accurate, and high-throughput discrimination of the viability status of Jurkat cells. Compared to previously reported devices for this application, this tool achieved effective discrimination of live and dead cells using a vertical sidewall electrode geometry that generated a vertically uniform electric field. This parallel sidewall geometry mitigates problems associated with positional dependence and current leakage that are more prominent in coplanar electrode geometries. The electrodes were fabricated using an accessible, CAD-driven negative manufacturing process demonstrating its potential for more widespread use. Furthermore, because the fundamental mechanisms and operation of this device do not require complex particle focusing or trapping equipment, this device provides a simple platform for single cell biophysical property analysis. Finally, the inclusion of a custom buffer solution highlights a potential mitigating action that can be used to overcome challenges of sensitivity and current leakage associated with impedance cytometry platforms.

The general approach taken by this study can also be considered for other applications of microfluidic impedance cytometry for single cell analysis. Simple modifications to the applied frequency, electrode size, cell suspension buffer, and signal processing algorithm can allow for interrogation of many cell types and extraction of a number of important biophysical properties on a single-cell basis.

Chapter 4. Conclusions and Future Directions

4.1. Conclusions

This work presents two similar but distinct approaches for the analysis of biological cell samples based on the connection between their biophysical properties and the frequency-dependent current responses they induce in the presence of applied AC electric fields. Micro-electrochemical impedance spectroscopy (μEIS) can be applied for rapid analysis of bulk samples of cells across a wide range of frequencies. A modular microfluidic assembly with an integrated reversible microelectrode connector unit was presented. This platform allowed for easy assembly and disassembly and did not require special fluid handling instruments for operation.

This platform was shown to be an effective reusable system for application of microfluidic technology to impedance spectroscopy testing by discrimination of zebrafish sperm cell concentrations in a low-conductivity isosmotic buffer. A linear relationship between sample conductance and cell concentration was observed at a goodness of fit (R^2) value of 0.998 ± 5.37e-4. The sensitivity of these measurements, as determined from the slope of the conductance vs. concentration plot, was determined to be 9.73E-7 ± 4.51E-12 mS (cells per mL)$^{-1}$. Similarly, the impedance spectra created by conditioned media altered by temporary suspension (then removal) of sperm cells were tested. A goodness of fit and sensitivity corresponding to this data were measured as 0.990 ± 6.61e-4 and 10.64E-7 ± 19.97E-12 mS (cells per mL)$^{-1}$, respectively. Comparison of data from each of these conditions, e.g. cell-containing samples and cell-free conditioned media, suggest

that the sperm cells affect sucrose media in such a way that its conductivity is increased while the presence of cells and debris reduce the extent of this increase.

Observation of the cells in sucrose by phase-contrast microscopy indicated that cell membranes are disrupted by 20 minutes after suspension. Furthermore, time-series measurements suggest that impedance measurements corresponding to cells suspended in the sucrose solution reach a steady state after approximately 12 minutes. While yet to be documented for sperm cells, increases in sample conductance have been observed in studies applied to cell detection and concentration measurements of various other cell types including peripheral blood mononuclear cells (Cheng et al. 2007), synthetic liposomes (Damhorst et al. 2013), HIV cells (Demircan Yalçın et al. 2019), and parasitic bacteria (Houssin et al. 2010) based on ion release from both intact and lysed cells. The pH of the non-buffered sucrose solution was found to be 5.6, likely due to the absorption and conversion of carbon dioxide to carbonic acid. This acidity, with the reduced number of cells that can be observed in the sucrose solution over time, suggests that cell concentration can be measured on the basis of the ions released from the cells upon membrane disruption. As a result, it is proposed that a likely candidate for the phenomena observed in this study is ion-release resulting from cell membrane disruption.

The second variation of dielectric spectroscopy applied herein, microfluidic impedance cytometry, can be applied for high-throughput analysis of cellular properties on a single-cell basis. A micromilling method was presented for the fabrication of an impedance cytometry device consisting of parallel vertical sidewall electrodes. A physical basis for fixed-frequency single-cell interrogation was presented by consideration of the frequency-dependence of biological cells' dielectric properties. Cell detection events were

isolated from background signals amidst noise and baseline drift using a custom signal processing algorithm. A comparison of the cell analysis prior to versus with this signal processing algorithm showed improved noise suppression, more sensitive cell detection, and better discrimination between live and necrotic cells.

4.2. Future Directions

4.2.1. Modular Microfluidic Assembly and Microelectrode Connector

The design and application of the modular microfluidic assembly and microelectrode connector units used in this study were intended to be applied as a proof-of-concept evaluation. These tools were easily assembled and disassembled during testing and cleaning efforts.

While the clamping forces of the magnets were shown not to compress the PDMS gasket to a statistically significant degree, the larger variance in gasket height in the clamping assembly compared to the measurements outside of the assembly suggest that there may be some inconsistency in the extent of PDMS compression. In the event that future measurements are conducted on this device that are sensitive to variations in chamber height, the possibility of such inconsistencies should be further evaluated by measuring the height of a given PDMS gasket with the top and bottom pieces of the assembly at variable positions. However, it should be noted that measurements conducted on the basis of the bulk sample properties, as in the study reported in Chapter 2 herein, the height of the microfluidic chamber may not be important.

Similarly, while the microelectrode connector unit appeared to produce sufficiently consistent impedance measurements for cell counting in the target concentration

range, the consistency and effect of the application of the connector to electrode pads should be evaluated. That is, the consistency of impedance measurements of simple, well-characterized electrolyte solutions over some number of runs should be evaluated. This can be done on the basis of calculation and monitoring of a cell constant value, calculated as the ratio of measured sample resistance to solution resistivity. This term represents a ratio of electrode dimensions and is well-established as a parameter for IDEA characterization ("Impedance Instrumentation, Testing, and Data Validation" 2012).

The design of this device should also be advanced to improve the throughput of sample analysis. Capabilities for easy driving of fluids through the interrogation volume perhaps by addition of simple elements for interfacing with common fluid driving instruments can be considered.

4.2.2. Evaluation of Other Cell Properties in Custom Buffers

While the basis for zebrafish sperm cell concentration measurement in this study appears to be ion release resulting from cell lysis, the approach taken suggests a platform for the analysis of other cell properties. For example, because contributions of cell membranes to measured impedance values above beta-dispersion events, cell interrogation at higher frequencies can reveal information regarding the biophysical properties of cell membranes. For example, the resistance and/or capacitance of cell membranes may be able to be correlated to the fraction of cells in a sample with intact membranes, thereby providing a form of an estimate of sperm cell sample quality that does not require their activation for motility analysis, which is standard practice.

These studies highlighted the importance of appropriate solution parameters for sensitive electrophysiological measurements of intact cells. This solution should be biocompatible to maintain cell viability, and also remain isosmotic so as to not causing activation of motility. Additionally, the buffer should be sufficiently conductive to carry applied electric fields to the cells in the solution without being so conductive that their contributions to measured impedance values cannot be detected.

The microfabricated chamber and interdigitated electrodes used in this study could also be used for stimulating electrical fields that could be used in the evaluation of the ion-transport properties of cell. In a solution with controlled ion content probed at a controlled voltage, ion transport might be able to be induced and evaluated. This information could provide an insight into the transport behavior of zebrafish sperm cell membranes in static and activated states that may provide insights that typical motility studies cannot, so is worthy of future exploration.

Appendix A. Microfluidic Assembly Dimensional Drawings

Dimensional drawings for the top and bottom components are shown below. All units are in mm.

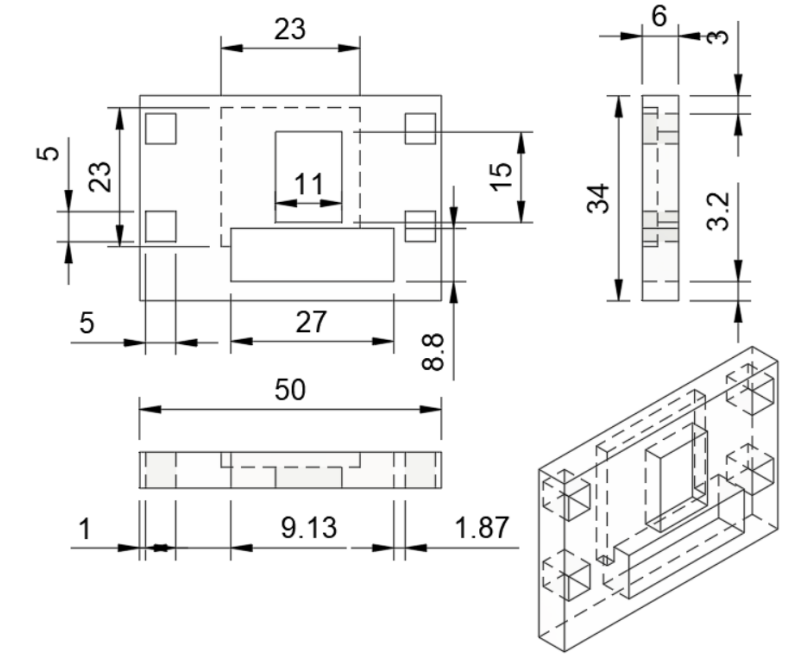

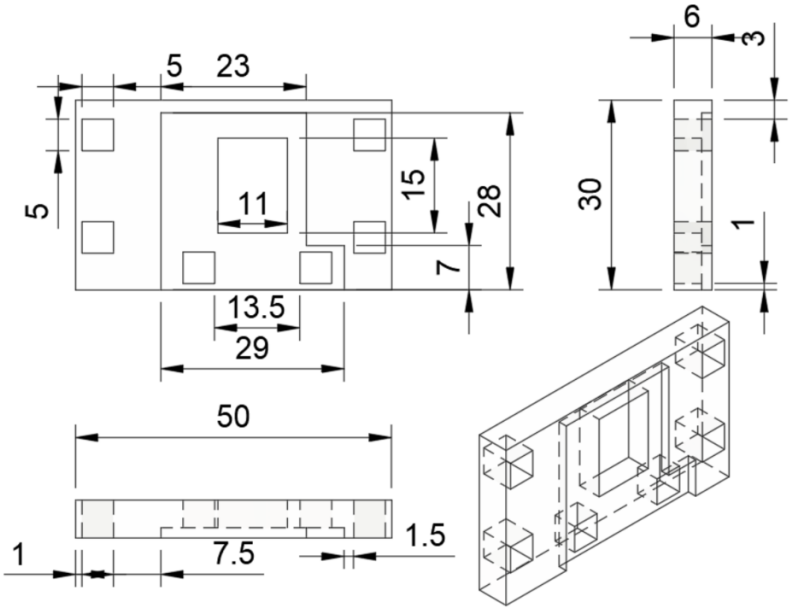

Appendix B. Impedance Cytometry Electric Field Simulations and Signal Processing

The approach taken to simulate the effects of electrode geometry on impedance cytometry, and the general approach used to process time course impedance data is presented below.

Simulation of Device Design

Computational simulations were created to model the impedance signal generated by a cell passing through the interrogation region of the device presented in this study. The method described by Cottet et al. [1], which involves defining a region of the model geometry as having dielectric properties corresponding to the cell of interest distinct from those of the cell-carrying buffer, was adapted herein.

Model Geometry

The model geometry was constructed to represent the detection region of the microfluidic device presented in this study as shown below.

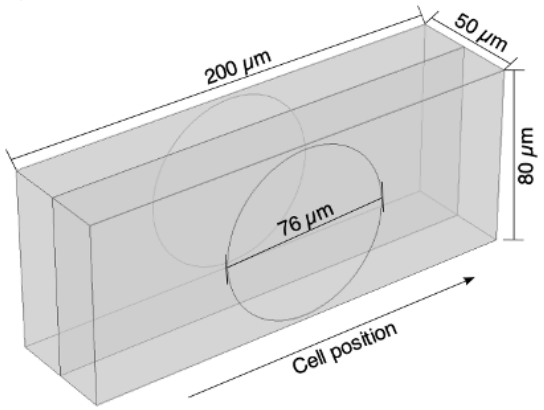

Figure S1 Schematic diagram of the model geometry representing the device design used in this study.

A 200 μm length of the microchannel was selected in order to encompass the entire electric field in the system. Though the actual height of the microchannel may vary due to limits of resolution of micromilling instrumentation and extents of surface modification resulting from hot embossing, the model geometry was specified to have a height of 80 μm in order to encompass the full diameter of the electrodes thereby revealing the extent of potential positional variance in measured impedance signals. The circles on the periphery of the geometry represent the area of the interface between the platinum electrodes and the fluid microchannel. One of these represents the excitation electrode and is defined as an electrical terminal with an applied voltage of 1 V while the other represents the sensing electrode and is defined as a ground boundary.

Material Definitions

The input specifications used to define the material properties described below.

Table S1 Dielectric material properties used in computational model of reported device.

Property	Symbol	Unit	Value	Basis
Solution Conductivity	sigma_sol	S/m	0.12	Conductivity of custom TrisGly + Sucrose + BSA buffer used in this study
Solution Relative Permittivity	eps_r_sol	--	80	Relative permittivity based on properties of PBS and custom buffer [2]
Particle Conductivity	sigma_par	S/m	1E-12	Median value of commonly reported membrane conductivities of biological cells [3]
Particle Relative Conductivity	eps_r_par	--	6	Median value of commonly reported membrane conductivities of biological cells [3]

The radius of the cell is defined as r0, and the position of its center is defined using Cartesian coordinates (x0, y0, z0). The properties of the material in the model are then defined using a conditional expression that applies the properties of the "particle" (or cell) within the radius of the cell and the properties of the "solution" outside of that region. The movement of the cell is achieved by varying the position of its center using an auxiliary parametric sweep.

Meshing

A free tetrahedral mesh element shape with the following size settings was used throughout the full extent of the geometry. Standard adaptive meshing was used, but no boundary layer or other distributive modifications were made. The mesh element size settings were established as follows:

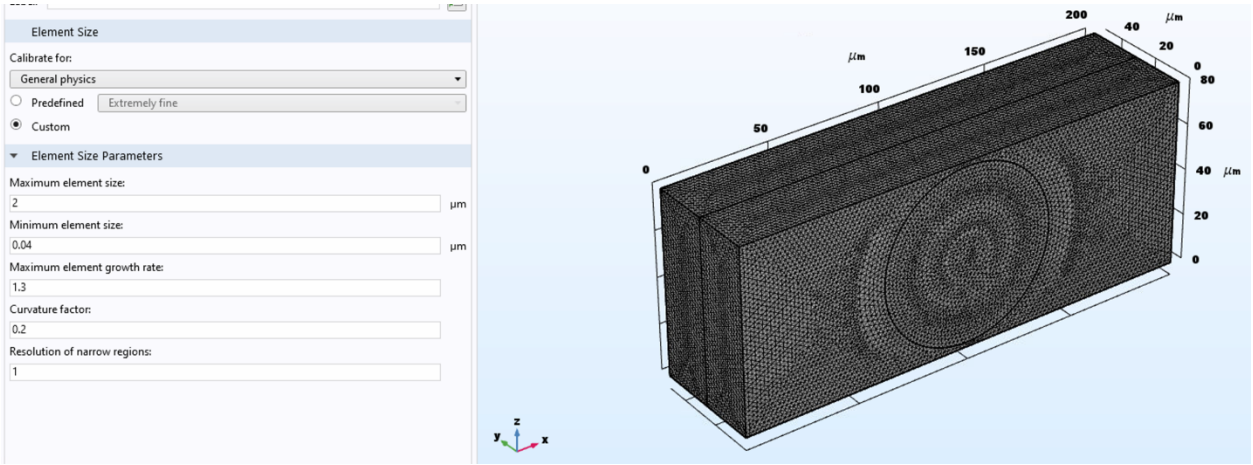

Figure S2 Meshing parameters and completed mesh of model geometry.

Synthetic Impedance Data

COMSOL's AC/DC module calculates electrical properties as lumped parameters. When a voltage is applied in the Electrostatics physics package, an admittance matrix, Y, is determined. Specifically, as only one voltage is applied, the system admittance is represented as the first element in Y, Y11. Therefore, by definition, the system impedance can be calculated by defining a new variable as Z11 = 1/Y11 and assigning a global variable probe. Because impedance data is measured as the cell is outside of the induced electric field, the contribution of the buffer impedance to the synthetic data stream can be removed.

Impedance Data Processing

Experimental data was collected using an Agilent E4980A LCR Meter controlled by LabView. Output impedance magnitude and phase data was collected and imported into Matlab. An algorithm was developed to process control sample data by a three-step process. First, a segment of data is taken whose length is based on the velocity of the cells in the microchannel and the length of the detection region. The data segment is then fitted against a mathematical single pulse Gaussian function, of the form $y_{pred} = a * \exp\left(\frac{t-b}{c}\right)^2$ where t is time in seconds; a, b, and c are fitting parameters. The quality of the fits of data segments corresponding to cell detection events (as confirmed by video microscopy) were recorded. Data that does not correspond to a cell event is passed by the algorithm as noise and is detrended to remove baseline drift. The data segments are then recombined and expressed together. No data smoothing is applied to avoid artificially suppressing important trends.

Supplementary References

[1] Cottet J, Kehren A, van Lintel H, Buret F, Frénéa-Robin M, Renaud P. How to improve the sensitivity of coplanar electrodes and micro channel design in electrical impedance flow cytometry: a study. Microfluid Nanofluidics 2019;23:1–11. https://doi.org/10.1007/s10404-018-2178-6.

[2] Gavish N, Promislow K. Dependence of the dielectric constant of electrolyte solutions on ionic concentration: A microfield approach. Phys Rev E 2016;94:12611. https://doi.org/10.1103/PhysRevE.94.012611.

[3] Markx GH, Davey CL. The dielectric properties of biological cells at radiofrequencies: applications in biotechnology. Enzyme Microb Technol 1999;25:161–71. https://doi.org/10.1016/S0141-0229(99)00008-3.

Appendix C. Signal Processing Code

Matlab code for processing single cell cytometry data is presented below.

```
function [ ] = ControlSamples( )
%The purpose of this function is as follows:
%1. Detrend raw signals for live and dead control samples
%2. Identify and extract cell event signals from detrended data
%3. Filter noise to improve signal-to-noise ratio
%4. Plot results

try

clear
clc

%-------------------------------------------------------------------
---------------------------------
%1. This section reads the live and dead cell control sample data and
%detrends the nonlinear data prior to event extraction

%1.1 Read data from file with prescribed name on a prescribed sheet
over a
%prescribed range. This can be extended later to create a loop wherein
the
%function will search a certain sheet within a certain file but will
loop
%through the data until an empty cell is reached. This way, any
dataset of
%any length can be processed
% tlive = xlsread('Sample_Data','Live_2MHz','G2:G650');
% Mlive = xlsread('Sample_Data','Live_2MHz','H2:H650');
% Plive = xlsread('Sample_Data','Live_2MHz','I2:I650');
% tdead = xlsread('Sample_Data','Dead_2MHz','B143:B1010');
% Mdead = xlsread('Sample_Data','Dead_2MHz','C143:C1010');
% Pdead = xlsread('Sample_Data','Dead_2MHz','D143:D1010');

t1 = linspace(1,4400,4400);
R1 = xlsread('5e4-RX-04_06_21-15-31.csv','5e4-
RX-04_06_21-15-31','A2:A4401');
X1 = xlsread('5e4-RX-04_06_21-16-47_v2.csv','5e4-
RX-04_06_21-16-47_v2','B2:B4401');
M1 = sqrt(R1.^2+X1.^2);
P1 = atan(X1./R1)*180/3.14159;
```

```
M1 = M1.*-1;

% Pdlive = round(length(tlive)/100);
% Pddead = round(length(tdead)/100);

%1.2 The Matlab "polyfit" function reads data in an [x,y,n] format to
%create coefficients, p, that fit a polynomial that fits the y data
over
%the x range with an order of n. Mu corresponds to the mean of the
dataset
% [p1,s1,mu1] = polyfit(tdead,Mdead,0);
% [p2,s2,mu3] = polyfit(tlive,Plive,0);
% [p3,s3,mu3] = polyfit(tdead,Pdead,0);
% [p4,s4,mu4] = polyfit(tlive,Mlive,0);
% [p1,s1,mu1] = polyfit(tdead,Mdead,1);
% [p2,s2,mu3] = polyfit(tlive,Plive,1);
% [p3,s3,mu3] = polyfit(tdead,Pdead,1);
% [p4,s4,mu4] = polyfit(tlive,Mlive,1);

[p1,s1,mu1] = polyfit(t1,M1,0);

%1.3 The Matlab "polyval" function reads data in an [p,x,[],mu] format
to
%create a polynomial function based on the polynomial coefficients
%described by p over the range x. Mu causes the polynomial to
incorporate
%a mean of mu by x' = (x-mu1)/mu2
% PolyVal1 = polyval(p1,tdead,[],mu1);
% PolyVal2 = polyval(p2,tlive,[],mu3);
% PolyVal3 = polyval(p3,tdead,[],mu3);
% PolyVal4 = polyval(p4,tlive,[],mu4);

PolyVal1 = polyval(p1,t1,[],mu1);

%The code below subtracts the polynomial created by the polyfit and
polyval
%functions from the raw data
% DetrendedMagdead = Mdead - PolyVal1;
% DetrendedPhlive = Plive - PolyVal2;
% DetrendedPhdead = Pdead - PolyVal3;
% DetrendedMaglive = Mlive - PolyVal4;

DetrendedM1 = M1 - PolyVal1;

% mintlive = min(tlive);
% tliveraw = tlive'-mintlive;
% mintdead = min(tdead);
% tdeadraw = tdead'-mintdead;

mint1 = min(t1);
```

```
t1raw = t1'-mint1;

% figure(2)
% subplot(2,2,1)
% p1 = plot(tliveraw,DetrendedMaglive);
% title('Raw Output - Impedance Magnitude of Live Cells');
% ylim([-40 120])
% a = get(gca,'XTickLabel');
% set(gca,'XTickLabel',a,'fontsize',23)
% set(gca,'XTickLabelMode','auto')
% b = get(gca,'YTickLabel');
% set(gca,'YTickLabel',b,'fontsize',23)
% set(gca,'YTickLabelMode','auto')
% p1.LineWidth = 3;
% p1.Color = [0, 1.0, 0, 0.5];
% xlabel('Time (s)','FontSize',29)
% ylabel('Impedance Magnitude (Ohms)','FontSize',29)
% subplot(2,2,3)
% p2 = plot(tliveraw,DetrendedPhlive);
% title('Raw Output - Impedance Phase of Live Cells');
% ylim([-0.14 0.04])
% a = get(gca,'XTickLabel');
% set(gca,'XTickLabel',a,'fontsize',23)
% set(gca,'XTickLabelMode','auto')
% b = get(gca,'YTickLabel');
% set(gca,'YTickLabel',b,'fontsize',23)
% set(gca,'YTickLabelMode','auto')
% p2.LineWidth = 3;
% p2.Color = [0, 1.0, 0, 0.5];
% xlabel('Time (s)','FontSize',29)
% ylabel('Impedance Phase (Degrees)','FontSize',29)
% subplot(2,2,2)
% p3 = plot(tdeadraw,DetrendedMagdead);
% title('Raw Output - Impedance Magnitude of Dead Cells');
% ylim([-40 120])
% a = get(gca,'XTickLabel');
% set(gca,'XTickLabel',a,'fontsize',23)
% set(gca,'XTickLabelMode','auto')
% b = get(gca,'YTickLabel');
% set(gca,'YTickLabel',b,'fontsize',23)
% set(gca,'YTickLabelMode','auto')
% p3.LineWidth = 3;
% p3.Color = [1.0, 0, 0, 0.5];
% xlabel('Time (s)','FontSize',29)
% ylabel('Impedance Magnitude (Ohms)','FontSize',29)
% subplot(2,2,4)
% p4 = plot(tdeadraw,DetrendedPhdead);
% title('Raw Output - Impedance Phase of Dead Cells');
% ylim([-0.14 0.04])
% a = get(gca,'XTickLabel');
```

```
% set(gca,'XTickLabel',a,'fontsize',23)
% set(gca,'XTickLabelMode','auto')
% b = get(gca,'YTickLabel');
% set(gca,'YTickLabel',b,'fontsize',23)
% set(gca,'YTickLabelMode','auto')
% p4.LineWidth = 3;
% p4.Color = [1.0, 0, 0, 0.5];
% xlabel('Time (s)','FontSize',29)
% ylabel('Impedance Phase (Degrees)','FontSize',29)

%-------------------------------------------------------------------
-----------------------------------
%2. This section fits standardized Magnitude data to a Gaussian
polynomial,
%keeps the data that fits the Gaussian profile and 3. detrends and
filters the
%data determined to be noise using the polyfit/polyval functions and
%Savitsky-Golay Filtering, respectively

%Define new vectors as vectors of ones to reduce run time
% DetrendedPhdeadInv = ones(length(tdead)-1,1);
DetrendedPh1Inv = ones(length(t1)-1,1);
% tdeadnorm = ones(length(tdead)-1,1);
t1norm = ones(length(t1)-1,1);
% DetrendedPhliveInv = ones(length(tlive)-1,1);
% tlivenorm = ones(length(tlive)-1,1);
% xdead = ones(length(tdead),1);
x1 = ones(length(t1),1);
% xlive = ones(length(tlive),1);
% y1 = ones(length(tdead),1);
y1 = ones(length(t1),1);
% y2 = ones(length(tlive),1);
% y3 = ones(length(tdead),1);
% y4 = ones(length(tlive),1);
% MagFit1 = zeros(length(tdead),1);
MagFit1 = zeros(length(t1),1);
% MagFit1Data = zeros(length(tdead),1);
MagFit1Data = zeros(length(t1),1);
% PhFit2 = zeros(length(tlive),1);
PhFit1 = zeros(length(t1),1);
% PhFit2Inv = zeros(length(tlive),1);
PhFit1Inv = zeros(length(t1),1);
% PhFit2Data = zeros(length(tlive),1);
% PhFit2DataInv = zeros(length(tlive),1);
% PhFit3 = zeros(length(tdead),1);
% PhFit3Inv = zeros(length(tdead),1);
% PhFit3Data = zeros(length(tdead),1);
% PhFit3DataInv = zeros(length(tdead),1);
% MagFit4 = zeros(length(tlive),1);
% MagFit4Data = zeros(length(tlive),1);
```

```
% Rsq1 = zeros(length(tdead),1);
Rsq1 = zeros(length(t1),1);
% Rsq3 = zeros(length(tdead),1);
% Rsq2 = zeros(length(tlive),1);
% Rsq4 = zeros(length(tlive),1);

%Create inverse vectors for Phase signals so that findpeaks can be
applied
% DetrendedPhdeadInv = DetrendedPhdead.*-1;
% DetrendedPhliveInv = DetrendedPhlive.*-1;

DetrendedPh1Inv = DetrnededPh1.*-1;

%Define length of vectors constructed for testing for signal detection
%events, approximate interval for length of signal corresponding to
%detection events, and minimum thresholds for goodness-of-fit values
to
%extract detection events from noise
% VectorLengthdead = 120;
% PeakIntervaldead = 70;
% VectorLengthlive = 70;
% PeakIntervallive = ceil(VectorLengthlive/2);
% RSquareLimMag1 = 0.67;
% RSquareLimMag4 = 0.67;
% RSquareLimPh2 = 0.6;
% RSquareLimPh3 = 0.6;
% i = 1; j = 1; k = 1; l = 1;
%i = 252; %Added for troubleshooting

VectorLength1 = 50;
i = 1; k = 1;
RSquareLimMag1 = 0.5;
RSquareLimPh1 = 0.5;

% %2.1 Construct loop for length of dead control sample data. This
means
% %that, if used for processing future impedance data, the sample must
be run
% %for an additional time (~1-2 s) with no cells present
% while i <= (length(tdead)-VectorLengthdead)
%     %2.1.1 Construct vectors of 'VectorLength' number of points
after the ith
%     %point in the loop. Vectors correspond to time data and
detrended
%     %impedance magnitude over the set vector length
%     xdead = tdead(i:i+VectorLengthdead-1);
%     y1 = DetrendedMagdead(i:i+VectorLengthdead-1);
%     %2.1.2 Fit each vector to a single two-sided Gaussian profile
%     fitOptions1 = fitoptions('gauss1','Lower',[-1000 -1000
-1000],'Upper',[1000 1000 1000]);
```

```
%     [fitf1,gof1] = fit(xdead,y1,'gauss1',fitOptions1);
%     %2.1.3 Quantify goodness-of-fit with r-squared values
%     Rsq1(i,1) = gof1.rsquare;
%     %2.1.4 If r-squared values are greater than the minimum
threshold set
%     %execute code below to extract event signals and fit to a
Gaussian
%     %profile
%     if Rsq1(i,1) > RSquareLimMag1
%         %2.1.4.1 Create vectors corresponding to the fit Gaussian
profile
%         %and the detrended impedance magnitude signal over the
vector
%         %length
%         MagFit1(i:i+VectorLengthdead-1) = fitf1(xdead);
%         MagFit1Data(i:i+VectorLengthdead-1) = y1;
%         %2.1.4.2 Identify the maximum and location of the maximum of
the
%         %Gaussian fit profile and the detrended impedance magnitude
signal
%         [maxMagFit1,Loc1] =
max(abs(MagFit1(i:i+VectorLengthdead-1)));
%         [maxMagFit1Data,Loc1Data] =
max(abs(MagFit1Data(i:i+VectorLengthdead-1)));
%         %2.1.4.3 Define new i values as the locations of the two
maxima
%         iNew = i + Loc1Data;
%         iDataNew = i + Loc1Data;
%         %2.1.4.4 Define minumum and maximum time points
corresponding to
%         %the assumed length of the detection event signal for
Gaussian fit
%         %and impedance data
%         Loc1Min = max(i,iNew-PeakIntervaldead);
%         Loc1DataMin = max(i,iDataNew-PeakIntervaldead);
%         Loc1Max = min(length(tdead)-
VectorLengthdead,iNew+PeakIntervaldead);
%         Loc1DataMax = min(length(tdead)-
VectorLengthdead,iDataNew+PeakIntervaldead);
%         %2.1.4.5 Define new x vector corresponding to the peak data
%         xdeadNew = tdead(Loc1DataMin:Loc1DataMax);
%         %2.1.4.6 Define new y vector corresponding to the peak data
%         y1New = DetrendedMagdead(Loc1DataMin:Loc1DataMax);
%         %2.1.4.7 Create new Gaussian fit centered around the maximum
of the
%         %detection event signal to ensure that all associated data
is
%         %processed
%         [fitf1New,gof1New] =
fit(xdeadNew,y1New,'gauss1',fitOptions1);
```

```
%         %2.1.4.8 Redefine the curve for the fit as 0 outside of
assumed
%         %peak length and assign new curve for the data in the peak
length
%         MagFit1(i:Loc1Min) = 0;
%         MagFit1(Loc1Min:Loc1DataMax) = fitf1New(xdeadNew);
%         if Loc1Max < i+VectorLengthdead-1
%         MagFit1(Loc1Max:i+VectorLengthdead-1) = 0;
%         end
%         %2.1.4.9 Redefine the impedance as 0 outside of assumed peak
length
%         %and keep the data within the detection event
%         MagFit1Data(i:Loc1Min) = DetrendedMagdead(i:Loc1Min);
%         MagFit1Data(Loc1DataMin:Loc1DataMax) = y1New;
%         if Loc1DataMax < i+VectorLengthdead-1
%         MagFit1Data(Loc1DataMax:i+VectorLengthdead-1) =
DetrendedMagdead(Loc1DataMax:i+VectorLengthdead-1);
%         end
%         MagFit1Noise(i:i+VectorLengthdead-1) = 0;
%         %2.1.4.10 Skip to end of detection event data to ensure that
it
%         %doesn't get erased or processed as noise
%         i = Loc1DataMax;
%     %3.1 If r-squared is less than the specified limit, use polyfit
and
%     %polyval functions to detrend noise then use Savitsky-Golay
Filtering
%     %to filter noise to ensure that no events were missed and
increase
%     %signal-to-noise ratio
%     else
%         %3.1.1 Create new polyfit and polyval functions to detrend
noise
%         %data over "VectorLength"-length interval
%         %[p1Noise,s1Noise,mu1Noise] = polyfit(xdead,y1,6);
%         %PolyVal1Noise = polyval(p1Noise,xdead,[],mu1Noise);
%         %3.1.2 Subtract polynomial from previously detrended data to
better
%         %detrend smaller section of noise
%         %MagFit1Data(i:i+length(y1)-1) = y1-PolyVal1Noise;
%         %3.1.3 Filter detrended noise data by Savitsky-Golay Filter
of
%         %order and frame length specified
%         %order = 3;
%         %framelen = VectorLength/10 + 1;
%         %MagFit1Data(i:i+length(y1)-1) =
sgolayfilt(MagFit1Data(i:i+length(y1)-1),order,framelen);
%         MagFit1Data(i:i+length(y1)-1) = 0;
%         MagFit1Noise(i:i+length(y1)-1) =
DetrendedMagdead(i:i+length(y1)-1);
```

```
%         %3.1.4 Skip to end of vector to avoid reprocessing
%         i = i + VectorLengthdead-1;
%     end
%     i = i + 1;
% end
%
% MagFit1Data(i:length(tdead)) = 0;
% MagFit1Noise(i:length(tdead)) = DetrendedMagdead(i:length(tdead));
%
% %2.3 Construct loop for length of dead control sample data. This
means
% %that, if used for processing future impedance data, the sample must
be run
% %for an additional time (~1-2 s) with no cells present
% while k <= (length(tdead)-VectorLengthdead)
%     %2.3.1 Construct vectors of 'VectorLength' number of points
after the
%     %kth point in the loop. Vectors correspond to time data and
detrended
%     %impedance phase over the set vector length
%     xdead = tdead(k:k+VectorLengthdead-1);
%     y3 = DetrendedPhdeadInv(k:k+VectorLengthdead-1);
%     %2.3.2 Fit each vector to a single two-sided Gaussian profile
%     fitOptions3 = fitoptions('gauss1','Lower',[-1000 -1000
-1000],'Upper',[1000 1000 1000]);
%     [fitf3,gof3] = fit(xdead,y3,'gauss1',fitOptions3);
%     %2.3.3 Quantify goodness-of-fit with r-squared values
%     Rsq3(k,1) = gof3.rsquare;
%     %2.3.4 If r-squared values are greater than the minimum
threshold set
%     %execute code below to extract event signals and fit to a
Gaussian
%     %profile
%     if Rsq3(k,1) > RSquareLimPh3
%         %2.3.4.1 Create vectors corresponding to the fit Gaussian
profile
%         %and the detrended impedance phase signal over the vector
%         %length
%         PhFit3Inv(k:k+VectorLengthdead-1) = fitf3(xdead);
%         PhFit3DataInv(k:k+VectorLengthdead-1) = y3;
%         %2.3.4.2 Identify the maximum and location of the maximum of
the
%         %Gaussian fit profile and the detrended impedance phase
signal
%         [maxPhFit3Inv,Loc3] =
max(abs(PhFit3Inv(k:k+VectorLengthdead-1)));
%         [maxPhFit3DataInv,Loc3Data] =
max(abs(PhFit3DataInv(k:k+VectorLengthdead-1)));
%         %2.3.4.3 Define new j values as the locations of the two
maxima
```

```
%         kNew = k + Loc3Data;
%         kDataNew = k + Loc3Data;
%         %2.3.4.4 Define minumum and maximum time points
corresponding to
%         %the assumed length of the detection event signal for
Gaussian fit
%         %and impedance data
%         Loc3Min = max(k,kNew-PeakIntervaldead);
%         Loc3DataMin = max(k,kDataNew-PeakIntervaldead);
%         Loc3Max = min(length(tdead)-
VectorLengthdead,kNew+PeakIntervaldead);
%         Loc3DataMax = min(length(tdead)-
VectorLengthdead,kDataNew+PeakIntervaldead);
%         %2.3.4.5 Define new x vector corresponding to the peak data
%         xdeadNew = tdead(Loc3DataMin:Loc3DataMax);
%         %2.3.4.6 Define new y vector corresponding to the peak data
%         y3New = DetrendedPhdead(Loc3DataMin:Loc3DataMax);
%         %2.3.4.7 Create new Gaussian fit centered around the maximum
of the
%         %detection event signal to ensure that all associated data
is
%         %processed
%         [fitf3New,gof3New] =
fit(xdeadNew,y3New,'gauss1',fitOptions3);
%         %2.3.4.8 Redefine the curve for the fit as 0 outside of
assumed
%         %peak length and assign new curve for the data in the peak
length
%         PhFit3Inv(k:Loc3Min) = 0;
%         PhFit3Inv(Loc3Min:Loc3DataMax) = fitf3New(xdeadNew);
%         if Loc3Max < k+VectorLengthdead-1
%         PhFit3Inv(Loc3Max:k+VectorLengthdead-1) = 0;
%         end
%         %2.3.4.9 Redefine the impedance as 0 outside of assumed peak
length
%         %and keep the data within the detection event
%         PhFit3DataInv(k:Loc3Min) = DetrendedPhdead(k:Loc3Min).*-1;
%         PhFit3DataInv(Loc3DataMin:Loc3DataMax) = y3New;
%         if Loc3DataMax < k+VectorLengthdead-1
%         PhFit3DataInv(Loc3DataMax:k+VectorLengthdead-1) =
DetrendedPhdead(Loc3DataMax:k+VectorLengthdead-1).*-1;
%         end
%         PhFit3Noise(k:k+VectorLengthdead-1) = 0;
%         %2.3.4.10 Skip to end of detection event data to ensure that
it
%         %doesn't get erased or processed as noise
%         k = Loc3DataMax;
%     %3.3 If r-squared is less than the specified limit, use polyfit
and
%     %polyval functions to detrend noise then use Savitsky-Golay
```

```
Filtering
%     %to filter noise to ensure that no events were missed and
increase
%     %signal-to-noise ratio
%     else
%         %3.3.1 Create new polyfit and polyval functions to detrend
noise
%         %data over "VectorLength"-length interval
%         %[p3Noise,s3Noise,mu3Noise] = polyfit(xdead,y3,6);
%         %PolyVal3Noise = polyval(p3Noise,xdead,[],mu3Noise);
%         %3.3.2 Subtract polynomial from previously detrended data to
better
%         %detrend smaller section of noise
%         %PhFit3DataInv(k:k+length(y3)-1) = y3-PolyVal3Noise;
%         %3.3.3 Filter detrended noise data by Savitsky-Golay Filter
of
%         %order and frame length specified
%         %order = 3;
%         %framelen = VectorLength/10 + 1;
%         %PhFit3DataInv(k:k+length(y3)-1) =
sgolayfilt(PhFit3DataInv(k:k+length(y3)-1),order,framelen);
%         PhFit3DataInv(k:k+length(y3)-1) = 0;
%         PhFit3Noise(k:k+length(y3)-1) =
DetrendedPhdead(k:k+length(y3)-1).*-1;
%         %3.2.4 Skip to end of vector to avoid reprocessing
%         k = k + VectorLengthdead-1;
%     end
%     k = k + 1;
% end
%
% PhFit3Data(k:length(tdead)) = 0;
% PhFit3Noise(k:length(tdead)) = DetrendedPhdead(k:length(tdead));
%
% %2.2 Construct loop for length of live control sample data. This
means
% %that, if used for processing future impedance data, the sample must
be run
% %for an additional time (~1-2 s) with no cells present
% while j <= (length(tlive)-VectorLengthlive)
%     %2.2.1 Construct vectors of 'VectorLength' number of points
after the
%     %jth point in the loop. Vectors correspond to time data and
detrended
%     %impedance phase over the set vector length
%     xlive = tlive(j:j+VectorLengthlive-1);
%     y2 = DetrendedPhliveInv(j:j+VectorLengthlive-1);
%     %2.2.2 Fit each vector to a single two-sided Gaussian profile
%     fitOptions2 = fitoptions('gauss1','Lower',[-1000 -1000
-1000],'Upper',[1000 1000 1000]);
%     [fitf2,gof2] = fit(xlive,y2,'gauss1',fitOptions2);
```

```
%     %2.2.3 Quantify goodness-of-fit with r-squared values
%     Rsq2(j,1) = gof2.rsquare;
%     %2.2.4 If r-squared values are greater than the minimum
threshold set
%     %execute code below to extract event signals and fit to a
Gaussian
%     %profile
%     if Rsq2(j,1) > RSquareLimPh2
%         %2.2.4.1 Create vectors corresponding to the fit Gaussian
profile
%         %and the detrended impedance phase signal over the vector
%         %length
%         PhFit2Inv(j:j+VectorLengthlive-1) = fitf2(xlive);
%         PhFit2DataInv(j:j+VectorLengthlive-1) = y2;
%         %2.2.4.2 Identify the maximum and location of the maximum of
the
%         %Gaussian fit profile and the detrended impedance phase
signal
%         [maxPhFit2Inv,Loc2] =
max(abs(PhFit2Inv(j:j+VectorLengthlive-1)));
%         [maxPhFit2DataInv,Loc2Data] =
max(abs(PhFit2DataInv(j:j+VectorLengthlive-1)));
%         %2.2.4.3 Define new j values as the locations of the two
maxima
%         jNew = j + Loc2Data;
%         jDataNew = j + Loc2Data;
%         %2.2.4.4 Define minumum and maximum time points
corresponding to
%         %the assumed length of the detection event signal for
Gaussian fit
%         %and impedance data
%         Loc2Min = max(j,jNew-PeakIntervallive);
%         Loc2DataMin = max(j,jDataNew-PeakIntervallive);
%         Loc2Max = min(length(tlive)-
VectorLengthlive,jNew+PeakIntervallive);
%         Loc2DataMax = min(length(tlive)-
VectorLengthlive,jDataNew+PeakIntervallive);
%         %2.2.4.5 Define new x vector corresponding to the peak data
%         xliveNew = tlive(Loc2DataMin:Loc2DataMax);
%         %2.2.4.6 Define new y vector corresponding to the peak data
%         y2New = DetrendedPhliveInv(Loc2DataMin:Loc2DataMax);
%         %2.2.4.7 Create new Gaussian fit centered around the maximum
of the
%         %detection event signal to ensure that all associated data
is
%         %processed
%         [fitf2New,gof2New] =
fit(xliveNew,y2New,'gauss1',fitOptions2);
%         %2.2.4.8 Redefine the curve for the fit as 0 outside of
assumed
```

```
%         %peak length and assign new curve for the data in the peak
length
%         PhFit2Inv(j:Loc2Min) = 0;
%         PhFit2Inv(Loc2Min:Loc2DataMax) = fitf2New(xliveNew);
%         if Loc2Max < j+VectorLengthlive-1
%         PhFit2Inv(Loc2Max:j+VectorLengthlive-1) = 0;
%         end
%         %2.2.4.9 Redefine the impedance as 0 outside of assumed peak
length
%         %and keep the data within the detection event
%         PhFit2DataInv(j:Loc2Min) = DetrendedPhlive(j:Loc2Min).*-1;
%         PhFit2DataInv(Loc2DataMin:Loc2DataMax) = y2New;
%         if Loc2DataMax < j+VectorLengthlive-1
%         PhFit2DataInv(Loc2DataMax:j+VectorLengthlive-1) =
DetrendedPhlive(Loc2DataMax:j+VectorLengthlive-1).*-1;
%         end
%         PhFit2Noise(j:j+VectorLengthlive-1) = 0;
%         %2.2.4.10 Skip to end of detection event data to ensure that
it
%         %doesn't get erased or processed as noise
%         j = Loc2DataMax;
%     %3.2 If r-squared is less than the specified limit, use polyfit
and
%     %polyval functions to detrend noise then use Savitsky-Golay
Filtering
%     %to filter noise to ensure that no events were missed and
increase
%     %signal-to-noise ratio
%     else
%         %3.2.1 Create new polyfit and polyval functions to detrend
noise
%         %data over "VectorLength"-length interval
%         %[p2Noise,s2Noise,mu2Noise] = polyfit(xlive,y2,6);
%         %PolyVal2Noise = polyval(p2Noise,xlive,[],mu2Noise);
%         %3.2.2 Subtract polynomial from previously detrended data to
better
%         %detrend smaller section of noise
%         %PhFit2DataInv(j:j+length(y2)-1) = y2-PolyVal2Noise;
%         %3.2.3 Filter detrended noise data by Savitsky-Golay Filter
of
%         %order and frame length specified
%         %order = 3;
%         %framelen = VectorLength/10 + 1;
%         %PhFit2DataInv(j:j+length(y2)-1) =
sgolayfilt(PhFit2DataInv(j:j+length(y2)-1),order,framelen);
%         PhFit2DataInv(j:j+length(y2)-1) = 0;
%         PhFit2Noise(j:j+length(y2)-1) =
DetrendedPhlive(j:j+length(y2)-1).*-1;
%         %3.2.4 Skip to end of vector to avoid reprocessing
%         j = j + VectorLengthlive-1;
```

```
%     end
%     j = j + 1;
% end
%
% PhFit2Data(j:length(tlive)) = 0;
% PhFit2Noise(j:length(tlive)) = DetrendedPhlive(j:length(tlive));
%
% %2.4 Processing live control sample magnitude will be conducted
differently
% %as there is assumed to be no magnitude response. This will be
confirmed
% %later
% while l <= (length(tlive)-VectorLengthlive)
%     %2.4.1 Construct vectors of 'VectorLength' number of points
after the lth
%     %point in the loop. Vectors correspond to time data and
detrended
%     %impedance magnitude over the set vector length
%     xlive = tlive(l:l+VectorLengthlive-1);
%     y4 = DetrendedMaglive(l:l+VectorLengthlive-1);
%     %2.4.2 Fit each vector to a single two-sided Gaussian profile
%     fitOptions4 = fitoptions('gauss1','Lower',[-1000 -1000
-1000],'Upper',[1000 1000 1000]);
%     [fitf4,gof4] = fit(xlive,y4,'gauss1',fitOptions4);
%     %2.4.3 Quantify goodness-of-fit with r-squared values
%     Rsq4(l,1) = gof4.rsquare;
%     %2.4.4 If r-squared values are greater than the minimum
threshold set
%     %execute code below to extract event signals and fit to a
Gaussian
%     %profile
%     if Rsq4(l,1) > RSquareLimMag4
%         %2.4.4.1 Create vectors corresponding to the fit Gaussian
profile
%         %and the detrended impedance magnitude signal over the
vector
%         %length
%         MagFit4(l:l+VectorLengthlive-1) = fitf4(xlive);
%         MagFit4Data(l:l+VectorLengthlive-1) = y4;
%         %2.4.4.2 Identify the maximum and location of the maximum of
the
%         %Gaussian fit profile and the detrended impedance magnitude
signal
%         [maxMagFit4,Loc4] =
max(abs(MagFit4(l:l+VectorLengthlive-1)));
%         [maxMagFit4Data,Loc4Data] =
max(abs(MagFit4Data(l:l+VectorLengthlive-1)));
%         %2.4.4.3 Define new l values as the locations of the two
maxima
%         lNew = l + Loc4Data;
```

```
%         lDataNew = l + Loc4Data;
%         %2.4.4.4 Define minumum and maximum time points
corresponding to
%         %the assumed length of the detection event signal for
Gaussian fit
%         %and impedance data
%         Loc4Min = max(l,lNew-PeakIntervallive);
%         Loc4DataMin = max(l,lDataNew-PeakIntervallive);
%         Loc4Max = min(length(tlive)-
VectorLengthlive,lNew+PeakIntervallive);
%         Loc4DataMax = min(length(tlive)-
VectorLengthlive,lDataNew+PeakIntervallive);
%         %2.4.4.5 Define new x vector corresponding to the peak data
%         xliveNew = tlive(Loc4DataMin:Loc4DataMax);
%         %2.4.4.6 Define new y vector corresponding to the peak data
%         y4New = DetrendedMaglive(Loc4DataMin:Loc4DataMax);
%         %2.4.4.7 Create new Gaussian fit centered around the maximum
of the
%         %detection event signal to ensure that all associated data
is
%         %processed
%         [fitf4New,gof4New] =
fit(xliveNew,y4New,'gauss1',fitOptions4);
%         %2.4.4.8 Redefine the curve for the fit as 0 outside of
assumed
%         %peak length and assign new curve for the data in the peak
length
%         MagFit4(l:Loc4Min) = 0;
%         MagFit4(Loc4Min:Loc4DataMax) = fitf4New(xliveNew);
%         if Loc4Max < l+VectorLengthlive-1
%         MagFit1(Loc4Max:l+VectorLengthlive-1) = 0;
%         end
%         %2.4.4.9 Redefine the impedance as 0 outside of assumed peak
length
%         %and keep the data within the detection event
%         MagFit4Data(l:Loc1Min) = DetrendedMaglive(l:Loc4Min);
%         MagFit4Data(Loc4DataMin:Loc4DataMax) = y4New;
%         if Loc4DataMax < l+VectorLengthlive-1
%         MagFit4Data(Loc4DataMax:i+VectorLengthlive-1) =
DetrendedMaglive(Loc4DataMax:l+VectorLengthlive-1);
%         end
%         MagFit4Noise(l:l+VectorLengthlive-1) = 0;
%         %2.4.4.10 Skip to end of detection event data to ensure that
it
%         %doesn't get erased or processed as noise
%         l = Loc4DataMax;
%     %3.4 If r-squared is less than the specified limit, use polyfit
and
%     %polyval functions to detrend noise then use Savitsky-Golay
Filtering
```

```
%     %to filter noise to ensure that no events were missed and
increase
%     %signal-to-noise ratio
%     else
%         %3.4.1 Create new polyfit and polyval functions to detrend
noise
%         %data over "VectorLength"-length interval
%         %[p4Noise,s4Noise,mu4Noise] = polyfit(xlive,y4,6);
%         %PolyVal4Noise = polyval(p4Noise,xlive,[],mu4Noise);
%         %3.4.2 Subtract polynomial from previously detrended data to
better
%         %detrend smaller section of noise
%         %MagFi41Data(l:l+length(y4)-1) = y4-PolyVal4Noise;
%         %3.4.3 Filter detrended noise data by Savitsky-Golay Filter
of
%         %order and frame length specified
%         %order = 3;
%         %framelen = VectorLength/10 + 1;
%         %MagFit4Data(l:l+length(y4)-1) =
sgolayfilt(MagFit4Data(l:l+length(y4)-1),order,framelen);
%         MagFit4Data(l:l+length(y4)-1) = 0;
%         MagFit4Noise(l:l+length(y4)-1) =
DetrendedMaglive(l:l+length(y4)-1);
%         %3.4.4 Skip to end of vector to avoid reprocessing
%         l = l + VectorLengthlive-1;
%     end
%     l = l + 1;
% end
%
% MagFit4Data(l:length(tlive)) = 0;
% MagFit4Noise(l:length(tlive)) = DetrendedMaglive(l:length(tlive));

while i <= (length(t1)-VectorLength1)
    x1 = t1(i:i+VectorLength1-1);
    y1 = DetrendedMag1(i:i+VectorLength1-1);
    fitOptions1 = fitoptions('gauss1','Lower',[-1000 -1000
-1000],'Upper',[1000 1000 1000]);
    [fitf1,gof1] = fit(x1,y1,'gauss1',fitOptions1);
    Rsq1(i,1) = gof1.rsquare;
    if Rsq1(i,1) > RSquareLimMag1
        MagFit1(i:i+VectorLength1-1) = fitf1(x1);
        MagFit1Data(i:i+VectorLength1-1) = y1;
        [maxMagFit1,Loc1] = max(abs(MagFit1(i:i+VectorLength1-1)));
        [maxMagFit1Data,Loc1Data] =
max(abs(MagFit1Data(i:i+VectorLength1-1)));
        iNew = i + Loc1Data;
        iDataNew = i + Loc1Data;
        Loc1Min = max(i,iNew-PeakInterval1);
        Loc1DataMin = max(i,iDataNew-PeakInterval1);
        Loc1Max = min(length(t1)-VectorLength1,iNew+PeakInterval1);
```

```
        Loc1DataMax = min(length(t1)-
VectorLength1,iDataNew+PeakInterval1);
        x1New = t1(Loc1DataMin:Loc1DataMax);
        y1New = DetrendedMag1(Loc1DataMin:Loc1DataMax);
        [fitf1New,gof1New] = fit(x1New,y1New,'gauss1',fitOptions1);
        MagFit1(i:Loc1Min) = 0;
        MagFit1(Loc1Min:Loc1DataMax) = fitf1New(x1New);
        if Loc1Max < i+VectorLength1-1
        MagFit1(Loc1Max:i+VectorLength1-1) = 0;
        end
        MagFit1Data(i:Loc1Min) = DetrendedMag1(i:Loc1Min);
        MagFit1Data(Loc1DataMin:Loc1DataMax) = y1New;
        if Loc1DataMax < i+VectorLength1-1
        MagFit1Data(Loc1DataMax:i+VectorLength1-1) =
DetrendedMag1(Loc1DataMax:i+VectorLength1-1);
        end
        MagFit1Noise(i:i+VectorLength1-1) = 0;
        i = Loc1DataMax;
    else
        MagFit1Data(i:i+length(y1)-1) = 0;
        MagFit1Noise(i:i+length(y1)-1) =
DetrendedMag1(i:i+length(y1)-1);
        i = i + VectorLength1-1;
    end
    i = i + 1;
end

MagFit1Data(i:length(t1)) = 0;
MagFit1Noise(i:length(t1)) = DetrendedMag1(i:length(t1));

while k <= (length(t1)-VectorLength1)
    x1 = t1(k:k+VectorLength1-1);
    y1 = DetrendedPh1Inv(k:k+VectorLength1-1);
    fitOptions1 = fitoptions('gauss1','Lower',[-1000 -1000
-1000],'Upper',[1000 1000 1000]);
    [fitf1,gof1] = fit(x1,y1,'gauss1',fitOptions1);
    Rsq2(k,1) = gof1.rsquare;
    if Rsq2(k,1) > RSquareLimPh1
        PhFit1Inv(k:k+VectorLength1-1) = fitf1(x1);
        PhFit1DataInv(k:k+VectorLength1-1) = y2;
        [maxPhFit1Inv,Loc1] =
max(abs(PhFit1Inv(k:k+VectorLength1-1)));
        [maxPhFit1DataInv,Loc1Data] =
max(abs(PhFit1DataInv(k:k+VectorLength1-1)));
        kNew = k + Loc1Data;
        kDataNew = k + Loc1Data;
        Loc1Min = max(k,kNew-PeakInterval1);
        Loc1DataMin = max(k,kDataNew-PeakInterval1);
        Loc1Max = min(length(t1)-VectorLength1,kNew+PeakInterval1);
        Loc1DataMax = min(length(t1)-
```

```
VectorLength1,kDataNew+PeakInterval1);
        x1New = t1(Loc1DataMin:Loc1DataMax);
        y1New = DetrendedPhdead(Loc1DataMin:Loc1DataMax);
        [fitf1New,gof1New] = fit(x1New,y1New,'gauss1',fitOptions1);
        PhFit1Inv(k:Loc1Min) = 0;
        PhFit1Inv(Loc1Min:Loc1DataMax) = fitf1New(x1New);
        if Loc1Max < k+VectorLength1-1
        PhFit1Inv(Loc1Max:k+VectorLength1-1) = 0;
        end
        PhFit1DataInv(k:Loc1Min) = DetrendedPh1(k:Loc1Min).*-1;
        PhFit1DataInv(Loc1DataMin:Loc1DataMax) = y1New;
        if Loc1DataMax < k+VectorLength1-1
        PhFit1DataInv(Loc1DataMax:k+VectorLength1-1) =
DetrendedPh1(Loc1DataMax:k+VectorLength1-1).*-1;
        end
        PhFit1Noise(k:k+VectorLength1-1) = 0;
        k = Loc1DataMax;
    else
        PhFit1DataInv(k:k+length(y1)-1) = 0;
        PhFit1Noise(k:k+length(y1)-1) =
DetrendedPh1(k:k+length(y1)-1).*-1;
        k = k + VectorLength1-1;
    end
    k = k + 1;
end

PhFit1Data(k:length(t1)) = 0;
PhFit1Noise(k:length(t1)) = DetrendedPh1(k:length(t1));

% MagFit1Noise = MagFit1Noise(:);
% MagFit4Noise = MagFit4Noise(:);
% PhFit3Noise = PhFit3Noise(:);
% PhFit2Noise = PhFit2Noise(:);

MagFit1Noise = MagFit1Noise(:);
PhFit1Noise = PhFit1Noise(:);

% PhFit2 = PhFit2Inv.*-1;
% PhFit2Data = PhFit2DataInv.*-1;
% PhFit3 = PhFit3Inv.*-1;
% PhFit3Data = PhFit3DataInv.*-1;

PhFit1 = PhFit1Inv.*-1;
PhFit1Data = PhFit1DataInv.*-1;

% for i = 1:length(MagFit1Data)
%     if MagFit1Data(i) < 0
%         MagFit1Noise(i) = DetrendedMagdead(i);
%     end
% end
```

```
% for i = 1:length(MagFit4Data)
%     if MagFit4Data(i) < 0
%         MagFit4Noise(i) = DetrendedMaglive(i);
%     end
% end
% for i = 1:length(PhFit2Data)
%     if PhFit2Data(i) > 0
%         PhFit2Noise(i) = DetrendedPhlive(i);
%     end
% end
% for i = 1:length(PhFit3Data)
%     if PhFit3Data(i) > 0
%         PhFit3Noise(i) = DetrendedPhdead(i);
%     end
% end

for i = 1:length(MagFit1Data)
    if MagFit1Data(i) < 0
        MagFit1Noise(i) = DetrendedMag1(i);
    end
end
for i = 1:length(PhFit1Data)
    if PhFit1Data(i) > 0
        PhFit1Noise(i) = DetrendedPh1(i);
    end
end

% IncMagdead = floor(length(MagFit1Data)/5);
% IncMaglive = floor(length(MagFit4Data)/5);
% IncPhdead = floor(length(PhFit3Data)/5);
% IncPhlive = floor(length(PhFit2Data)/5);

IncMag1 = floor(length(MagFit1Data)/5);
IncPh1 = floor(length(PhFit1Data)/5);

% tMagdead = tdead(1:IncMagdead);
% tMaglive = tlive(1:IncMaglive);
% tPhdead = tdead(1:IncPhdead);
% tPhlive = tlive(1:IncPhlive);

tMag1 = t1(1:IncMag1);
tPh1 = t1(1:IncMag1);

% [pMagdeadNoise,sMagdeadNoise,muMagdeadNoise] =
polyfit(tMagdead,MagFit1Noise(1:IncMagdead),5);
% [pMagliveNoise,sMagliveNoise,muMagliveNoise] =
polyfit(tMaglive,MagFit4Noise(1:IncMaglive),5);
% [pPhdeadNoise,sPhdeadNoise,muPhdeadNoise] =
polyfit(tPhdead,PhFit3Noise(1:IncPhdead),5);
% [pPhliveNoise,sPhliveNoise,muPhliveNoise] =
```

```
polyfit(tPhlive,PhFit2Noise(1:IncPhlive),5);

[pMag1Noise,sMag1Noise,muMag1Noise] =
polyfit(tMag1,MagFit1Noise(1:IncMag1),5);
[pPh1Noise,sPh1Noise,muPh1Noise] =
polyfit(tPh1,PhFit1Noise(1:IncPh1),5);

% PolyValMagdeadNoise = polyval(pMagdeadNoise,tdead(1:IncMagdead),
[],muMagdeadNoise);
% PolyValMagliveNoise = polyval(pMagliveNoise,tlive(1:IncMaglive),
[],muMagliveNoise);
% PolyValPhdeadNoise = polyval(pPhdeadNoise,tdead(1:IncPhdead),
[],muPhdeadNoise);
% PolyValPhliveNoise = polyval(pPhliveNoise,tlive(1:IncPhlive),
[],muPhliveNoise);

PolyValMag1Noise = polyval(pMag1Noise,t1(1:IncMag1),[],muMag1Noise);
PolyValPh1Noise = polyval(pPh1Noise,t1(1:IncPh1),[],muPh1Noise);

% DetrendedMagdeadNoise(1:IncMagdead) = MagFit1Noise(1:IncMagdead) -
PolyValMagdeadNoise;
% DetrendedMagliveNoise(1:IncMaglive) = MagFit4Noise(1:IncMaglive) -
PolyValMagliveNoise;
% DetrendedPhdeadNoise(1:IncPhdead) = PhFit3Noise(1:IncPhdead) -
PolyValPhdeadNoise;
% DetrendedPhliveNoise(1:IncPhlive) = PhFit2Noise(1:IncPhlive) -
PolyValPhliveNoise;

DetrendedMag1Noise(1:IncMag1) = MagFit1Noise(1:IncMag1) -
PolyValMag1Noise;
DetrendedPh1Noise(1:IncPh1) = PhFit1Noise(1:IncPh1) - PolyValPh1Noise;

% tMagdead = tdead(IncMagdead:IncMagdead*2);
% tMaglive = tlive(IncMaglive:IncMaglive*2);
% tPhdead = tdead(IncPhdead:IncPhdead*2);
% tPhlive = tlive(IncPhlive:IncPhlive*2);

tMag1 = t1(IncMag1:IncMag1*2);
tPh1 = t1(IncPh1:IncPh1*2);

% [pMagdeadNoise,sMagdeadNoise,muMagdeadNoise] =
polyfit(tMagdead,MagFit1Noise(IncMagdead:IncMagdead*2),5);
% [pMagliveNoise,sMagliveNoise,muMagliveNoise] =
polyfit(tMaglive,MagFit4Noise(IncMaglive:IncMaglive*2),5);
% [pPhdeadNoise,sPhdeadNoise,muPhdeadNoise] =
polyfit(tPhdead,PhFit3Noise(IncPhdead:IncPhdead*2),5);
% [pPhliveNoise,sPhliveNoise,muPhliveNoise] =
polyfit(tPhlive,PhFit2Noise(IncPhlive:IncPhlive*2),5);

[pMag1Noise,sMag1Noise,muMag1Noise] =
```

```
polyfit(tMag1,MagFit1Noise(IncMag1:IncMag1*2),5);
[pPh1Noise,sPh1Noise,muPh1Noise] =
polyfit(tPh1,PhFit1Noise(IncPh1:IncPh1*2),5);

% PolyValMagdeadNoise =
polyval(pMagdeadNoise,tdead(IncMagdead:IncMagdead*2),
[],muMagdeadNoise);
% PolyValMagliveNoise =
polyval(pMagliveNoise,tlive(IncMaglive:IncMaglive*2),
[],muMagliveNoise);
% PolyValPhdeadNoise =
polyval(pPhdeadNoise,tdead(IncPhdead:IncPhdead*2),[],muPhdeadNoise);
% PolyValPhliveNoise =
polyval(pPhliveNoise,tlive(IncPhlive:IncPhlive*2),[],muPhliveNoise);

PolyValMag1Noise = polyval(pMag1Noise,t1(IncMag1:IncMag1*2),
[],muMag1Noise);
PolyValPh1Noise = polyval(pPh1Noise,t1(IncPh1:IncPh1*2),
[],muPh1Noise);

% DetrendedMagdeadNoise(IncMagdead:IncMagdead*2) =
MagFit1Noise(IncMagdead:IncMagdead*2) - PolyValMagdeadNoise;
% DetrendedMagliveNoise(IncMaglive:IncMaglive*2) =
MagFit4Noise(IncMaglive:IncMaglive*2) - PolyValMagliveNoise;
% DetrendedPhdeadNoise(IncPhdead:IncPhdead*2) =
PhFit3Noise(IncPhdead:IncPhdead*2) - PolyValPhdeadNoise;
% DetrendedPhliveNoise(IncPhlive:IncPhlive*2) =
PhFit2Noise(IncPhlive:IncPhlive*2) - PolyValPhliveNoise;

DetrendedMag1Noise(IncMag1:IncMag1*2) =
MagFit1Noise(IncMag1:IncMag1*2) - PolyValMag1Noise;
DetrendedPh1Noise(IncPh1:IncPh1*2) = PhFit1Noise(IncPh1:IncPh1*2) -
PolyValPh1Noise;

% tMagdead = tdead(2*IncMagdead:IncMagdead*3);
% tMaglive = tlive(2*IncMaglive:IncMaglive*3);
% tPhdead = tdead(2*IncPhdead:IncPhdead*3);
% tPhlive = tlive(2*IncPhlive:IncPhlive*3);

tMag1 = t1(2*IncMag1:IncMag1*3);
tPh1 = t1(2*IncPh1:IncPh1*3);

% [pMagdeadNoise,sMagdeadNoise,muMagdeadNoise] =
polyfit(tMagdead,MagFit1Noise(2*IncMagdead:IncMagdead*3),5);
% [pMagliveNoise,sMagliveNoise,muMagliveNoise] =
polyfit(tMaglive,MagFit4Noise(2*IncMaglive:IncMaglive*3),5);
% [pPhdeadNoise,sPhdeadNoise,muPhdeadNoise] =
polyfit(tPhdead,PhFit3Noise(2*IncPhdead:IncPhdead*3),5);
% [pPhliveNoise,sPhliveNoise,muPhliveNoise] =
polyfit(tPhlive,PhFit2Noise(2*IncPhlive:IncPhlive*3),5);
```

```
[pMag1Noise,sMag1Noise,muMag1Noise] =
polyfit(tMag1,MagFit1Noise(2*IncMag1:IncMag1*3),5);
[pPh1Noise,sPh1Noise,muPh1Noise] =
polyfit(tPh1,PhFit3Noise(2*IncPh1:IncPh1*3),5);

% PolyValMagdeadNoise =
polyval(pMagdeadNoise,tdead(2*IncMagdead:IncMagdead*3),
[],muMagdeadNoise);
% PolyValMagliveNoise =
polyval(pMagliveNoise,tlive(2*IncMaglive:IncMaglive*3),
[],muMagliveNoise);
% PolyValPhdeadNoise =
polyval(pPhdeadNoise,tdead(2*IncPhdead:IncPhdead*3),[],muPhdeadNoise);
% PolyValPhliveNoise =
polyval(pPhliveNoise,tlive(2*IncPhlive:IncPhlive*3),[],muPhliveNoise);

PolyValMag1Noise = polyval(pMag1Noise,t1(2*IncMag1:IncMag1*3),
[],muMag1Noise);
PolyValPh1Noise = polyval(pPh1Noise,t1(2*IncPh1:IncPh1*3),
[],muPh1Noise);

% DetrendedMagdeadNoise(2*IncMagdead:IncMagdead*3) =
MagFit1Noise(2*IncMagdead:IncMagdead*3) - PolyValMagdeadNoise;
% DetrendedMagliveNoise(2*IncMaglive:IncMaglive*3) =
MagFit4Noise(2*IncMaglive:IncMaglive*3) - PolyValMagliveNoise;
% DetrendedPhdeadNoise(2*IncPhdead:IncPhdead*3) =
PhFit3Noise(2*IncPhdead:IncPhdead*3) - PolyValPhdeadNoise;
% DetrendedPhliveNoise(2*IncPhlive:IncPhlive*3) =
PhFit2Noise(2*IncPhlive:IncPhlive*3) - PolyValPhliveNoise;

DetrendedMag1Noise(2*IncMag1:IncMag1*3) =
MagFit1Noise(2*IncMag1:IncMag1*3) - PolyValMag1Noise;
DetrendedPh1Noise(2*IncPh1:IncPh1*3) = PhFit3Noise(2*IncPh1:IncPh1*3)
- PolyValPh1Noise;

% tMagdead = tdead(3*IncMagdead:IncMagdead*4);
% tMaglive = tlive(3*IncMaglive:IncMaglive*4);
% tPhdead = tdead(3*IncPhdead:IncPhdead*4);
% tPhlive = tlive(3*IncPhlive:IncPhlive*4);

tMag1 = t1(3*IncMag1:IncMag1*4);
tPh1 = t1(3*IncPh1:IncPh1*4);

% [pMagdeadNoise,sMagdeadNoise,muMagdeadNoise] =
polyfit(tMagdead,MagFit1Noise(3*IncMagdead:IncMagdead*4),5);
% [pMagliveNoise,sMagliveNoise,muMagliveNoise] =
polyfit(tMaglive,MagFit4Noise(3*IncMaglive:IncMaglive*4),5);
% [pPhdeadNoise,sPhdeadNoise,muPhdeadNoise] =
polyfit(tPhdead,PhFit3Noise(3*IncPhdead:IncPhdead*4),5);
```

```
% [pPhliveNoise,sPhliveNoise,muPhliveNoise] =
polyfit(tPhlive,PhFit2Noise(3*IncPhlive:IncPhlive*4),5);

[pMag1Noise,sMag1Noise,muMag1Noise] =
polyfit(tMag1,MagFit1Noise(3*IncMag1:IncMag1*4),5);
[pPh1Noise,sPh1Noise,muPh1Noise] =
polyfit(tPh1,PhFit3Noise(3*IncPh1:IncPh1*4),5);

% PolyValMagdeadNoise =
polyval(pMagdeadNoise,tdead(3*IncMagdead:IncMagdead*4),
[],muMagdeadNoise);
% PolyValMagliveNoise =
polyval(pMagliveNoise,tlive(3*IncMaglive:IncMaglive*4),
[],muMagliveNoise);
% PolyValPhdeadNoise =
polyval(pPhdeadNoise,tdead(3*IncPhdead:IncPhdead*4),[],muPhdeadNoise);
% PolyValPhliveNoise =
polyval(pPhliveNoise,tlive(3*IncPhlive:IncPhlive*4),[],muPhliveNoise);

PolyValMag1Noise = polyval(pMag1Noise,t1(3*IncMag1:IncMag1*4),
[],muMag1Noise);
PolyValPh1Noise = polyval(pPh1Noise,t1(3*IncPh1:IncPh1*4),
[],muPh1Noise);

% DetrendedMagdeadNoise(3*IncMagdead:IncMagdead*4) =
MagFit1Noise(3*IncMagdead:IncMagdead*4) - PolyValMagdeadNoise;
% DetrendedMagliveNoise(3*IncMaglive:IncMaglive*4) =
MagFit4Noise(3*IncMaglive:IncMaglive*4) - PolyValMagliveNoise;
% DetrendedPhdeadNoise(3*IncPhdead:IncPhdead*4) =
PhFit3Noise(3*IncPhdead:IncPhdead*4) - PolyValPhdeadNoise;
% DetrendedPhliveNoise(3*IncPhlive:IncPhlive*4) =
PhFit2Noise(3*IncPhlive:IncPhlive*4) - PolyValPhliveNoise;

DetrendedMag1Noise(3*IncMag1:IncMag1*4) =
MagFit1Noise(3*IncMag1:IncMag1*4) - PolyValMag1Noise;
DetrendedPh1Noise(3*IncPh1:IncPh1*4) = PhFit3Noise(3*IncPh1:IncPh1*4)
- PolyValPh1Noise;

% tMagdead = tdead(4*IncMagdead:IncMagdead*5);
% tMaglive = tlive(4*IncMaglive:IncMaglive*5);
% tPhdead = tdead(4*IncPhdead:IncPhdead*5);
% tPhlive = tlive(4*IncPhlive:IncPhlive*5);

tMag1 = t1(4*IncMag1:IncMag1*5);
tPh1 = t1(4*IncPh1:IncPh1*5);

% [pMagdeadNoise,sMagdeadNoise,muMagdeadNoise] =
polyfit(tMagdead,MagFit1Noise(4*IncMagdead:IncMagdead*5),5);
% [pMagliveNoise,sMagliveNoise,muMagliveNoise] =
polyfit(tMaglive,MagFit4Noise(4*IncMaglive:IncMaglive*5),5);
```

```
% [pPhdeadNoise,sPhdeadNoise,muPhdeadNoise] =
polyfit(tPhdead,PhFit3Noise(4*IncPhdead:IncPhdead*5),5);
% [pPhliveNoise,sPhliveNoise,muPhliveNoise] =
polyfit(tPhlive,PhFit2Noise(4*IncPhlive:IncPhlive*5),5);

[pMag1Noise,sMag1Noise,muMag1Noise] =
polyfit(tMag1,MagFit1Noise(4*IncMag1:IncMag1*5),5);
[pPh1Noise,sPh1Noise,muPh1Noise] =
polyfit(tPh1,PhFit3Noise(4*IncPh1:IncPh1*5),5);

% PolyValMagdeadNoise =
polyval(pMagdeadNoise,tdead(4*IncMagdead:IncMagdead*5),
[],muMagdeadNoise);
% PolyValMagliveNoise =
polyval(pMagliveNoise,tlive(4*IncMaglive:IncMaglive*5),
[],muMagliveNoise);
% PolyValPhdeadNoise =
polyval(pPhdeadNoise,tdead(4*IncPhdead:IncPhdead*5),[],muPhdeadNoise);
% PolyValPhliveNoise =
polyval(pPhliveNoise,tlive(4*IncPhlive:IncPhlive*5),[],muPhliveNoise);

PolyValMag1Noise = polyval(pMag1Noise,t1(4*IncMag1:IncMag1*5),
[],muMag1Noise);
PolyValPh1Noise = polyval(pPh1Noise,t1(4*IncPh1:IncPh1*5),
[],muPh1Noise);

% DetrendedMagdeadNoise(4*IncMagdead:IncMagdead*5) =
MagFit1Noise(4*IncMagdead:IncMagdead*5) - PolyValMagdeadNoise;
% DetrendedMagliveNoise(4*IncMaglive:IncMaglive*5) =
MagFit4Noise(4*IncMaglive:IncMaglive*5) - PolyValMagliveNoise;
% DetrendedPhdeadNoise(4*IncPhdead:IncPhdead*5) =
PhFit3Noise(4*IncPhdead:IncPhdead*5) - PolyValPhdeadNoise;
% DetrendedPhliveNoise(4*IncPhlive:IncPhlive*5) =
PhFit2Noise(4*IncPhlive:IncPhlive*5) - PolyValPhliveNoise;

DetrendedMag1Noise(4*IncMag1:IncMag1*5) =
MagFit1Noise(4*IncMag1:IncMag1*5) - PolyValMag1Noise;
DetrendedPh1Noise(4*IncPh1:IncPh1*5) = PhFit3Noise(4*IncPh1:IncPh1*5)
- PolyValPh1Noise;

% DetrendedMagdeadNoise = DetrendedMagdeadNoise(:);
% DetrendedMagliveNoise = DetrendedMagliveNoise(:);
% DetrendedPhdeadNoise = DetrendedPhdeadNoise(:);
% DetrendedPhliveNoise = DetrendedPhliveNoise(:);

DetrendedMag1Noise = DetrendedMag1Noise(:);
DetrendedPh1Noise = DetrendedPh1Noise(:);

% [TFMagdead,LMagdead,UMagdead,CMagdead] =
filloutliers(DetrendedMagdeadNoise,0);
```

```
% [TFMaglive,LMaglive,UMaglive,CMaglive] =
filloutliers(DetrendedMagliveNoise,0);
% [TFPhdead,LPhdead,UPhdead,CPhdead] =
filloutliers(DetrendedPhdeadNoise,0);
% [TFPhlive,LPhlive,UPhlive,CPhlive] =
filloutliers(DetrendedPhliveNoise,0);

[TFMag1,LMag1,UMag1,CMag1] = filloutliers(DetrendedMag1Noise,0);
[TFPh1,LPh1,UPh1,CPh1] = filloutliers(DetrendedPh1Noise,0);

% DetrendedMagdeadNoise = TFMagdead;
% DetrendedMagliveNoise = TFMaglive;
% DetrendedPhdeadNoise = TFPhdead;
% DetrendedPhliveNoise = TFPhlive;

DetrendedMag1Noise = TFMag1;
DetrendedPh1Noise = TFPh1;

% DetrendedMagdeadNoise(length(DetrendedMagdeadNoise)+1:length(tdead))
= 0;
% DetrendedMagliveNoise(length(DetrendedMagliveNoise)+1:length(tlive))
= 0;
% DetrendedPhdeadNoise(length(DetrendedPhdeadNoise)+1:length(tdead)) =
0;
% DetrendedPhliveNoise(length(DetrendedPhliveNoise)+1:length(tlive)) =
0;

DetrendedMagdeadNoise(length(DetrendedMagdeadNoise)+1:length(tdead)) =
0;
DetrendedPhdeadNoise(length(DetrendedPhdeadNoise)+1:length(tdead)) =
0;

% MagdeadData = zeros(length(DetrendedMagdead),1);
% MagliveData = zeros(length(DetrendedMaglive),1);
% PhdeadData = zeros(length(DetrendedPhdead),1);
% PhliveData = zeros(length(DetrendedPhlive),1);

i = 1;
for i = 1:length(DetrendedMagdeadNoise)
    if MagFit1Data(i) > 0
        MagFit1Data(i) = MagFit1Data(i);
    else
        MagFit1Data(i) = DetrendedMagdeadNoise(i);
    end
end
i = 1;
for i = 1:length(DetrendedMagliveNoise)
    if MagFit4Data(i) > 0
        MagFit4Data(i) = MagFit4Data(i);
    else
```

```
        MagFit4Data(i) = DetrendedMagliveNoise(i);
    end
end
i = 1;
for i = 1:length(DetrendedPhdeadNoise)
    if PhFit3Data(i) < 0
        PhFit3Data(i) = PhFit3Data(i);
    else
        PhFit3Data(i) = DetrendedPhdeadNoise(i);
    end
end
i = 1;
for i = 1:length(DetrendedPhliveNoise)
    if PhFit2Data(i) < 0
        PhFit2Data(i) = PhFit2Data(i);
    else
        PhFit2Data(i) = DetrendedPhliveNoise(i);
    end
end

for i = 1:length(tdead)
    if MagFit1(i) > 1
        if MagFit1Data(i) > -5
            DetrendedMagdeadNoise(i) = MagFit1Data(i);
        else
            DetrendedMagdeadNoise(i) = DetrendedMagdeadNoise(i);
        end
    end
end
for i = 1:length(tlive)
    if MagFit4(i) > 1
        if MagFit4Data(i) > -5
            DetrendedMagliveNoise(i) = MagFit4Data(i);
        else
            DetrendedMagliveNoise(i) = DetrendedMagliveNoise(i);
        end
    end
end
for i = 1:length(tdead)
    if PhFit3(i) < -0.001
        if PhFit3Data(i) < 0.02
            DetrendedPhdeadNoise(i) = PhFit3Data(i);
        else
            DetrendedPhdeadNoise(i) = DetrendedPhdeadNoise(i);
        end
    end
end
for i = 1:length(tlive)
    if PhFit2(i) < -0.001
        if PhFit2Data(i) < 0.02
```

```
            DetrendedPhliveNoise(i) = PhFit2Data(i);
        else
            DetrendedPhliveNoise(i) = DetrendedPhliveNoise(i);
        end
    end
end

mintlive = min(tlive);
tlive = tlive'-mintlive;
mintdead = min(tdead);
tdead = tdead'-mintdead;

%Create normalized time series so that live and dead cell samples can
be
%plotted together (for comparison of magnitude and phase data for each
%collection of data)
for i = 1:length(tlive)
    tlivenorm(i) = tlive(i)/max(tlive)*100;
end
for i = 1:length(tdead)
    tdeadnorm(i) = tdead(i)/max(tdead)*100;
end

%Plot data
figure(1)
%subplot(2,2,1)
p1 = plot(tlive,MagFit4,tlive,DetrendedMagliveNoise);
%title('Impedance Magnitude of Live Cells');
xlim([0 25])
ylim([-20 80])
a = get(gca,'XTickLabel');
set(gca,'XTickLabel',a,'fontname','Helvetica','fontsize',32)
set(gca,'XTickLabelMode','auto')
b = get(gca,'YTickLabel');
set(gca,'YTickLabel',b,'fontname','Helvetica','fontsize',32)
set(gca,'YTickLabelMode','auto')
p1(1).LineWidth = 2;
p1(1).Color = [0.4660, 0.6740, 0.1880];
p1(2).Color = [0.4660, 0.6740, 0.1880, 0.7];
xlabel('Time (s)')
ylabel('Impedance Magnitude (Ohms)')
legendMaglive = legend('Signal Detection Algorithm Output','Detrended
Raw Impedance Signal');
%legendMaglive.FontSize = 22;
%legendMaglive.Location = 'northwest';
export_fig /Users/jasoneades/Desktop/FIG5A.eps -RGB -Painters
-transparent
figure(2)
%subplot(2,2,3)
p2 = plot(tlive,PhFit2,tlive,DetrendedPhliveNoise);
```

```
%title('Impedance Phase of Live Cells');
xlim([0 25])
ylim([-0.10 0.02])
a = get(gca, 'XTickLabel');
set(gca,'XTickLabel',a,'fontname','Helvetica','fontsize',32)
set(gca,'XTickLabelMode','auto')
b = get(gca,'YTickLabel');
set(gca,'YTickLabel',b,'fontname','Helvetica','fontsize',32)
set(gca,'YTickLabelMode','auto')
p2(1).LineWidth = 2;
p2(1).Color = [0.4660, 0.6740, 0.1880];
p2(2).Color = [0.4660, 0.6740, 0.1880, 0.7];
xlabel('Time (s)')
ylabel('Impedance Phase (Degrees)')
legendPhlive = legend('Signal Detection Algorithm Output','Detrended
Raw Impedance Signal');
%legendPhlive.FontSize = 22;
legendPhlive.Location = 'southeast';
export_fig /Users/jasoneades/Desktop/FIG5C.eps -RGB -Painters
-transparent
figure(3)
%subplot(2,2,2)
p3 = plot(tdead,MagFit1,tdead,DetrendedMagdeadNoise);
%title('Impedance Magnitude of Dead Cells');
xlim([0 25])
ylim([-20 80])
a = get(gca,'XTickLabel');
set(gca,'XTickLabel',a,'fontname','Helvetica','fontsize',32)
set(gca,'XTickLabelMode','auto')
b = get(gca,'YTickLabel');
set(gca,'YTickLabel',b,'fontname','Helvetica','fontsize',32)
set(gca,'YTickLabelMode','auto')
p3(1).LineWidth = 2;
p3(1).Color = [0.6350, 0.0780, 0.1840];
p3(2).Color = [0.6350, 0.0780, 0.1840, 0.7];
xlabel('Time (s)')
ylabel('Impedance Magnitude (Ohms)')
legendMagdead = legend('Signal Detection Algorithm Output','Detrended
Raw Impedance Signal');
%legendMagdead.FontSize = 22;
%legendMagdead.Location = 'northwest';
export_fig /Users/jasoneades/Desktop/FIG5B.eps -RGB -Painters
-transparent
figure(4)
%subplot(2,2,4)
p4 = plot(tdead,PhFit3,tdead,DetrendedPhdeadNoise);
%title('Impedance Phase of Dead Cells');
xlim([0 25])
ylim([-0.10 0.02])
a = get(gca,'XTickLabel');
```

```
set(gca,'XTickLabel',a,'fontname','Helvetica','fontsize',32)
set(gca,'XTickLabelMode','auto')
b = get(gca,'YTickLabel');
set(gca,'YTickLabel',b,'fontname','Helvetica','fontsize',32)
set(gca,'YTickLabelMode','auto')
p4(1).LineWidth = 2;
p4(1).Color = [0.6350, 0.0780, 0.1840];
p4(2).Color = [0.6350, 0.0780, 0.1840, 0.7];
xlabel('Time (s)')
ylabel('Impedance Phase (Degrees)')
legendPhdead = legend('Signal Detection Algorithm Output','Detrended
Raw Impedance Signal');
%legendPhdead.FontSize = 22;
legendPhdead.Location = 'southeast';
export_fig /Users/jasoneades/Desktop/FIG5D.eps -RGB -Painters
-transparent

% order = 3;
% framelen = 11;
%
% MagdeadSG = sgolayfilt(DetrendedMagdead,order,framelen);
% PhdeadSG = sgolayfilt(DetrendedPhdead,order,framelen);
% MagliveSG = sgolayfilt(DetrendedMaglive,order,framelen);
% PhliveSG = sgolayfilt(DetrendedPhlive,order,framelen);
%
% figure(3)
% subplot(2,2,1)
% p1 = plot(tlive,MagliveSG,tlive,DetrendedMaglive);
% title('Impedance Magnitude of Live Cells by Savitzky-Golay
Filtering');
% a = get(gca,'XTickLabel');
% set(gca,'XTickLabel',a,'fontsize',20)
% set(gca,'XTickLabelMode','auto')
% b = get(gca,'YTickLabel');
% set(gca,'YTickLabel',b,'fontsize',20)
% set(gca,'YTickLabelMode','auto')
% p1(1).LineWidth = 3;
% p1(1).Color = [1.0, 0, 0];
% p1(2).Color = [1.0, 0, 0, 0.7];
% xlabel('Time (s)','FontSize',26)
% ylabel('Impedance Magnitude (Ohms)','FontSize',26)
% subplot(2,2,2)
% p2 = plot(tlive,PhliveSG,tlive,DetrendedPhlive);
% title('Impedance Phase of Live Cells by Savitzky-Golay Filtering');
% a = get(gca, 'XTickLabel');
% set(gca,'XTickLabel',a,'fontsize',20)
% set(gca,'XTickLabelMode','auto')
% b = get(gca,'YTickLabel');
% set(gca,'YTickLabel',b,'fontsize',20)
% set(gca,'YTickLabelMode','auto')
```

```
% p2(1).LineWidth = 3;
% p2(1).Color = [1.0, 0, 0];
% p2(2).Color = [1.0, 0, 0, 0.7];
% xlabel('Time (s)','FontSize',26)
% ylabel('Impedance Phase (Degrees)','FontSize',26)
% subplot(2,2,3)
% p3 = plot(tdead,MagdeadSG,tdead,DetrendedMagdead);
% title('Impedance Magnitude of Dead Cells by Savitzky-Golay
Filtering');
% a = get(gca,'XTickLabel');
% set(gca,'XTickLabel',a,'fontsize',20)
% set(gca,'XTickLabelMode','auto')
% b = get(gca,'YTickLabel');
% set(gca,'YTickLabel',b,'fontsize',20)
% set(gca,'YTickLabelMode','auto')
% p3(1).LineWidth = 3;
% p3(1).Color = [0, 0, 1.0];
% p3(2).Color = [0, 0, 1.0, 0.7];
% xlabel('Time (s)','FontSize',26)
% ylabel('Impedance Magnitude (Ohms)','FontSize',26)
% subplot(2,2,4)
% p4 = plot(tdead,PhdeadSG,tdead,DetrendedPhdead);
% title('Impedance Phase of Dead Cells by Savitzky-Golay Filtering');
% a = get(gca,'XTickLabel');
% set(gca,'XTickLabel',a,'fontsize',20)
% set(gca,'XTickLabelMode','auto')
% b = get(gca,'YTickLabel');
% set(gca,'YTickLabel',b,'fontsize',20)
% set(gca,'YTickLabelMode','auto')
% p4(1).LineWidth = 3;
% p4(1).Color = [0, 0, 1.0];
% p4(2).Color = [0, 0, 1.0, 0.7];
% xlabel('Time (s)','FontSize',26)
% ylabel('Impedance Phase (Degrees)','FontSize',26)

assignin('base','Rsq1',Rsq1)
Rsq1(Rsq1>0)
assignin('base','Rsq2',Rsq2)
Rsq2(Rsq2>0)
assignin('base','Rsq3',Rsq3)
assignin('base','Rsq4',Rsq4)

%-------------------------------------------------------------------------
--------------------------------
%Below catches errors and returns the error and values for i, j, k,
and l
%in loops

catch exception
    disp(exception.identifier);
```

```
    disp(exception.message);
    disp(exception.stack.line);
    i
    j
    k
    l
end


end
```

```
function [ ] = MixedSample ( )
%This code processes sample data for live and dead cells mixed in one
%sample

try

clear
clc

t = xlsread('Sample_Data','Mixed_2MHz','A950:A1350');
M = xlsread('Sample_Data','Mixed_2MHz','B950:B1350');
P = xlsread('Sample_Data','Mixed_2MHz','C950:C1350');

[pM,sM,muM] = polyfit(t,M,10);
[pP,sP,muP] = polyfit(t,P,10);

PolyValM = polyval(pM,t,[],muM);
PolyValP = polyval(pP,t,[],muP);

DetrendedM = M - PolyValM;
DetrendedP = P - PolyValP;

DetrendedPInv = zeros(length(t)-1,1);
x = zeros(length(t)-1,1);
yM = zeros(length(t)-1,1);
yP = zeros(length(t)-1,1);
MFit = zeros(length(t),1);
MFitData = zeros(length(t),1);
PFit = zeros(length(t),1);
PFitInv = zeros(length(t),1);
PFitData = zeros(length(t),1);
PFitDataInv = zeros(length(t),1);

DetrendedPInv = DetrendedP.*-1;

VectorLength = 80;
PeakInterval = 50;
RSquareLimM = 0.15;
RSquareLimP = 0.15;
i = 1; j = 1;
%order = 3; framelen = 79;

while i <= length(t)-VectorLength
    x = t(i:i+VectorLength-1);
    yM = DetrendedM(i:i+VectorLength-1);
    fitOptionsM = fitoptions('gauss1','Lower',[0 0 0],'Upper',[1000
1000 1000]);
    [fitfM,gofM] = fit(x,yM,'gauss1',fitOptionsM);
    RsqM = gofM.rsquare;
    if RsqM > RSquareLimM
```

```
        MFit(i:i+VectorLength-1) = fitfM(x);
        MFitData(i:i+VectorLength-1) = yM;
        [maxMFit,LocM] = max(abs(MFit(i:i+VectorLength-1)));
        [maxMFitData,LocMData] =
max(abs(MFitData(i:i+VectorLength-1)));
        iNew = i + LocMData;
        iDataNew = i + LocMData;
        LocMMin = max(i,iNew-PeakInterval);
        LocMDataMin = max(i,iDataNew-PeakInterval);
        LocMMax = iNew+PeakInterval;
        LocMDataMax = iDataNew+PeakInterval;
        xNew = t(LocMDataMin:LocMDataMax);
        yMNew = DetrendedM(LocMDataMin:LocMDataMax);
        [fitfMNew,gofMNew] = fit(xNew,yMNew,'gauss1',fitOptionsM);
        MFit(i:LocMMin) = 0;
        MFit(LocMMin:LocMDataMax) = fitfMNew(xNew);
        if LocMMax < i+VectorLength-1
        MFit(LocMMax:i+VectorLength-1) = 0;
        end
        MFitData(i:LocMMin) = DetrendedM(i:LocMMin);
        MFitData(LocMDataMin:LocMDataMax) = yMNew;
        if LocMDataMax < i+VectorLength-1
        MFitData(LocMDataMax:i+VectorLength-1) =
DetrendedM(LocMDataMax:i+VectorLength-1);
        end
        MFitNoise(i:i+VectorLength-1) = 0;
        i = LocMDataMax;
    else
        %[pMNoise,sMNoise,muMNoise] = polyfit(x,yM,6);
        %PolyValMNoise = polyval(pMNoise,x,[],muMNoise);
        %MFitData(i:i+length(yM)-1) = yM-PolyValMNoise;
        %MFitData(i:i+length(yM)-1) =
sgolayfilt(MFitData(i:i+length(yM)-1),order,framelen);
        MFit(i:i+length(yM)-1) = 0;
        MFitData(i:i+length(yM)-1) = DetrendedM(i:i+length(yM)-1);
        MFitNoise(i:i+length(yM)-1) = DetrendedM(i:i+length(yM)-1);
        i = i + VectorLength-1;
    end
    i = i + 1;
end

MFit(i:length(t)) = 0;
MFitData(i:length(t)) = DetrendedM(i:length(t));
MFitNoise(i:length(t)) = DetrendedM(i:length(t));

while j <= length(t)-VectorLength
    x = t(j:j+VectorLength-1);
    yP = DetrendedPInv(j:j+VectorLength-1);
    fitOptionsP = fitoptions('gauss1','Lower',[-1000 -1000
-1000],'Upper',[1000 1000 1000]);
```

```
    [fitfP,gofP] = fit(x,yP,'gauss1',fitOptionsP);
    RsqP = gofP.rsquare;
    if RsqP > RSquareLimP
        PFitInv(j:j+VectorLength-1) = fitfP(x);
        PFitDataInv(j:j+VectorLength-1) = yP;
        [maxPFit,LocP] = max(abs(PFitInv(j:j+VectorLength-1)));
        [maxPFitData,LocPData] =
max(abs(PFitDataInv(j:j+VectorLength-1)));
        jNew = j + LocPData;
        jDataNew = j + LocPData;
        LocPMin = max(j,jNew-PeakInterval);
        LocPDataMin = max(j,jDataNew-PeakInterval);
        LocPMax = jNew+PeakInterval;
        LocPDataMax = jDataNew+PeakInterval;
        xNew = t(LocPDataMin:LocPDataMax);
        yPNew = DetrendedPInv(LocPDataMin:LocPDataMax);
        [fitfPNew,gofPNew] = fit(xNew,yPNew,'gauss1',fitOptionsP);
        PFitInv(j:LocPMin) = 0;
        PFitInv(LocPMin:LocPDataMax) = fitfPNew(xNew);
        if LocPMax < j+VectorLength-1
        PFitInv(LocPMax:j+VectorLength-1) = 0;
        end
        PFitDataInv(j:LocPMin) = DetrendedPInv(j:LocPMin);
        PFitDataInv(LocPDataMin:LocPDataMax) = yPNew;
        if LocPDataMax < j+VectorLength-1
        PFitDataInv(LocPDataMax:j+VectorLength-1) =
DetrendedPInv(LocPDataMax:j+VectorLength-1);
        end
        j = LocPDataMax;
    else
        %[pPNoise,sPNoise,muPNoise] = polyfit(x,yP,6);
        %PolyValPNoise = polyval(pPNoise,x,[],muPNoise);
        %PFitDataInv(j:j+length(yP)-1) = yP-PolyValPNoise;
        %PFitDataInv(j:j+length(yP)-1) =
sgolayfilt(PFitDataInv(j:j+length(yP)-1),order,framelen);
        PFitInv(j:j+length(yP)-1) = 0;
        PFitDataInv(j:j+length(yP)-1) =
DetrendedPInv(j:j+length(yP)-1);
        PFitNoise(j:j+length(yP)-1) = DetrendedPInv(j:j+length(yP)-1);
        j = j + VectorLength-1;
    end
    j = j + 1;
end

PFitInv(i:length(t)) = 0;
PFitDataInv(i:length(t)) = DetrendedPInv(i:length(t));
PFitNoise(i:length(t)) = DetrendedPInv(i:length(t));


MFitNoise = MFitNoise(:);
```

```
PFitNoise = PFitNoise(:);

PFit = PFitInv.*-1;
PFitData = PFitDataInv.*-1;

for i = 1:length(t)
    if MFit(i) < 0
        MFitNoise(i) = DetrendedM(i);
    end
end
for i = 1:length(t)
    if PFit(i) > 0
        PFitNoise(i) = DetrendedP(i);
    end
end

IncM = floor(length(MFitData)/5);
IncP = floor(length(PFitData)/5);

tM = t(1:IncM);
tP = t(1:IncP);

[pMNoise,sMNoise,muMNoise] = polyfit(tM,MFitNoise(1:IncM),5);
[pPNoise,sPNoise,muPNoise] = polyfit(tP,PFitNoise(1:IncP),5);

PolyValMNoise = polyval(pMNoise,t(1:IncM),[],muMNoise);
PolyValPNoise = polyval(pPNoise,t(1:IncP),[],muPNoise);

DetrendedMNoise(1:IncM) = MFitNoise(1:IncM) - PolyValMNoise;
DetrendedPNoise(1:IncP) = PFitNoise(1:IncP) - PolyValPNoise;

tM = t(IncM:IncM*2);
tP = t(IncP:IncP*2);

[pMNoise,sMNoise,muMNoise] = polyfit(tM,MFitNoise(IncM:IncM*2),5);
[pPNoise,sPNoise,muPNoise] = polyfit(tP,PFitNoise(IncP:IncP*2),5);

PolyValMNoise = polyval(pMNoise,t(IncM:IncM*2),[],muMNoise);
PolyValPNoise = polyval(pPNoise,t(IncP:IncP*2),[],muPNoise);

DetrendedMNoise(IncM:IncM*2) = MFitNoise(IncM:IncM*2) - PolyValMNoise;
DetrendedPNoise(IncP:IncP*2) = PFitNoise(IncP:IncP*2) - PolyValPNoise;

tM = t(2*IncM:IncM*3);
tP = t(2*IncP:IncP*3);

[pMNoise,sMNoise,muMNoise] = polyfit(tM,MFitNoise(2*IncM:IncM*3),5);
[pPNoise,sPNoise,muPNoise] = polyfit(tP,PFitNoise(2*IncP:IncP*3),5);

PolyValMNoise = polyval(pMNoise,t(2*IncM:IncM*3),[],muMNoise);
```

```
PolyValPNoise = polyval(pPNoise,t(2*IncP:IncP*3),[],muPNoise);

DetrendedMNoise(2*IncM:IncM*3) = MFitNoise(2*IncM:IncM*3) -
PolyValMNoise;
DetrendedPNoise(2*IncP:IncP*3) = PFitNoise(2*IncP:IncP*3) -
PolyValPNoise;

tM = t(3*IncM:IncM*4);
tP = t(3*IncP:IncP*4);

[pMNoise,sMNoise,muMNoise] = polyfit(tM,MFitNoise(3*IncM:IncM*4),5);
[pPNoise,sPNoise,muPNoise] = polyfit(tP,PFitNoise(3*IncP:IncP*4),5);

PolyValMNoise = polyval(pMNoise,t(3*IncM:IncM*4),[],muMNoise);
PolyValPNoise = polyval(pPNoise,t(3*IncP:IncP*4),[],muPNoise);

DetrendedMNoise(3*IncM:IncM*4) = MFitNoise(3*IncM:IncM*4) -
PolyValMNoise;
DetrendedPNoise(3*IncP:IncP*4) = PFitNoise(3*IncP:IncP*4) -
PolyValPNoise;

tM = t(4*IncM:IncM*5);
tP = t(4*IncP:IncP*5);

[pMNoise,sMNoise,muMNoise] = polyfit(tM,MFitNoise(4*IncM:IncM*5),5);
[pPNoise,sPNoise,muPNoise] = polyfit(tP,PFitNoise(4*IncP:IncP*5),5);

PolyValMNoise = polyval(pMNoise,t(4*IncM:IncM*5),[],muMNoise);
PolyValPNoise = polyval(pPNoise,t(4*IncP:IncP*5),[],muPNoise);

DetrendedMNoise(4*IncM:IncM*5) = MFitNoise(4*IncM:IncM*5) -
PolyValMNoise;
DetrendedPNoise(4*IncP:IncP*5) = PFitNoise(4*IncP:IncP*5) -
PolyValPNoise;

[TFMNoise,LMNoise,UMNoise,CMNoise] = filloutliers(DetrendedMNoise,0);
[TFPNoise,LPNoise,UPNoise,CPNoise] = filloutliers(DetrendedPNoise,0);

DetrendedMNoise = TFMNoise;
DetrendedPNoise = TFPNoise;

DetrendedMNoise(length(DetrendedMNoise)+1:length(t)) = 0;
DetrendedPNoise(length(DetrendedPNoise)+1:length(t)) = 0;

for i = 1:length(t)
    if MFit(i) > 1
        if MFitData(i) > -5
            DetrendedMNoise(i) = MFitData(i);
        else
            DetrendedMNoise(i) = DetrendedMNoise(i);
```

```
        end
    end
end
for i = 1:length(t)
    if PFit(i) < -0.001
        if PFitData(i) < 0.02
            DetrendedPNoise(i) = PFitData(i);
        else
            DetrendedPNoise(i) = DetrendedPNoise(i);
        end
    end
end

MFit = normalize(MFit,'range');
MFitData = normalize(MFitData,'range');
PFit = normalize(PFit,'range');
PFitData = normalize(PFitData,'range');
PFit = PFit'-1;
PFitData = PFitData'-1;

figure(1)
subplot(2,1,1)
p1 = plot(t,MFitData,t,PFitData);
a = get(gca,'XTickLabel');
set(gca,'XTickLabel',a,'fontsize',20)
set(gca,'XTickLabelMode','auto')
b = get(gca,'YTickLabel');
set(gca,'YTickLabel',b,'fontsize',1420)
set(gca,'YTickLabelMode','auto')
p1(1).LineWidth = 2;
p1(1).Color = [0, 0, 1.0, 0.7];
p1(2).LineWidth = 2;
p1(2).Color = [1.0, 0, 0, 0.7];
xlabel('Time (s)','FontSize',20)
ylabel('Impedance','FontSize',20)
legend('Impedance Magnitude Detrended Raw Signal','Impedance Phase
Detrended Raw Signal')
subplot(2,1,2)
p2 = plot(t,MFit,t,PFit);
a = get(gca,'XTickLabel');
set(gca,'XTickLabel',a,'fontsize',20)
set(gca,'XTickLabelMode','auto')
b = get(gca,'YTickLabel');
set(gca,'YTickLabel',b,'fontsize',20)
set(gca,'YTickLabelMode','auto')
p2(1).LineWidth = 2;
p2(1).Color = 'b';
p2(2).LineWidth = 2;
p2(2).Color = 'r';
xlabel('Time (s)','FontSize',20)
```

```
ylabel('Impedance','FontSize',20)
legend('Impedance Magnitude (Ohms) - Signal Detection Algorithm
Output','Impedance Phase (Degrees) - Signal Detection Algorithm
Output')



catch exception
    disp(exception.identifier);
    disp(exception.message);
    disp(exception.stack.line);
    i
    j
end



end
```

References

Adams, André A. et al. (July 1, 2008). "Highly Efficient Circulating Tumor Cell Isolation from Whole Blood and Label-Free Enumeration Using Polymer-Based Microfluidics with an Integrated Conductivity Sensor". In: *Journal of the American Chemical Society* 130.27, pp. 8633–8641. ISSN: 0002-7863, 1520-5126. DOI: 10 . 1021 / ja8015022.

Anwar, Khalid, Taeheon Han, and Sun Min Kim (Apr. 2011). "Reversible Sealing Techniques for Microdevice Applications". In: *Sensors and Actuators B: Chemical* 153.2, pp. 301–311. ISSN: 09254005. DOI: 10.1016/j.snb.2010.11.002.

Auger, J. (Nov. 1, 2000). "Intra- and Inter-Individual Variability in Human Sperm Concentration, Motility and Vitality Assessment during a Workshop Involving Ten Laboratories". In: *Human Reproduction* 15.11, pp. 2360–2368. ISSN: 14602350. DOI: 10.1093/humrep/15.11.2360.

Barsoukov, Evgenij and J. Ross Macdonald, eds. (Apr. 4, 2005). *Impedance Spectroscopy*. 1st ed. Wiley. ISBN: 978-0-471-64749-2. DOI: 10.1002/0471716243.fmatter.

Bernabini, Catia, David Holmes, and Hywel Morgan (2011). "Micro-Impedance Cytometry for Detection and Analysis of Micron-Sized Particles and Bacteria". In: *Lab on a Chip* 11.3, pp. 407–412. ISSN: 1473-0197, 1473-0189. DOI: 10.1039/C0LC00099J.

Brito, Leonardo F.C. et al. (June 2016). "Andrology Laboratory Review: Evaluation of Sperm Concentration". In: *Theriogenology* 85.9, pp. 1507–1527. ISSN: 0093691X. DOI: 10.1016/j.theriogenology.2016.01.002.

Brosel-Oliu, Sergi et al. (Dec. 2019). "Impedimetric Transducers Based on Interdigitated Electrode Arrays for Bacterial Detection – A Review". In: *Analytica Chimica Acta* 1088, pp. 1–19. ISSN: 00032670. DOI: 10.1016/j.aca.2019.09.026.

Buettner, Florian et al. (Feb. 2015). "Computational Analysis of Cell-to-Cell Heterogeneity in Single-Cell RNA-Sequencing Data Reveals Hidden Subpopulations of Cells". In: *Nature Biotechnology* 33.2, pp. 155–160. ISSN: 1087-0156, 1546-1696. DOI: 10.1038/nbt.3102.

Caselli, Federica and Paolo Bisegna (Feb. 2016). "A Simple and Robust Event-Detection Algorithm for Single-Cell Impedance Cytometry". In: *IEEE Transactions on Biomedical Engineering* 63.2, pp. 415–422. ISSN: 0018-9294, 1558-2531. DOI: 10 . 1109/TBME.2015.2462292.

Caselli, Federica, Adele De Ninno, et al. (Mar. 2018). "A Novel Wiring Scheme for Standard Chips Enabling High-Accuracy Impedance Cytometry". In: *Sensors and*

Actuators B: Chemical 256, pp. 580–589. ISSN: 09254005. DOI: 10.1016/j.snb.2017.10.113.

Cesewski, Ellen and Blake N. Johnson (July 2020). "Electrochemical Biosensors for Pathogen Detection". In: *Biosensors and Bioelectronics* 159, p. 112214. ISSN: 09565663. DOI: 10.1016/j.bios.2020.112214.

Chen, Jian et al. (Mar. 2011). "A Microfluidic Device for Simultaneous Electrical and Mechanical Measurements on Single Cells". In: *Biomicrofluidics* 5.1, p. 014113. ISSN: 1932-1058. DOI: 10.1063/1.3571530.

Cheng, Xuanhong et al. (2007). "Cell Detection and Counting through Cell Lysate Impedance Spectroscopy in Microfluidic Devices". In: *Lab on a Chip* 7.6, pp. 746–755. ISSN: 1473-0197, 1473-0189. DOI: 10.1039/B705082H.

Cheung, Karen, Shady Gawad, and Philippe Renaud (June 2005). "Impedance Spectroscopy Flow Cytometry: On-Chip Label-Free Cell Differentiation". In: *Cytometry Part A* 65A.2, pp. 124–132. ISSN: 1552-4922, 1552-4930. DOI: 10.1002/cyto.a.20141.

Clausen, Casper et al. (Oct. 2018). "Bacteria Detection and Differentiation Using Impedance Flow Cytometry". In: *Sensors* 18.10, p. 3496. ISSN: 1424-8220. DOI: 10.3390/s18103496.

Cottet, Jonathan et al. (Jan. 2019). "How to Improve the Sensitivity of Coplanar Electrodes and Micro Channel Design in Electrical Impedance Flow Cytometry: A Study". In: *Microfluidics and Nanofluidics* 23.1, p. 11. ISSN: 1613-4982, 1613-4990. DOI: 10.1007/s10404-018-2178-6.

Couniot, N. et al. (May 2015). "Capacitive Biosensing of Bacterial Cells: Analytical Model and Numerical Simulations". In: *Sensors and Actuators B: Chemical* 211, pp. 428–438. ISSN: 09254005. DOI: 10.1016/j.snb.2015.01.108.

Daguerre, Hugo et al. (2020). "Positional Dependence of Particles and Cells in Microfluidic Electrical Impedance Flow Cytometry: Origin, Challenges and Opportunities". In: *Lab on a Chip* 20.20, pp. 3665–3689. ISSN: 1473-0197, 1473-0189. DOI: 10.1039/D0LC00616E.

Damhorst, Gregory L. et al. (Oct. 2013). "A Liposome-Based Ion Release Impedance Sensor for Biological Detection". In: *Biomedical Microdevices* 15.5, pp. 895–905. ISSN: 1387-2176, 1572-8781. DOI: 10.1007/s10544-013-9778-4.

Daniels, Jonathan S. and Nader Pourmand (June 2007). "Label-Free Impedance Biosensors: Opportunities and Challenges". In: *Electroanalysis* 19.12, pp. 1239–1257. ISSN: 10400397, 15214109. DOI: 10.1002/elan.200603855.

De Ninno, Adele, Vito Errico, et al. (2017). "Coplanar Electrode Microfluidic Chip Enabling Accurate Sheathless Impedance Cytometry". In: *Lab on a Chip* 17.6, pp. 1158–1166. ISSN: 1473-0197, 1473-0189. DOI: 10.1039/C6LC01516F.

De Ninno, Adele, Riccardo Reale, et al. (Feb. 2020). "High-Throughput Label-Free Characterization of Viable, Necrotic and Apoptotic Human Lymphoma Cells in a Coplanar-Electrode Microfluidic Impedance Chip". In: *Biosensors and Bioelectronics* 150, p. 111887. ISSN: 09565663. DOI: 10.1016/j.bios.2019.111887.

Dekker, S. et al. (Nov. 2018). "Standardized and Modular Microfluidic Platform for Fast Lab on Chip System Development". In: *Sensors and Actuators B: Chemical* 272, pp. 468–478. ISSN: 09254005. DOI: 10.1016/j.snb.2018.04.005.

Demircan Yalçın, Yağmur et al. (July 2019). "Exploring the Relationship between Cytoplasmic Ion Content Variation and Multidrug Resistance in Cancer Cells via Ion-Release Based Impedance Spectroscopy". In: *Sensors and Actuators B: Chemical* 290, pp. 180–187. ISSN: 09254005. DOI: 10.1016/j.snb.2019.03.084.

Dong, Qiaoxiang, Changjiang Huang, and Terrence R. Tiersch (Feb. 2007). "Control of Sperm Concentration Is Necessary for Standardization of Sperm Cryopreservation in Aquatic Species: Evidence from Sperm Agglutination in Oysters". In: *Cryobiology* 54.1, pp. 87–98. ISSN: 00112240. DOI: 10.1016/j.cryobiol.2006.11.007.

Evander, Mikael et al. (2013). "Microfluidic Impedance Cytometer for Platelet Analysis". In: *Lab on a Chip* 13.4, p. 722. ISSN: 1473-0197, 1473-0189. DOI: 10.1039/c2lc40896a.

Farka, Zdeněk et al. (Aug. 2016). "Rapid Immunosensing of *Salmonella* Typhimurium Using Electrochemical Impedance Spectroscopy: The Effect of Sample Treatment". In: *Electroanalysis* 28.8, pp. 1803–1809. ISSN: 10400397. DOI: 10.1002/elan.201600093.

Gale, Bruce et al. (Aug. 28, 2018). "A Review of Current Methods in Microfluidic Device Fabrication and Future Commercialization Prospects". In: *Inventions* 3.3, p. 60. ISSN: 2411-5134. DOI: 10.3390/inventions3030060.

Gawad, S., L. Schild, and Ph. Renaud (2001). "Micromachined Impedance Spectroscopy Flow Cytometer for Cell Analysis and Particle Sizing". In: *Lab on a Chip* 1.1, p. 76. ISSN: 1473-0197, 1473-0189. DOI: 10.1039/b103933b.

Hagedorn, M. et al. (Feb. 2009). "Biophysics of Zebrafish (Danio Rerio) Sperm". In: *Cryobiology* 58.1, pp. 12–19. ISSN: 00112240. DOI: 10.1016/j.cryobiol.2008.09.013.

Heath, James R., Antoni Ribas, and Paul S. Mischel (Mar. 2016). "Single-Cell Analysis Tools for Drug Discovery and Development". In: *Nature Reviews Drug Discovery* 15.3, pp. 204–216. ISSN: 1474-1776, 1474-1784. DOI: 10.1038/nrd.2015.16.

Heileman, Khalil, Jamal Daoud, and Maryam Tabrizian (Nov. 2013). "Dielectric Spectroscopy as a Viable Biosensing Tool for Cell and Tissue Characterization and Analysis". In: *Biosensors and Bioelectronics* 49, pp. 348–359. ISSN: 09565663. DOI: 10.1016/j.bios.2013.04.017.

Hierlemann, A. et al. (June 2003). "Microfabrication Techniques for Chemical/Biosensors". In: *Proceedings of the IEEE* 91.6, pp. 839–863. ISSN: 0018-9219. DOI: 10.1109/JPROC.2003.813583.

Hollingsworth, A.D. and D.A. Saville (Jan. 2003). "A Broad Frequency Range Dielectric Spectrometer for Colloidal Suspensions: Cell Design, Calibration, and Validation". In: *Journal of Colloid and Interface Science* 257.1, pp. 65–76. ISSN: 00219797. DOI: 10.1016/S0021-9797(02)00029-2.

Honrado, Carlos et al. (2021). "Single-Cell Microfluidic Impedance Cytometry: From Raw Signals to Cell Phenotypes Using Data Analytics". In: *Lab on a Chip* 21.1, pp. 22–54. ISSN: 1473-0197, 1473-0189. DOI: 10.1039/D0LC00840K.

Houssin, T. et al. (Jan. 15, 2010). "Label-Free Analysis of Water-Polluting Parasite by Electrochemical Impedance Spectroscopy". In: *Biosensors and Bioelectronics* 25.5, pp. 1122–1129. ISSN: 09565663. DOI: 10.1016/j.bios.2009.09.039.

"Impedance Instrumentation, Testing, and Data Validation" (July 2, 2012). In: Lvovich, Vadim F. *Impedance Spectroscopy*. Hoboken, NJ, USA: John Wiley & Sons, Inc., pp. 163–204. ISBN: 978-1-118-16407-5. DOI: 10.1002/9781118164075.ch8.

Jing, Rongyan et al. (May 2009). "Optimization of Activation, Collection, Dilution, and Storage Methods for Zebrafish Sperm". In: *Aquaculture* 290.1-2, pp. 165–171. ISSN: 00448486. DOI: 10.1016/j.aquaculture.2009.02.027.

Jönsson, Mats et al. (May 2006). "Bacteria Counting with Impedance Spectroscopy in a Micro Probe Station". In: *The Journal of Physical Chemistry B* 110.20, pp. 10165–10169. ISSN: 1520-6106, 1520-5207. DOI: 10.1021/jp060148q.

Kadan-Jamal, Kian et al. (Nov. 2020). "Electrical Impedance Spectroscopy of Plant Cells in Aqueous Biological Buffer Solutions and Their Modelling Using a Unified Electrical Equivalent Circuit over a Wide Frequency Range: 4Hz to 20 GHz". In: *Biosensors and Bioelectronics* 168, p. 112485. ISSN: 09565663. DOI: 10.1016/j.bios.2020.112485.

Kumar, K Vijaya, B Ram Reddy, and K Sai Krishna (n.d.). "Comparison of Different Methods for Assessing Sperm Concentration in Infertility Workup: A Review". In: (), p. 5.

Lasia, Andrzej (2014). *Electrochemical Impedance Spectroscopy and Its Applications*. New York, NY: Springer New York. ISBN: 978-1-4614-8932-0. DOI: 10.1007/978-1-4614-8933-7.

Lawrence, Christian (Sept. 2007). "The Husbandry of Zebrafish (Danio Rerio): A Review". In: *Aquaculture* 269.1-4, pp. 1–20. ISSN: 00448486. DOI: 10.1016/j.aquaculture.2007.04.077.

Lei, Kin (Jan. 7, 2014). "Review on Impedance Detection of Cellular Responses in Micro/Nano Environment". In: *Micromachines* 5.1, pp. 1–12. ISSN: 2072-666X. DOI: 10.3390/mi5010001.

Lieschke, Graham J. and Peter D. Currie (May 2007). "Animal Models of Human Disease: Zebrafish Swim into View". In: *Nature Reviews Genetics* 8.5, pp. 353–367. ISSN: 1471-0056, 1471-0064. DOI: 10.1038/nrg2091.

Liu, Jia, Yuhao Qiang, and E Du (Mar. 2021). "Dielectric Spectroscopy of Red Blood Cells in Sickle Cell Disease". In: *ELECTROPHORESIS* 42.5, pp. 667–675. ISSN: 0173-0835, 1522-2683. DOI: 10.1002/elps.202000143.

Luongo, Kevin et al. (May 2013). "Microfluidic Device for Trapping and Monitoring Three Dimensional Multicell Spheroids Using Electrical Impedance Spectroscopy". In: *Biomicrofluidics* 7.3, p. 034108. ISSN: 1932-1058. DOI: 10.1063/1.4809590.

Macdonald, Niall P. et al. (Apr. 4, 2017). "Comparing Microfluidic Performance of Three-Dimensional (3D) Printing Platforms". In: *Analytical Chemistry* 89.7, pp. 3858–3866. ISSN: 0003-2700, 1520-6882. DOI: 10.1021/acs.analchem.7b00136.

Mernier, Guillaume, Enri Duqi, and Philippe Renaud (2012). "Characterization of a Novel Impedance Cytometer Design and Its Integration with Lateral Focusing by Dielectrophoresis". In: *Lab on a Chip* 12.21, p. 4344. ISSN: 1473-0197, 1473-0189. DOI: 10.1039/c2lc40551b.

Murbach, Matthew et al. (Aug. 2020). "Impedance.Py: A Python Package for Electrochemical Impedance Analysis". In: *Journal of Open Source Software* 5.52, p. 2349. ISSN: 2475-9066. DOI: 10.21105/joss.02349.

Murphy, Travis W. et al. (2018). "Recent Advances in the Use of Microfluidic Technologies for Single Cell Analysis". In: *The Analyst* 143.1, pp. 60–80. ISSN: 0003-2654, 1364-5528. DOI: 10.1039/C7AN01346A.

Narayanan, Shree et al. (May 2010). "Analysis of the Passivation Layer by Testing and Modeling a Cell Impedance Micro-Sensor". In: *Sensors and Actuators A: Physical* 159.2, pp. 241–247. ISSN: 09244247. DOI: 10.1016/j.sna.2009.12.036.

Nielsen, Anna V et al. (2020). "3D Printed Microfluidics". In: p. 23.

Ohno, Ryuzo et al. (Feb. 2013). "Electrochemical Impedance Spectroscopy Biosensor with Interdigitated Electrode for Detection of Human Immunoglobulin A". In: *Biosensors and Bioelectronics* 40.1, pp. 422–426. ISSN: 09565663. DOI: 10.1016/j.bios.2012.07.052.

Ostermann, Melanie et al. (Dec. 2020). "Label-Free Impedance Flow Cytometry for Nanotoxicity Screening". In: *Scientific Reports* 10.1, p. 142. ISSN: 2045-2322. DOI: 10.1038/s41598-019-56705-3.

Palego, C. et al. (June 2013). "Broadband Microchamber for Electrical Detection of Live and Dead Biological Cells". In: *2013 IEEE MTT-S International Microwave Symposium Digest (MTT)*. Seattle, WA, USA: IEEE, pp. 1–3. ISBN: 978-1-4673-6177-3. DOI: 10.1109/MWSYM.2013.6697355.

Petchakup, Chayakorn, King Li, and Han Hou (Mar. 12, 2017). "Advances in Single Cell Impedance Cytometry for Biomedical Applications". In: *Micromachines* 8.3, p. 87. ISSN: 2072-666X. DOI: 10.3390/mi8030087.

Raicu, V (Apr. 1, 1995). "A Simple Theoretical and Practical Approach to Measuring Dielectric Properties with an Open-Ended Coaxial Probe". In: *Measurement Science and Technology* 6.4, pp. 410–414. ISSN: 0957-0233, 1361-6501. DOI: 10.1088/0957-0233/6/4/011.

Randviir, Edward P. and Craig E. Banks (2013). "Electrochemical Impedance Spectroscopy: An Overview of Bioanalytical Applications". In: *Analytical Methods* 5.5, p. 1098. ISSN: 1759-9660, 1759-9679. DOI: 10.1039/c3ay26476a.

Rasponi, Marco et al. (May 2011). "Reliable Magnetic Reversible Assembly of Complex Microfluidic Devices: Fabrication, Characterization, and Biological Validation". In: *Microfluidics and Nanofluidics* 10.5, pp. 1097–1107. ISSN: 1613-4982, 1613-4990. DOI: 10.1007/s10404-010-0738-5.

Research, WHO Special Program of (1992). *WHO Laboratory Manual for the Examination of Human Semen and Sperm-Cervicle Mucus Interaction*.

Rollo, Enrica et al. (Aug. 2017). "Label-Free Identification of Activated T Lymphocytes through Tridimensional Microsensors on Chip". In: *Biosensors and Bioelectronics* 94, pp. 193–199. ISSN: 09565663. DOI: 10.1016/j.bios.2017.02.047.

Schade-Kampmann, G. et al. (Oct. 2008). "On-Chip Non-Invasive and Label-Free Cell Discrimination by Impedance Spectroscopy". In: *Cell Proliferation* 41.5, pp. 830–840. ISSN: 09607722, 13652184. DOI: 10.1111/j.1365-2184.2008.00548.x.

Schönleber, M., D. Klotz, and E. Ivers-Tiffée (June 2014). "A Method for Improving the Robustness of Linear Kramers-Kronig Validity Tests". In: *Electrochimica Acta* 131, pp. 20–27. ISSN: 00134686. DOI: 10.1016/j.electacta.2014.01.034.

Schwan, Herman P. (1957). "Electrical Properties of Tissue and Cell Suspensions* *This Work Was Supported in Part by Grants from the United States Public Health Service, H-1253(C2-4) and in Part by the Office of Naval Research, 119–289." In: ed. by JOHN H. LAWRENCE and CORNELIUS A. TOBIAS. Vol. 5. Advances in Biological and Medical Physics. Elsevier, pp. 147–209. DOI: 10.1016/B978-1-4832-3111-2.50008-0.

Seidl, J., R. Knuechel, and L.A. Kunz-Schughart (Jan. 1999). "Evaluation of Membrane Physiology Following Fluorescence Activated or Magnetic Cell Separation". In: *Cytometry* 36.2, pp. 102–111.

Skafte-Pedersen, Peder et al. (May 2013). "Modular Microfluidic Systems Using Reversibly Attached PDMS Fluid Control Modules". In: *Journal of Micromechanics and Microengineering* 23.5, p. 055011. ISSN: 0960-1317, 1361-6439. DOI: 10.1088/0960-1317/23/5/055011.

Solsona, Miguel et al. (2019). "Gradient in the Electric Field for Particle Position Detection in Microfluidic Channels". In: *Lab on a Chip* 19.6, pp. 1054–1059. ISSN: 1473-0197, 1473-0189. DOI: 10.1039/C8LC01333K.

Spencer, Daniel and Hywel Morgan (Feb. 2020). "High-Speed Single-Cell Dielectric Spectroscopy". In: *ACS Sensors* 5.2, pp. 423–430. ISSN: 2379-3694, 2379-3694. DOI: 10.1021/acssensors.9b02119.

Sun, Tao et al. (Feb. 2009). "Digital Signal Processing Methods for Impedance Microfluidic Cytometry". In: *Microfluidics and Nanofluidics* 6.2, pp. 179–187. ISSN: 1613-4982, 1613-4990. DOI: 10.1007/s10404-008-0315-3.

Suresh, S (July 2007). "Biomechanics and Biophysics of Cancer Cells". In: *Acta Biomaterialia* 3.4, pp. 413–438. ISSN: 17427061. DOI: 10.1016/j.actbio.2007.04.002.

Taleat, Zahra, Alireza Khoshroo, and Mohammad Mazloum-Ardakani (July 2014). "Screen-Printed Electrodes for Biosensing: A Review (2008–2013)". In: *Microchimica Acta* 181.9-10, pp. 865–891. ISSN: 0026-3672, 1436-5073. DOI: 10.1007/s00604-014-1181-1.

Tan, Ereene, Huiping Yang, and Terrence R. Tiersch (June 2010). "Determination of Sperm Concentration for Small-Bodied Biomedical Model Fishes by Use of Microspectrophotometry". In: *Zebrafish* 7.2, pp. 233–240. ISSN: 1545-8547, 1557-8542. DOI: 10.1089/zeb.2010.0655.

Tang, Wenlai et al. (Mar. 2017). "Microfluidic Impedance Cytometer with Inertial Focusing and Liquid Electrodes for High-Throughput Cell Counting and Discrimination". In: *Analytical Chemistry* 89.5, pp. 3154–3161. ISSN: 0003-2700, 1520-6882. DOI: 10.1021/acs.analchem.6b04959.

Temiz, Yuksel et al. (Jan. 2015). "Lab-on-a-Chip Devices: How to Close and Plug the Lab?" In: *Microelectronic Engineering* 132, pp. 156–175. ISSN: 01679317. DOI: 10.1016/j.mee.2014.10.013.

Torres, Leticia et al. (Dec. 2017). "Challenges in Development of Sperm Repositories for Biomedical Fishes: Quality Control in Small-Bodied Species". In: *Zebrafish* 14.6, pp. 552–560. ISSN: 1545-8547, 1557-8542. DOI: 10.1089/zeb.2017.1426.

Tsouti, V. et al. (Sept. 2011). "Capacitive Microsystems for Biological Sensing". In: *Biosensors and Bioelectronics* 27.1, pp. 1–11. ISSN: 09565663. DOI: 10.1016/j.bios.2011.05.047.

Varshney, Madhukar and Yanbin Li (June 2009). "Interdigitated Array Microelectrodes Based Impedance Biosensors for Detection of Bacterial Cells". In: *Biosensors and Bioelectronics* 24.10, pp. 2951–2960. ISSN: 09565663. DOI: 10.1016/j.bios.2008.10.001.

Waheed, Sidra et al. (2016). "3D Printed Microfluidic Devices: Enablers and Barriers". In: *Lab on a Chip* 16.11, pp. 1993–2013. ISSN: 1473-0197, 1473-0189. DOI: 10.1039/C6LC00284F.

Wang, H., N. Sobahi, and A. Han (2017). "Impedance Spectroscopy-Based Cell/Particle Position Detection in Microfluidic Systems". In: *Lab on a Chip* 17.7, pp. 1264–1269. ISSN: 1473-0197, 1473-0189. DOI: 10.1039/C6LC01223J.

Westerfield, Monte (2000). "The Zebrafish Book, a Guide for the Laboratory Use of Zebrafish Danio Rerio". In: *The Zebrafish Book, a Guide for the Laboratory Use of Zebrafish Danio Rerio*. Eugene, OR: University of Oregon Press, pp. 1.1–11.93.

Wilson-Leedy, J.G., M.K. Kanuga, and R.L. Ingermann (Apr. 2009). "Influence of Osmolality and Ions on the Activation and Characteristics of Zebrafish Sperm Motility". In: *Theriogenology* 71.7, pp. 1054–1062. ISSN: 0093691X. DOI: 10.1016/j.theriogenology.2008.11.006.

Xu, Youchun et al. (Mar. 2016). “A Review of Impedance Measurements of Whole Cells”. In: *Biosensors and Bioelectronics* 77, pp. 824–836. ISSN: 09565663. DOI: 10.1016/j.bios.2015.10.027.

Yang, Huiping, Jonathan Daly, and Terrence R. Tiersch (Apr. 2016). “Determination of Sperm Concentration Using Flow Cytometry with Simultaneous Analysis of Sperm Plasma Membrane Integrity in Zebrafish *Danio Rerio*: Determination of Sperm Concentration by Flow Cytometry”. In: *Cytometry Part A* 89.4, pp. 350–356. ISSN: 15524922. DOI: 10.1002/cyto.a.22796.

Vita

Jason Eades was raised in Baton Rouge, LA. He received a B.S. in Chemical Engineering from Louisiana State University in 2016. He worked as a Process Engineering Specialist for Ford, Bacon, & Davis, LLC for four years. In June 2016, he enrolled part-time in the graduate program in the Department of Biological and Agricultural Engineering at Louisiana State University. In September 2019, he transitioned to full-time graduate study to pursue a Master's degree in Biological Engineering, which is anticipated to be awarded in August 2021.